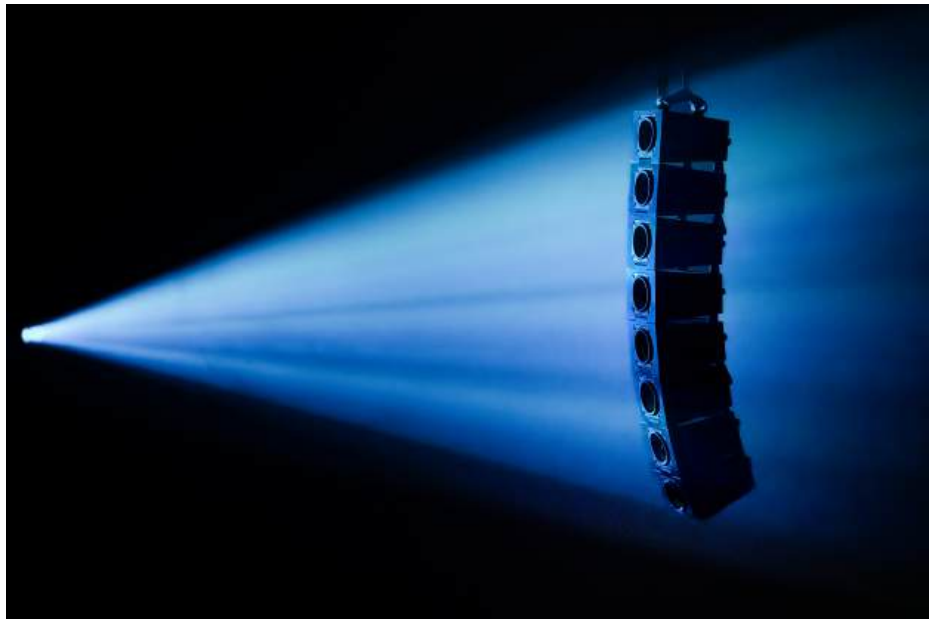


Immersive Sound Reinforcement

PhD Thesis



Lukas Gölles



Immersive Sound Reinforcement

PhD Thesis
submitted by

Dipl.-Ing. Lukas Gölles, BSc

Supervisors:

O.Univ.Prof. Mag.art. DI Dr.techn. Robert Höldrich
Univ.Prof. Dipl.-Ing. Dr.techn. Alois Sontacchi

Co-Supervisor:

Univ.Prof. DI Dr.rer.nat. Franz Zotter

External Reviewer:

Prof. Dr.-Ing. Anselm Goertz

submitted to

University of Music and Performing Arts Graz
PhD Program (Sound and Music Computing, UV 094 750)

January 8, 2025

Abstract

The requirements for many audio applications have increased with the boom of Augmented Reality (AR) and Virtual Reality (VR). As a result of the pressure to progress, there is also an increasing interest in using immersive audio technologies at concerts.

In venues with a capacity of 50 to 200 people, point-source loudspeakers are often employed in surround sound reinforcement systems, often with the goal to arrange direct sound objects and enveloping diffuse sounds around the audience. However, a setup of surrounding point-source loudspeakers causes different level balances between voices and instruments from different directions for each listener. Furthermore, they are not able to reproduce a preserved sense of feeling surrounded by sound, i.e. envelopment, at off-center listening positions.

This doctoral thesis investigates the effect of using small line arrays in different distance decay settings on the size of the area for which reproduction is acceptable, i.e. the sweet area. By modifying the curvature or phasing of line sources, the direct sound level roll-off on the listening area is designed, for which a design equation is introduced. The approach is also extended to define the phase load of planar arrays. To test and verify the formalism in practice, a miniature line array prototype with 3D printed enclosures is designed and presented. Simulations of the sweet area for surround sound reinforcement compare different line-array configurations considering the level balance and the envelopment. Using the miniature line-array prototype, a listening experiment confirms the results of the simulations in practice and proposes a dual-target design that realizes a hybrid approach of combining line-array curving and phasing. This dual-target design requires separate processing of the direct sound objects from the enveloping parts. A second listening experiment shows that simple design targets also achieve acceptable results in conventional concert scenarios and do not require splitting direct sound objects from the enveloping diffuse sounds.

Kurzfassung

Mit dem Aufschwung der erweiterten Realität (augmented reality) und der virtuellen Realität (virtual reality) sind die Anforderungen für viele Audioanwendungen gestiegen. Infolge des Fortschrittsdrucks steigt auch das Interesse, Rundumbeschallung bei Konzerten zu ermöglichen. Punktschallquellen verwenden häufig bei mittelgroßen Beschallungsszenarien eingesetzt, bei denen öfters Audioobjekte und einhüllende diffuse Klänge rund um das Publikum platziert werden. Jedoch ergibt sich bei einem Setup von Punktquellenlautsprechern eine unterschiedliche Lautstärkebalance der Audioobjekte für jede Hörposition. Weiters ist ein solches Setup nicht in der Lage, die Einhüllung, das Gefühl von Klang umgeben zu sein, an dezentralen Hörpositionen zu erhalten.

In dieser Dissertation wird die Auswirkung kleiner Line Arrays auf die Größe des Bereichs untersucht, der für akzeptable Wiedergabe genutzt werden kann, d.h. auf die Größe der Sweet Area. Der Direktschallpegelabfall auf der Hörfläche lässt sich durch Anpassen der Krümmung oder des Phasenbelags linienförmiger Schallquellen entwerfen. Für das Design der Krümmung und des Phasenbelags wird eine Designgleichung vorgestellt, die auf das Design des Phasenbelags von planaren Arrays erweitert wird. Um den Formalismus in der Praxis zu testen und zu verifizieren, wird ein Miniatur Line Array Prototyp mit 3D-gedruckten Gehäusen entworfen und vorgestellt. Simulationen der Sweet Area für Rundumbeschallung vergleichen unterschiedliche Line Array Konfigurationen unter Berücksichtigung der Lautstärkebalance und der Einhüllung. Unter Verwendung des Miniatur Line Array Prototyps bestätigt ein Hörversuch die Ergebnisse der Simulationen in der Praxis und schlägt ein Dual-Target-Design des Direktschallpegels vor, das einen hybriden Ansatz realisiert, welcher den Einsatz von Line Array Krümmung und elektronischen Beamforming kombiniert. Dieses Design erfordert in weiterer Folge eine getrennte Verarbeitung der Direktobjekte und der einhüllenden diffusen Klängen. Ein zweiter Hörversuch zeigt, dass auch einfache Designziele bei konventionellen Konzertszenarien akzeptable Ergebnisse erzielen und keine Trennung der Direktobjekte von den einhüllenden diffusen Klängen erfordern.

Preface

I am grateful for all the help and support I have received during the last three years, but also for the employment I have received at the Institute of Electronic Music and Acoustics (IEM) of the University of Music and Performing Arts (Kunstuniversität, KUG) in Graz within the project *Envelopment In Immersive Sound Reinforcement* (project number P 35254-N) funded by the Austrian Science Fund (FWF).

Personally, I would like to thank:

- Robert Höldrich, for being my main advisor, his expertise, and feedback.
- Alois Sontacchi for being my second advisor, and the possibility to present the mini line arrays to many visitors at the IEM.
- Franz Zotter, for being my co-advisor, for leading and acquiring the EnImSo project, for always being open to discussions, for co-authoring many papers and his advice on text, equation and presentation engineering.
- Anselm Goertz, for joining the committee and evaluation discussions as my external reviewer.
- Matthias Frank, for many discussions on listening experiment design, the listening experiment evaluations, co-authoring many papers, and for his strategic approach to inspiring practical demonstrations.
- Thomas Musil, for the modification and improvements of the CAD miniature line-array model that made them look like a commercial product and for building 48 enclosures.
- Stefan Warum, for his tireless willingness to be the first port of call when you are looking for equipment and for his support and advice in choosing the right equipment to be bought.
- Emanuel Brandl, for mounting and modifying the new amplifiers so that they can be used with the line-array prototype and the NL8 connectors.
- My office colleagues, the „residents of the Petersgasse“ („Petersgassenbewohner“), for all coffee breaks and always having fun while thinking of new ideas to decorate the wall in the kitchenette with funny quotes.
- Helmut Wagner and the Herzkraft team for the excellent and professional cooperation at numerous events at which I was able to learn the practical handling of professional line-source arrays and other things that helped me to look at problems from a practical point of view.
- Raphael Köstl, for the idea and for his great support in designing and taking the cover pictures.

Apart from all these people, I want to thank my parents, Elke and Erich, and my brother, Julian, for their unconditional support.

Erklärung

Mit meiner Unterschrift bestätige ich, dass mir der *Leitfaden für schriftliche Arbeiten an der KUG*¹ bekannt ist und ich die darin enthaltenen Bestimmungen eingehalten habe. Ich erkläre ehrenwörtlich, dass ich die vorliegende Arbeit selbständig verfasst, andere als die angegebenen Quellen nicht verwendet und die wörtlich oder inhaltlich entnommenen Stellen als solche kenntlich gemacht habe. Sofern fremde Hilfe (z.B. Korrekturlesen durch Native Speaker) und/oder KI-Dienste verwendet wurden (z.B. internetbasierte Übersetzungstools und/oder KI-basierte Sprachmodelle) habe ich dies ausgewiesen.

Graz, den 8. Januar 2025

.....
(Unterschrift)

¹Leitfaden für schriftliche Arbeiten an der KUG (laut Beschluss des Senats vom 7. November 2023)

Contents

1	Introduction	1
1.1	Challenges of medium-scale surround sound reinforcement	3
1.2	Organization of content	4
2	Curving and Phasing	5
2.1	Linear Sources	6
2.2	Planar Sources	8
3	Prototype Design	11
4	Successful Surround Sound Reinforcement	15
4.1	Optimal Design Targets	16
4.2	Dual-target vs. Single-target Design	21
4.3	Spatialization Techniques for Live Surround Sound Reinforcement	23
5	Concluding Remarks	25
	Publications	31

List of Publications

This thesis provides an overview of the publications listed below, which are referred to in the text by their Roman numerals.

Journal Papers:

- I Lukas Gölles**, and Franz Zotter, „Theory of continuously curved and phased line sources for sound reinforcement,“ *Acta Acust.*, vol. 7, p. 52, 2023. [Online]. Available: <https://doi.org/10.1051/aacus/2023045>
- II Lukas Gölles** and Franz Zotter, „Theory of continuously phased planar sources for sound reinforcement,“ *Acta Acust.*, [Accepted on October 1, 2024]

Conference Papers:

- III Lukas Gölles**, Franz Zotter, and Leon Merkel, “Miniature line array for immersive sound reinforcement,” in *Proceedings of AES SIA Conf.*, Huddersfield, 08 2023. [Online]. Available: <https://aes2.org/publications/elibrary-page/?id=22156>
- IV Lukas Gölles**, and Franz Zotter, “Dual-target design for large-scale sound reinforcement: Simulation and evaluation,” in *Audio Engineering Society Conference: AES 2024 International Conference on Acoustics & Sound Reinforcement*, Jan 2024, *peer-reviewed*. [Online]. Available: <https://aes2.org/publications/elibrary-page/?id=22369>
- V Lukas Gölles**, Matthias Frank, and Franz Zotter, “Simulating the sweet area of immersive sound reinforcement with surrounding mini line arrays,” in *Fortschritte der Akustik, DAGA*, Hannover, March 2024. [Online]. Available: https://pub.dega-akustik.de/DAGA_2024/files/upload/paper/188.pdf
- VI Lukas Gölles**, Matthias Frank, and Franz Zotter, “Improving surround sound reinforcement at off-center listening positions with miniature line arrays,” in *Audio Engineering Society Convention 156*, Madrid, June 2024, *peer-reviewed*. [Online]. Available: <https://aes2.org/publications/elibrary-page/?id=22504>
- VII Lukas Gölles**, Matthias Frank, and Franz Zotter, “Evaluating a dual-target line-array design for medium-scale surround sound reinforcement,” in *Audio Engineering Society Convention 156*, Madrid, June 2024. [Online]. Available: <https://aes2.org/publications/elibrary-page/?id=22560>
- VIII Lukas Gölles**, Maximilian Herczegh, and Matthias Frank, “MCPyPan3D: mixing console’s python-based panning tool for 3D audio at live events,” in *Proceedings of LEaTcon Science Talks*, Hamburg: October 2024. [presented, but not published yet]

Author's Contribution

In Publications I - VIII, I was the first author. Below, my role is referred to as "first author".

Publication I: Theory of continuously curved and phased line sources for sound reinforcement

The first and second author developed and described the formalism and required routines together. The first author developed the algorithm and performed the simulations and the measurements. The manuscript was primarily written by the first author with contributions from the second author.

Publication II: Theory of continuously phased planar sources for sound reinforcement

The formalism of Publication I was primarily extended to planar arrays by the first author. In an intensive mathematical internal revision with the second author, some mathematical improvements could be found. Simulations, measurements, and analysis were done by the first author. The text was mainly authored by the first author with editing contributions by the second author.

Publication III: Miniature line array for immersive sound reinforcement

The derivations were primarily done by the first author with contributions from the second author. The online solver was programmed by the first author. Measurements of coverage and directivity were done by all three authors. Analysis of the directivity measurements was done by the third author. The first author performed the analysis of the coverage measurements. The first author mainly wrote the paper, except the section dealing with the directivity measurement, which was written by the third author. The second author helped to edit the paper.

Publication IV: Dual-target design for large-scale sound reinforcement: Simulation and evaluation

The first author had the basic idea to perform a simulation study for large arrays and also wrote the paper, with support of the second author. The first author performed the simulations and analyzed the measurements. Both authors carried out the measurements.

Publication V: Simulating the sweet area of immersive sound reinforcement with surrounding mini line arrays

The first author wrote the paper and did the simulations with the support of scripts of the

energy vector provided by the second author. The second and third authors helped to edit the paper.

Publication VI: Improving surround sound reinforcement at off-center listening positions with miniature line arrays

The listening experiment design and the evaluation were carried out mainly by the first author. The second and third authors helped during the design and evaluation, as well as in writing the paper.

Publication VII: Evaluating a dual-target line-array design for medium-scale surround sound reinforcement

The first author was primarily responsible for the design and assessment of listening experiments. Along with their help in writing the paper, the second and third author contributed to the experimental design and assessment.

Publication VIII: MCPan3D: mixing console's python-based panning tool for 3D audio at live events

The idea was conceived by the first author. The python-based graphical interface was programmed by the second author. The first author did the mathematical derivations, performed the simulations, prepared the listening experiment, and wrote the paper. The third author helped to edit the paper and to make sure the experimental study was designed and evaluated properly.

1

Introduction

Today, state-of-the-art large-scale sound reinforcement systems largely focus on the use of line-(source) arrays [1], cf. Figure 1. Their direct sound pressure coverage can easily be designed by modifying the splay angles between the enclosures of such an array. Usually, a line source is mounted on each side of the stage. In many cases, the dimensions of the stages determine the distance between the arrays and also the mounting height. As large stages are usually very wide, accurate panning that works for the largest part of the listening area is practically infeasible. Therefore, the same signal is often reproduced by both arrays to preserve the level balance between the different instruments and voices of the mix for many listeners.



Figure 1: Example of a line-source array with ten L'Acoustics K3 enclosures, Photo: Raphael Köstl.

As a result of the growing popularity of spatial audio and the further development of home cinema systems, the usage of spatial audio techniques is gaining in importance, even at live events. Additional loudspeaker arrays can be placed above the stage to enable better localization of audio objects from different directions. These loudspeakers are often complemented with surrounding loudspeakers on the sides and in the back of the audience. A good system design is essential to provide a sweet area that should be as large as possible. The sweet area is a zone in which acceptable playback is achieved regarding a consistent localization of direct sound objects, a well-balanced mix of instruments and voices from different directions, and the impression of being surrounded by sound, whenever enveloping diffuse sounds are reproduced. For large sound reinforcement systems, there are already solutions, for example L'Acoustics L-ISA² or d&b Soundscape³. In [2, Ch. 2, p. 24ff], E. Corteel et. al. propose guidelines dealing with the system setup. However, most line-source arrays are designed to be used in large-scale sound reinforcement, making it difficult to use them in smaller systems. This might be a factor why point-source loudspeakers are most commonly employed in medium-scale surround sound reinforcement applications up to 200 listeners. One of the key motivations behind this thesis is to investigate and experimentally verify that smaller line array systems can have clear benefits, also in such smaller application scenarios.



Figure 2: Example of a medium-scale spatial audio system: IEM CUBE with 24 point-source loudspeakers, Tannoy Systems 1200, mounted in a hemispherical arrangement, Photo: Wolfgang Hummer.

²<https://l-isa.l-acoustics.com/>

³<https://www.dbsoundscape.com/global/en/>

1.1 Challenges of medium-scale surround sound reinforcement

At the University of Music and Performing Arts Graz, there are two rooms with permanent Ambisonic playback systems installed. Both setups employ point-source loudspeakers. The György Ligeti Hall at MUMUTH, is a $33\text{ m} \times 15\text{ m}$ concert hall with a reverberation time $T_{30} \approx 1.1\text{ s}$. The setup uses 25 point-source loudspeakers, Kling & Freitag CA 1001, mounted in a hemisphere. The second room, the IEM CUBE is a $10.3\text{ m} \times 12\text{ m}$ studio with $T_{30} \approx 0.5\text{ s}$. The setup uses 12 d&b 12S-D on the horizon and 13 d&b 8S on higher layers. Figure 2 shows the IEM CUBE with the older loudspeaker system, Tannoy Systems 1200, which was replaced by the d&b system in 2021. The IEM CUBE can hold up to 70 listeners, and the György Ligeti Hall can accommodate around 150 people, making them examples of medium-sized surround sound reinforcement spaces.

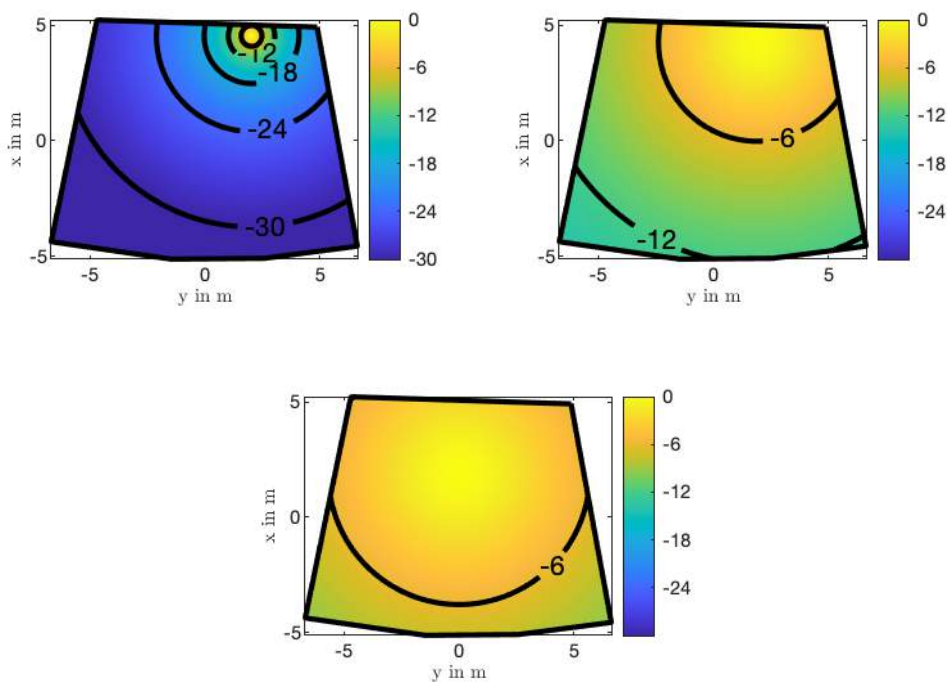


Figure 3: Maps of direct sound pressure level of point-source loudspeakers at the IEM CUBE mounted at different layers: horizontal (upper left), 30° layer (upper right), 60° layer (lower center).

Considering listeners outside the center of a surround setup using point-source loudspeakers, level differences between the loudspeakers become apparent due to different distances between the listening positions and various loudspeakers. Figure 3 compares the direct sound pressure levels on the listening area of ideal point sources at different heights at the IEM CUBE. It is apparent that loudspeakers on the horizontal layer exhibit the greatest level roll-off along the

listening area due to the strongest distance variation between source and receiver. This leads to a position-dependent level balance of instruments and voices positioned on the horizon in different directions.

When using loudspeakers whose direct sound level decays less than 6 dB per doubling of distance, the sweet area of the volume balance for horizontally placed direct sounds is expected to increase. As line arrays facilitate the design of customized direct sound level roll-off by adjusting the splay angles, line sources have to be investigated on the size of the sweet area. For loudspeakers mounted on higher layers, the simulation already shows acceptable coverage, cf. Figure 3. Only slight improvements in coverage are expected when using line-(source) loudspeakers. Therefore, this thesis limits the considerations to loudspeakers mounted along a horizontal ring. The main goal of this thesis is to present a strategy of how surround sound reinforcement systems must be designed to yield a large sweet area in terms of good localization, a well-balanced mix, and a preserved sense of envelopment. A miniature line array with small enclosures is designed for medium-scale sound requirement that is also used to verify the theory in practice. Simulations and listening experiments provide design targets for the direct sound level to enable successful surround sound reinforcement.

1.2 Organization of content

This thesis is structured into three parts that summarize the contributions attached in the appendix. Chapter 2 deals with the mathematical descriptions of Publication I and Publication II that introduce design equations for curving/phasing of linear and planar sources. Chapter 3 summarizes the design procedure for the miniature line array prototype with 3D printed enclosures of Publication III. These loudspeakers were used to verify the mathematical descriptions as well as in the listening experiments that evaluate different distance decay configurations. Chapter 4 discusses new guidelines for the design of surround sound reinforcement systems and provides an overview of the simulation results of Publication V and the results of the listening experiments of Publication VI and Publication VII. Furthermore, the outcomes of Publication VIII are presented that focus on how to use a conventional mixing desk for surround sound reinforcement. Finally, Chapter 5 summarizes the results of this thesis and provides an outlook for further work.

2

Curving and Phasing

One of the key aspects of this thesis is to find design equations for curving and phasing of linear and planar sources to achieve a desired direct sound level decay on the listening area. In practice, discrete line-(source) arrays or recently also planar sources are employed in sound reinforcement systems. In the first step of design, we assume a continuous line or planar source, for which we describe the sound pressure by the one-dimensional/two-dimensional integral of the delayed Green's function $G(r) = \frac{e^{-ik(r+w)}}{4\pi r}$, cf. Publication I and Publication II. i denotes the imaginary unit, k is the wave number, r is the distance between source and receiver, and $w = c\tau$ is the delay τ , expressed as an equivalent delay length, where c is the speed of sound. For a D -dimensional oscillatory integral, the stationary-phase method is applied to yield an approximated value of the integral [3, 4],

$$\int_{\mathbb{R}^D} \frac{e^{-ik(r+w)}}{4\pi r} dx \approx \sum_{x_n} \frac{e^{-ik(r+w)}}{4\pi r} \sqrt{\frac{(2\pi)^D}{k^D |\det\{H(r+w)\}|}} e^{i\frac{\pi}{4} \text{sig}\{H(r+w)\}} \Big|_{x_n}. \quad (1)$$

$H(\cdot)$ is the Hessian, $\det\{\cdot\}$ its determinant and $\text{sig}\{\cdot\}$ its signature. The integral is evaluated at each stationary-phase point x_n and summed over all these stationary-phase points. For each observation point, there is typically a single stationary phase point on the source, which is characterized by a minimum time of flight including the applied delay.

Figure 4 compares the exact description of the integral to the simplification assumed by the stationary-phase approximation. For simplicity, a straight line source without phasing is shown that is expanded along the vertical axis z . The listening area is assumed to lie on the x - y plane $\mathbf{x}_r = [x_r \ y_r \ 0]^T$ and therefore, the stationary-phase point on the source is at $z = 0$ for every receiver in on-axis direction. The binomial approximation is applied to the distance $r = \sqrt{r_0^2 + z^2} \approx r_0 + \frac{z^2}{2r_0}$, which is used to simplify the term in the exponent of the Green's function. For the amplitude term, $r \approx r_0$ is assumed. The main difference between the exact and approximate description lies in points on the source that are further away from

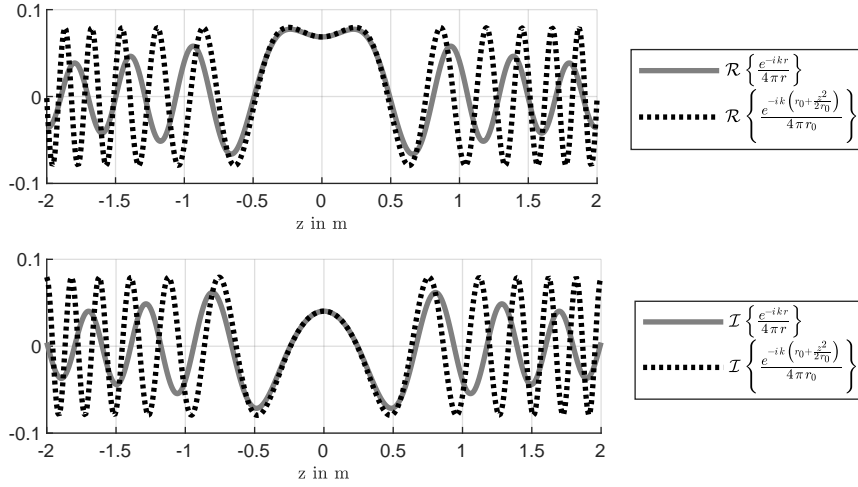


Figure 4: Simplifications for the integral over the Green's function defining the sound pressure level of a line source at $f = 1$ kHz.

the stationary-phase point at $z = 0$, cf. Figure 4. Nevertheless, these points have no stable contributions to the sound pressure anyway, as their parts are likely to cancel. Around the stationary phase point, the approximation is sufficiently accurate, allowing the method to be applied for calculating the sound pressure of linear and planar sources composed of ideal point sources.

The solution is discretized afterwards to make the formalism directly applicable to the design of curving/phasing for discrete line-(source) arrays and the design of the phase load of discrete planar arrays.

2.1 Linear Sources

The purpose of Publication I is to find the curving and/or phasing of a continuous linear source to achieve an equalized direct sound level roll of by $-6 \cdot \beta$ dB per distance doubling on the listening area. This publication introduces a differential equation for a hybrid approach that combines curving and phasing of linear sources,

$$\dot{\vartheta}_T = -\frac{r^{2\beta}}{g^2} \frac{1}{r^2 \cos \vartheta_w} + \frac{\cos \vartheta_w}{r}, \quad \text{with } r = \frac{z}{\sin \vartheta_T}, \quad (2)$$

where ϑ_T is the total inclination split linearly into a geometry part ϑ and a delay part ϑ_w , cf. Figure 5. g is a constant that is responsible for the radius of curvature at the highest point of the source and z is the current z position on the source.

The differential equation corresponds to that from the Wavefront Sculpture Technology literature

[5, 6] after discretization, rewriting of some variables, and omitting electronic beamforming ($\vartheta_w \equiv 0$).

According to the Frenet Serret formulas, that are used to describe arbitrary trajectories in space, the tangent at any point on the curved line source is $\mathbf{t} = [\sin \vartheta \ 0 \ \cos \vartheta]^\top$ and the geometry of the source is calculated by integration along the natural source length parameter,

$$\mathbf{x}(s) = \int_0^S \mathbf{t} ds + \mathbf{x}_0 \quad \mathbf{x}_0 = [0 \ 0 \ z_0] , \quad (3)$$

where z_0 defines the mounting height of the line source. The delay added along the curve acts as a progressive delay and sum beamformer for which we obtain the delay length by integration over the sine,

$$w = - \int_0^S \sin \vartheta_w ds . \quad (4)$$

Figure 5 shows the Frenet Serret trihedron containing the tangent vector \mathbf{t} , the normal vector \mathbf{n} and the bi-orthogonal vector \mathbf{b} . The direction of the stationary phase \mathbf{u} is shown as a vector that points from the stationary-phase point to its corresponding observation point on the listening area with minimum flight time and additional delay $\tau = w/c$ applied.

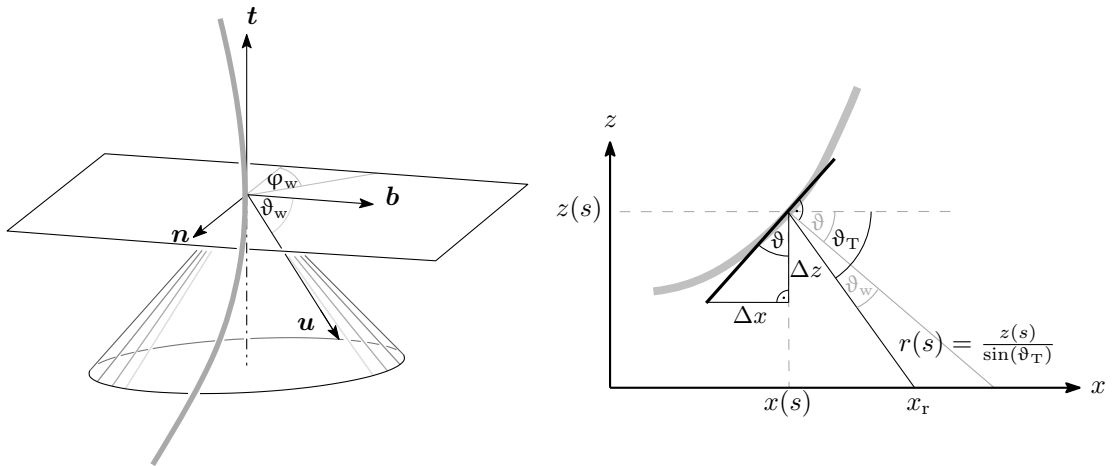


Figure 5: Continuous arc-shaped source (solid grey) with accompanying Frenet trihedron (top) at the point $\mathbf{x}(s) = [x(s) \ 0 \ z(s)]^\top$, showing the steering angle ϑ_w and inclination ϑ , for total inclination ϑ_T and the stationary-phase cone for ϑ_w containing the direction \mathbf{u} of the polar angle φ_w (right: side view), cf. Publication I.

The formalism is directly applicable to the line-array curvature design after discretization, and its effectiveness has been shown by simulations and measurements on a prototype line array in Publication I and also on professional line arrays in Publication IV, cf. Figure 6. The online line

array solver written in Javascript⁴ is intended to solve the differential equation with low effort and to propose tilt angles for a discrete line-(source) array.



Figure 6: Measurement on the miniature line array prototype (left) and measurement on a professional Nexo Geo S12 line array (right).

2.2 Planar Sources

In order to design the direct sound not only along a line that lies in the on-axis direction of the source but also across the width of the audience area, Publication II introduces three design equations for the delay length profile of planar sources,

$$\frac{\partial^2 w}{\partial h^2} = a + \frac{1}{r} \left(\frac{\partial w}{\partial h} \right)^2 \quad \frac{\partial^2 w}{\partial h \partial v} = b + \frac{1}{r} \frac{\partial w}{\partial h} \frac{\partial w}{\partial v} \quad (5)$$

$$\frac{\partial^2 w}{\partial v^2} = \frac{1}{r} \left[\frac{g^{-2} r^{2\beta} + r^2 b^2}{1 + r a} + \left(\frac{\partial w}{\partial v} \right)^2 - 1 \right] \quad (6)$$

$$\text{with } r = \frac{v \cos \eta + z_0}{-\frac{\partial w}{\partial v} \cos \eta + \sin \eta \sqrt{1 - \left(\frac{\partial w}{\partial h} \right)^2 - \left(\frac{\partial w}{\partial v} \right)^2}}. \quad (7)$$

η is the inclination of the planar source, v defines the source length in the vertical direction, i.e. $v \in [0, -V]$ and h the width in the horizontal direction $h \in [-\frac{H}{2}, \frac{H}{2}]$. z_0 is the mounting height of the planar source, i.e. the distance between the highest point of the source and the

⁴<https://enimso.iem.sh/post/line-array-designer-mixed-iterative/>

listening area, which is assumed to lie on the x - y plane. a and b are design parameters that control the horizontal coverage on the listening area. Figure 7 shows the geometry of the planar source with unit vectors $\mathbf{e}_h = [0 \ 1 \ 0]^\top$ and $\mathbf{e}_v = [\sin \eta \ 0 \ \cos \eta]^\top$,

$$\mathbf{x}_s = \mathbf{x}_0 + h \mathbf{e}_h + v \mathbf{e}_v \quad \text{with } \mathbf{x}_0 = [0 \ 0 \ z_0]^\top. \quad (8)$$

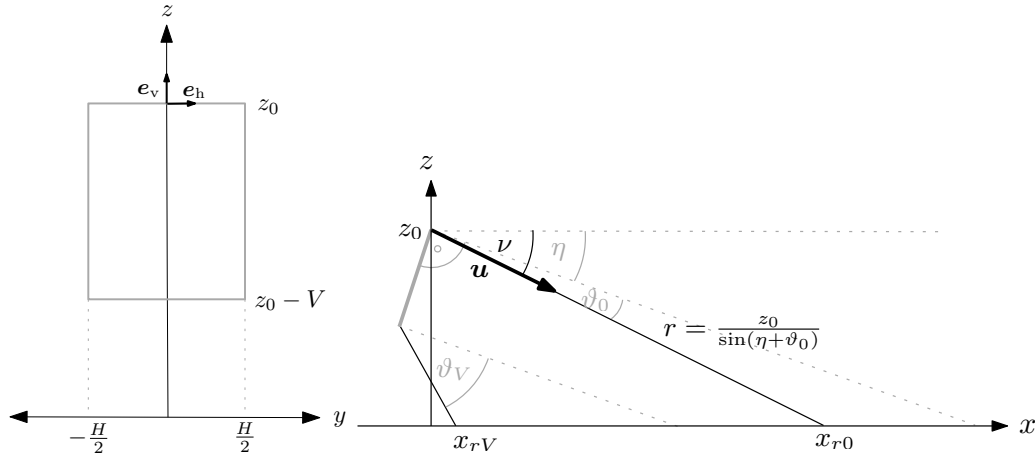


Figure 7: Front view (left) and Side view (right) of a planar source (solid gray) inclined by η showing the stationary-phase direction \mathbf{u} , and the beamforming angles $\vartheta_0 = -\arcsin \left. \frac{\partial w}{\partial v} \right|_{v=0, h=0}$ on top and $\vartheta_V = -\arcsin \left. \frac{\partial w}{\partial v} \right|_{v=-V, h=0}$ on the bottom of the source for a desired depth coverage between x_{r0} and x_{rV} , cf. Publication II.

In addition to simulations and measurements, Publication II also outlines the limits in terms of driver spacing. Although the delay lengths can be reduced by tilting the source, it still seems desirable to use smaller drivers in practice.

It is known from literature, that planar arrays are often considered in the works on Wave Field Synthesis [7, 8, 9, 10]. It is a recent and remarkable development that the company Holoplot⁵ has recently introduced planar arrays for professional sound reinforcement. They use delays and FIR filters to achieve the desired sound level coverage on the audience area.

On their downside, when driving all enclosures individually, planar arrays require an increase in use of hardware resources compared to single point sources, line-(source) arrays with curving or even such with phasing. In order to keep the effort manageable in this doctoral thesis, only line arrays with individually controllable elements are used to investigate the effect of different distance decays on the size of the sweet area.

⁵<https://holoplot.com/>

3

Prototype Design

To evaluate the mathematical descriptions of Publication I and Publication II, a prototype array is required, which is also used for listening experiments considering different direct sound level decays in medium-scale surround sound reinforcement applications. Previous own research presented a 3D printed waveguide prototype with two shells mounted on a compression driver [11, 12], cf. Figure 8. The aim of this prototype is to redirect the waves along paths with different lengths from the driver to a continuously curved outlet. The waveguide has been shown to be well suited for frequencies above 1 kHz and reduces the influence of room reflections due to its more directional radiation compared to point-source loudspeakers.

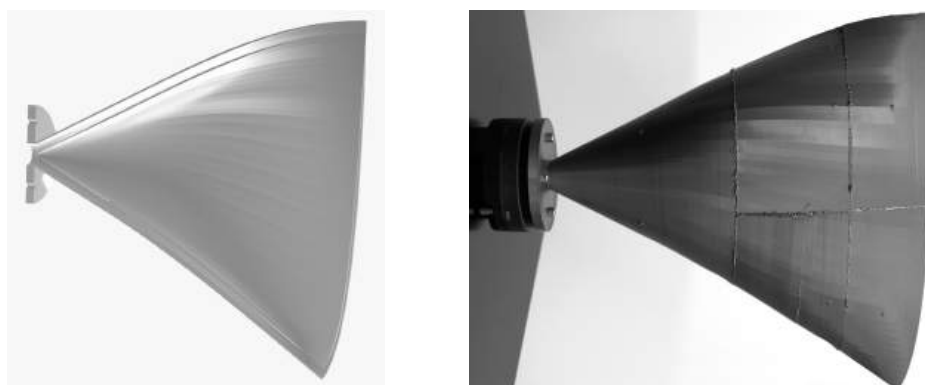


Figure 8: Optimally curved arc source, realized as 3D printed waveguide mounted on a compression driver [11, 12].

Because it is difficult to build such waveguides with a single driver for a broad frequency range, a line array with multiple broadband drivers appears to be a more feasible option, also due to its flexibility to adjust the curvature to the listening area by modifying the tilt angles between the enclosures. For the prototype, 2.5 inch drivers SB acoustics SB65WBAC25-4⁶, known from

⁶<https://sbacoustics.com/product/2-5in-sb65wbac25-4/>

3D-printed spherical 3-9-3 arrays [13], are chosen since they allow to reproduce low frequencies from 115 Hz and perform at higher frequencies with good quality. As with professional line array systems, the shape of an enclosure is chosen to be trapezoidal. The design procedure for these enclosures is described in Publication III in detail. The enclosures are designed in OpenSCAD⁷, a free software for creating 3D computer-aided design (CAD) objects. OpenSCAD is chosen because the design process is based on a human-readable script with simple syntax that is compiled to create stereolithography files (STL) for later use of the 3D printing software. Figure 10 presents the CAD model on the left side.

Templates to adjust the line-array splay angles between 0 degrees and 10 degrees in steps of 1 degree are also designed in OpenSCAD, cf. Figure 10 on the right side. The material used for printing is polylactic acid (PLA) because the material is biodegradable and recyclable as it is made from natural materials. However, the material has low UV and temperature resistance, which limits the arrays to be used indoors only. Figure 11 shows the 3D printer while printing four elements at the same time. A single element requires 22 hours of printing time and 210 g of filament. Figure 9 shows an example of a fully assembled miniature line array with 8 3D printed enclosures.



Figure 9: Fully assembled miniature line array with eight 3D printed enclosures and mounted drivers SB acoustics SB65WBAC25-4

⁷<https://openscad.org/>



Figure 10: CAD model of a single line-array enclosure (left) and CAD model of the template for adjusting the splay angles between the line-array enclosures (right).

Initially, 16 enclosures were printed to install at least one stereo playback system using two line arrays with eight enclosures each. It was planned to conduct listening experiments virtually for which Ambisonic impulse response measurements should be taken at the IEM CUBE considering a setup of eight surround line sources with eight enclosures each.

However, the results of these prototypical arrays were so convincing, that another batch of 48 elements was printed to build a setup for surround sound reinforcement on site and to carry out listening experiments with a full 8-direction surround layout without the need for headphone-based virtual experiments.

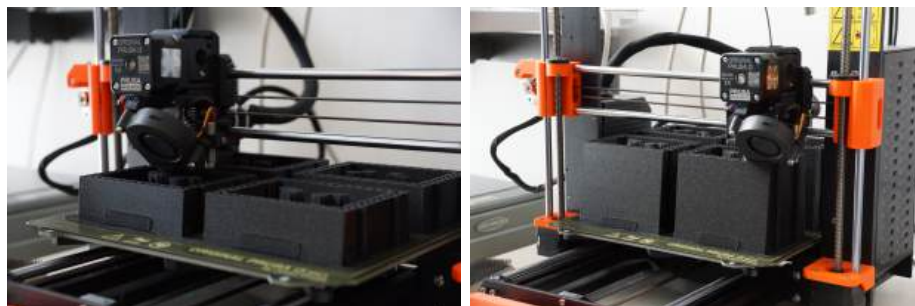


Figure 11: Prusa i3 MK3S printing 4 line-array enclosures.

For amplification, we choose to use innosonics MA32/LP2⁸ amplifiers that meet the requirements of driving all elements individually.

In addition to the design, Publication III shows measurements of coverage and directivity, as well as a filter for direct sound equalization. These line array prototypes are used to evaluate the theory of curved and phased line sources of Publication I. The frequency responses of the line arrays with eight enclosures each, as used in the listening experiments at the IEM CUBE, are presented in Publication V. Furthermore, the enclosures are used to build a prototype planar array and to evaluate its direct sound pressure level on the listening area using different delay profiles in Publication II.

⁸<https://www.innosonix.de/lp2>

4

Successful Surround Sound Reinforcement

Recommendations for surround sound reinforcement setups using line-source arrays have already been published [2, Ch. 2, p. 24ff]. E. Corteel et. al. suggest a direct sound level variation on the listening area of less than 6 dB to guarantee that all direct sound objects are reproduced with nearly the same loudness regardless of the listener position. To achieve a compromise between flat direct sound level and frequency homogeneity over large distances, it is recommended to design the direct sound level rolling off by 1 dB per 10 m.

Other studies have also been carried out by L'Acoustics that investigate the acceptable acoustic delay caused by loudspeakers placed at different distances from the listener [14, 15]. In large-scale surround sound systems, direct sound objects must be placed frontally in order to preserve the temporal structure and rhythmical groove, especially for percussive elements. The scene is then complemented with surrounding effects, such as delay, reverberation, etc.

However, these studies only take direct sounds, level and delay between instruments and voices from different directions into account. In addition, the envelopment, i.e. the sensation of being surrounded by sound [16, 17, 18], contributes to successful surround sound reinforcement. S. Riedel et. al. [19] have shown that the distance decay of ideal line sources (-3 dB per distance doubling) produces an enlarged area of envelopment.

Simulations [11, 12, 19] and listening experiments with simulated line sources [20] indicate that two different design targets for the direct sound level over distance are necessary for successful sound reinforcement: 0 dB per doubling of distance (dod) to preserve the mixing balance, i.e. the volume balance of instruments and voices from different directions, and -3 dB/dod to

preserve the envelopment at off-center listening positions. This chapter summarizes the results of simulations and listening experiments using the miniature line arrays to provide a guideline on how surround sound systems should be designed to achieve acceptable playback with low hardware and software efforts.

4.1 Optimal Design Targets

Preserving the mixing balance at off-center listening positions

F. Zotter et. al. have shown by experiment that a mixing imbalance of ± 3 dB is acceptable for direct sound objects [21]. In this experiment, listeners had to find their preferred level balance between two voices from different directions. Then they had to find an upper and lower limit, for which they found that the level balance is still acceptable.

Applied to a circular setup of radius r using 8 point sources, the sweet area is concentrated to a small area of approximately $1/6 \cdot r$ for which the level difference between the loudest and quietest source remains below 3 dB, cf. Figure 12. This means that only 2.78 % of the area covered by the loudspeaker arrangement falls within the 3 dB limit.

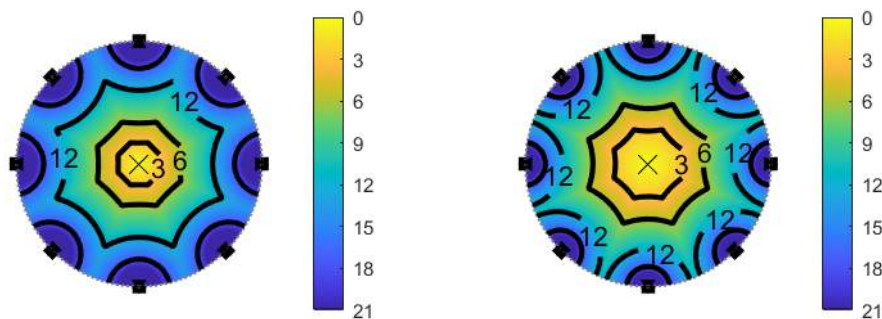


Figure 12: Level difference between loudest and quietest loudspeaker (left) and mixing balance (right) for a circular setup of 8 point sources.

In Publication V, a less strict measure is introduced to predict the sweet area of the mixing balance. Taking the direct sound level of all loudspeakers into account, the mixing balance is determined by the maximum absolute deviation from the median on each position. The 3 dB limit is reached roughly at $2/7 \cdot r$, cf. Figure 12. Under these conditions, only 8.16% of the area covered by the loudspeaker arrangement falls within the 3 dB threshold. Furthermore, even with a more relaxed 6 dB limit, the area (21.34%) still remains very small to ensure a preserved mixing balance across the majority of the listening area.

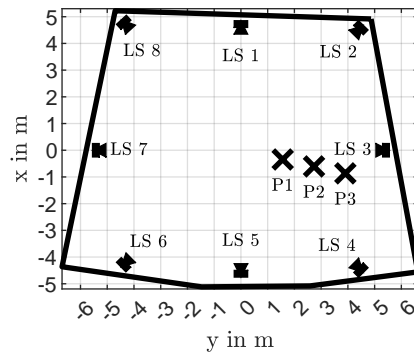


Figure 13: IEM CUBE: Loudspeaker setup and listening positions for listening experiments, cf. Publication VI.

Publication V presents a comparative analysis of sweet area simulations employing different line array distance decay configurations: 0 dB/dod, -3 dB/dod, and -6 dB/dod. This analysis uses the formalism presented in Publication I, which employs a hybrid approach that combines line-array curving and phasing. To make the results comparable to practical applications, it is assumed that eight line arrays with eight enclosures each are mounted in a circular setup at the IEM CUBE, cf. Figure 13. This studio measures 10.3 m by 12 m and has a reverberation time of approximately $T_{30} \approx 0.5$ s. First simulations deal with the localization and are carried out using the extended energy vector model [22, 23] as it has been successfully used to predict the sweet area of an Ambisonic playback system [24, 25],

$$r_E = \frac{\sum_L (w_{\tau,l} \cdot w_{d,l} \cdot g_l)^2 \theta_l}{\sum_L (w_{\tau,l} \cdot w_{d,l} \cdot g_l)^2}. \quad (9)$$

θ_l is a unit vector pointing from the observation point to the l -th loudspeaker of an arrangement consisting of L loudspeakers. $w_{\tau,l}$ is a time weight that incorporates the acoustic time of flight between the source and receiver. For the damping weights $w_{d,l}$ the A-weighted sum of direct sound level simulations of the line arrays is used. g denotes the gain weights resulting from Ambisonic encoding and decoding. The simulated sweet areas show only minor differences between different distance decay settings, cf. Publication V.

Further simulations are performed, using the mixing balance, i.e. the maximum absolute deviation from the median of the direct sound level. Here, the 0 dB/dod configuration yields the largest sweet area for the constant source, followed by the -3 dB/dod configuration, cf. Figure 15.

To verify the results of the simulations in practice, listening experiments were carried out at the IEM CUBE. Listeners had to compare different distance decay configurations at three off-center

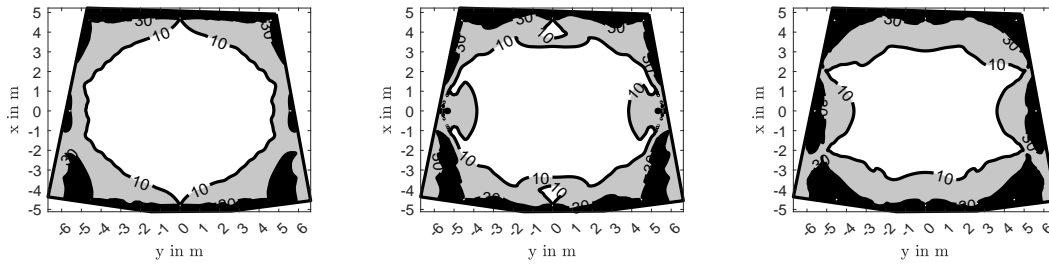


Figure 14: Simulation considering the localization error of three different array configurations, 0 dB/dod, -3 dB/dod and -6 dB/dod for a horizontal ring of eight loudspeakers at the IEM CUBE, cf. Publication V.

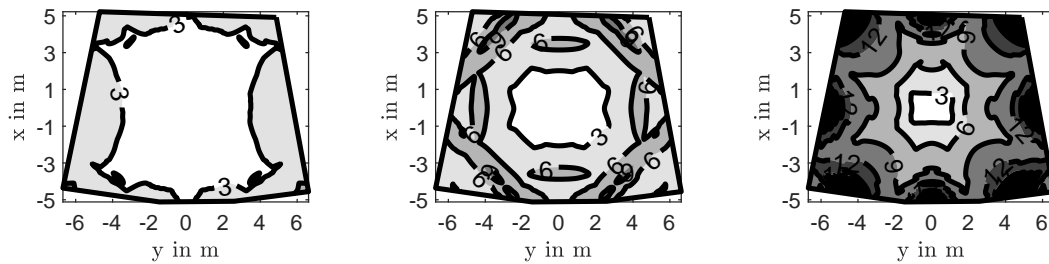


Figure 15: Simulation considering the mixing balance of three different array configurations, 0 dB/dod, -3 dB/dod and -6 dB/dod for a horizontal ring of eight loudspeakers at the IEM CUBE, cf. Publication V.

listening positions. Figure 13 shows the loudspeaker arrangement and the listening positions as used in the experiment. The results of the listening experiment presented in Publication VI show that the 0 dB/dod configuration is rated best, cf. Figure 16. Except at position 1 which is closest to the center of the loudspeaker arrangements, an analysis of the sign rank test with Bonferroni correction indicates significant differences at all positions. The impact effect size [26] denotes large effects at all positions. As an anchor to the scale, a configuration with -6 dB/dod and the center loudspeaker additionally attenuated by 9 dB was introduced. (Despite not targeted as a matter on its own in the experiment: Its low ratings could be used to underline the importance of a working center loudspeaker).

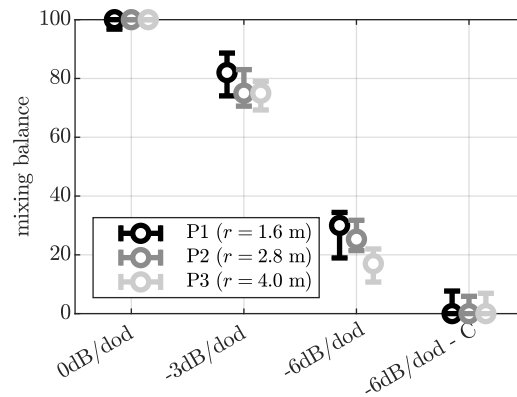


Figure 16: Listening experiment considering mixing balance: Median values and 95% confidence intervals of pooled results, cf. Publication VI.

Preserving the envelopment at off-center listening positions

For simulating the sweet area of envelopment, we assume that fully decorrelated signals are played back by the horizontal ring of 8 loudspeakers. As in Publication IV, these calculations are based on the energy vector of Equation 9. The diffuseness is calculated using the norm of the energy vector, $\psi = 1 - \|\mathbf{r}_E\|$. Figure 17 shows the sweet area for a point-source setup consisting of 8 loudspeakers in a horizontal ring. The diffuseness has to stay above 0.8 for acceptable playback. This limit is reached at $0.36 \cdot r$ which implies that only 12.96 % of the area that is spanned by the loudspeaker arrangement falls into the range of $\psi > 0.8$. Furthermore, Figure 17 shows that the perceived direction is dominated by the closest loudspeaker, whose contribution gets dominant at far off-center listening positions. Therefore, a setup consisting of surrounding point sources neither preserves the envelopment, cf. Figure 17, nor the mixing balance, cf. Figure 12, at off-center listening positions.

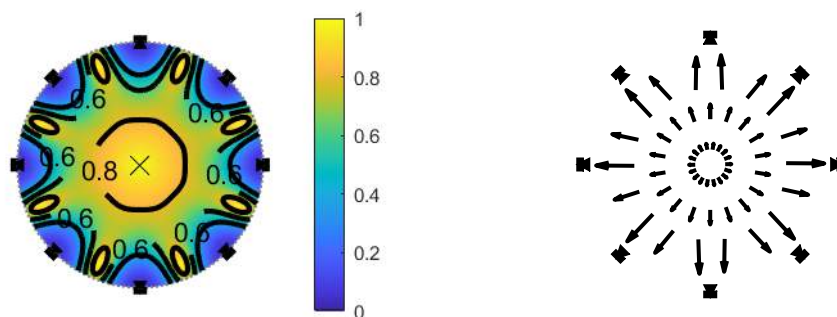


Figure 17: Diffuseness $1 - \|\mathbf{r}_E\|$ (left) and energy vectors (right) for a circular ring of 8 point sources.

By contrast, Figure 18 shows the diffuseness and the energy vectors for a setup of ideal constant sources whose sound pressure is independent of the distance $p(r) = \text{const.}$. The radius for which the diffuseness stays above 0.8 increases slightly to $\frac{2}{5} \cdot r$. However, considering the directions of the energy vectors, it is noticeable that they point inwards in Figure 18 (right), while they are point outwards in Figure 17. When moving out of the center now, the opposite side dominates the perceived direction. This can be explained by the distant loudspeaker outnumber the closer ones. For instance, in a ring of 8 loudspeakers, laterally moving right off-center can cause that 5 of the 8 loudspeakers are rather left, while 3 of them are rather on the right. If levels are all the same and signals uncorrelated, 5 on the left win over 3 on the right, in number and level.

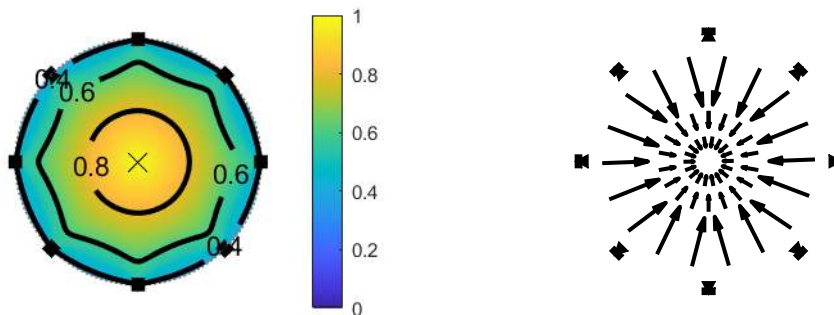


Figure 18: Diffuseness $1 - \|\mathbf{r}_E\|$ (left) and energy vectors (right) for a circular ring of 8 ideal constant sources.

Publication V compares the sweet area of envelopment using different line-array distance decay configurations at the IEM CUBE. Listeners had to rate the envelopment, i.e. the feeling of being surrounded by sound, of different line-array configurations. The largest area is denoted for the -3 dB/dod ($\beta = 0.5$) configuration, cf. Figure 19.

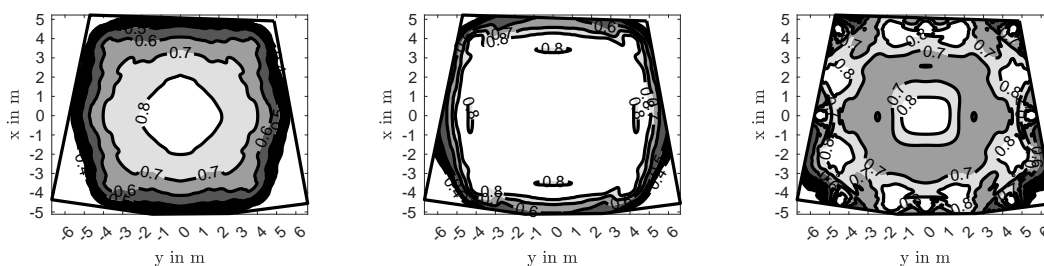


Figure 19: Simulation considering the envelopment of three different array configurations, 0 dB/dod , -3 dB/dod and -6 dB/dod for a horizontal ring of eight loudspeakers at the IEM CUBE, cf. Publication V.

To verify the findings in practice, a listening experiment was carried out, cf. Publication VI. The results confirm the -3 dB/dod configuration as best in terms of envelopment, cf. Figure 20.

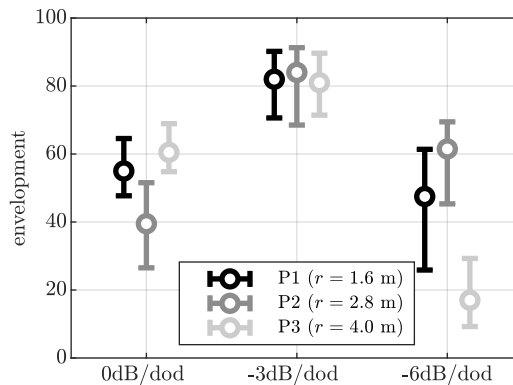


Figure 20: Listening experiment considering the envelopment: Median values and 95% confidence intervals of pooled results, cf. Publication VI.

4.2 Dual-target vs. Single-target Design

The results of the listening experiment in Publication VI show that two targets would be necessary for successful surround sound reinforcement that separately treat the direct sounds and the enveloping parts of a scene. For a setup of eight line arrays of eight elements each, a mixing desk with two eight-channel buses is necessary to render both parts separately. To avoid the need for a dual line-array setup with individual curving, a processor is mandatory, which distributes the signals to the array elements correspondingly. This processor implements the idea of a dual-target design applying the hybrid approach of combined curving and phasing, as described in Publication I and verified in Publication IV for professional line-source arrays. The processor must add precise sample-wise delays to each channel of the envelopment bus to achieve -3 dB/dod , assuming that the line-array curvature is designed for 0 dB/dod . Furthermore, 64 individual controllable amplifiers are necessary to drive each array element individually. The block diagram for such a system is shown in Figure 21. For audio productions, this would also mean that the direct sound objects have to be routed separately from the enveloping parts to enable separate playback.

However, the listening experiment in Publication VI only investigates isolated scenarios, where either direct sound or envelopment is considered separately. Publication VII investigates a more realistic scenario, in which direct sounds are complemented with enveloping effects, such as reverberation. In our setup at the IEM CUBE, the number of necessary amplifiers is reduced to

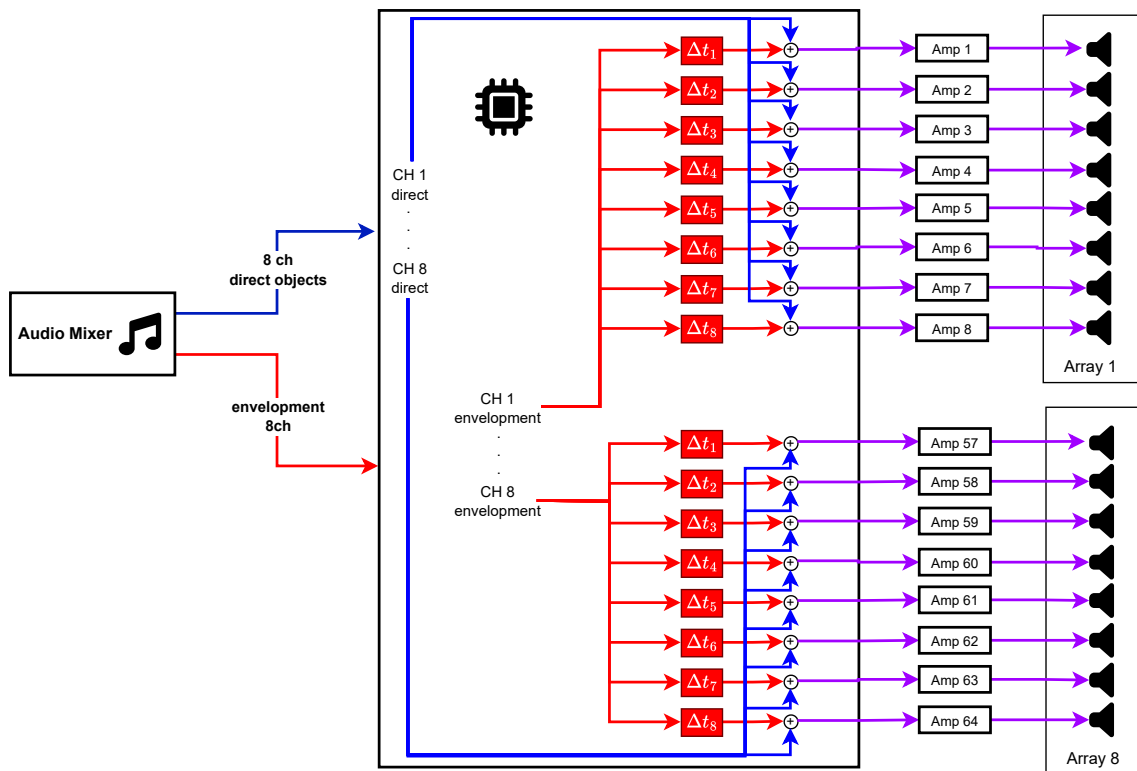


Figure 21: Block diagram of a processor for surround sound reinforcement using 8 line arrays with 8 enclosures each, implementing the dual-target design.

8, if a single-target design between 0 dB/dod and -3 dB/dod could be sufficient. Moreover, a single-target design omits the need for a second bus and the procedure of adding delays to the array elements. Assuming that the mixing desk is able to perform spatialization, the entire processor could be omitted, saving hardware and software efforts.

Correspondingly, the listening experiment described in Publication VII compares the dual-target design with different single-target designs for a live sound reinforcement scenario with direct sounds placed frontally. Two configurations were tested; the first denotes a wide mix where direct sounds are distributed around $\varphi = \pm 90^\circ$, the second represents a scenario with a stage in the front where direct sounds are distributed around $\varphi = \pm 45^\circ$. These direct sound objects are complemented with surrounding reverberation. The same loudspeaker arrangement and the same positions as in Publication VI are used to make the results comparable to the first experiment. Listeners had to rate the similarity between the conditions of 0, -1.5 and -3 dB/dod and the dual-target design that renders direct sound objects with 0 dB/dod and enveloping ones with -3 dB/dod. This reference was also hidden in the configurations to be rated.

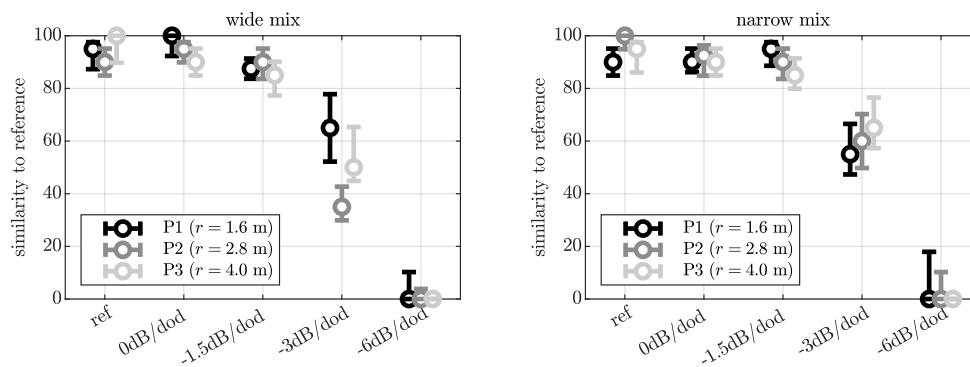


Figure 22: Listening experiment: Median values and 95% confidence intervals of pooled results for a wide mix (left) and a narrow mix (right) of the direct sounds, cf. Publication VII.

The results in Figure 22 show that the expert listeners could not always distinguish between the reference and the single-target configurations 0 dB/dod and -1.5 dB/dod. Considering the impact effect size, it is noticeable that small effects are denoted for pairwise comparisons between the reference and the 0 dB/dod configurations as well as between the reference and the -1.5 dB/dod configuration. This leads to the conclusion that, in a conventional live concert scenario in which isolated envelopment is not predominant, a preserved mixing balance is more important to listeners than a preserved envelopment. Therefore, distance decays between 0 dB/dod and -1.5 dB/dod are recommended. More relaxed distance decays than 0 dB/dod should be preferred, because their frequency response is less distance dependent⁹. In addition, the surrounding line sources can also be designed to reach a level decay of -3 dB/dod as they are mainly responsible for the envelopment.

This listening experiment deals with a conventional concert scenario with frontally placed direct sounds. It is important to note that there are concerts or installations in which enveloping sounds are used primarily. For these, a consistent setting of -3 dB/dod is clearly preferred.

4.3 Spatialization Techniques for Live Surround Sound Reinforcement

L'Acoustics L-ISA¹⁰, d&b Soundscape¹¹ or Adamson Fletcher Machine¹² are well-known processors that are employed in spatial sound reinforcement systems. What they all have in common is that they receive the multi-channel signals from a conventional mixing console via a digital interface, such as MADI/DANTE/AVB MILAN, distribute them to a loudspeaker array

⁹close to the line array, there is too much bass, far away the high-frequency end is over-emphasized

¹⁰<https://l-isa.l-acoustics.com/>

¹¹<https://www.dbsoundscape.com/global/en/>

¹²<https://adamson-fletcher-machine.com/>

using amplitude-based and/or delay-based algorithms, and complement them with reverberation. Another approach for spatialization is to use a PC or Laptop in combination with a Digital Audio Workstation (DAW), for example, REAPER¹³, and VST-Plugins for spazialisation, such as the IEM plugins¹⁴. The signals for the loudspeakers are then sent to the mixing desk, which distributes them to the corresponding loudspeakers. To effectively minimize latency in live sound reinforcement systems, it is essential that the buffer size remains sufficiently small. This requirement frequently results in increased computational demands that may compromise the stability of the system.

As a way to circumvent both a processor and PC/DAW processing, MCPyPan3D (mixing console's python-based panning tool for 3D audio at live events) was devised here to rely solely on the mixing console for the purpose of signal processing and signal distribution, cf. Publication VIII. For each audio source, a python-based script calculates the loudspeaker gains based on Ambisonic panning. The sound engineer controls determines the positions of the objects in a graphical interface, and MCPyPan3D updates the (positive-valued) channel gains to the auxiliary channels of the mixing desk through a network connect. On the Allen & Heath SQ-5, as an exemplary mixing desk, stereo auxiliary channles have to be used to increase the number of loudspeakers from 12 (when using mono buses) to 24. Publication VIII shows that these adjustments result only in negligible variations in the mean localization error. In terms of reverberation, conventional mixing consoles are restricted to rendering stereo effects. In a typical live sound reinforcement setup featuring direct sound sources positioned at the front, it has been demonstrated in Publication VIII that left-right panning of stereo reverberation, spatialized using first-order Ambisonics, yields acceptable results.

¹³<https://www.reaper.fm/>

¹⁴<https://plugins.iem.at/>

5

Concluding Remarks

This thesis proposed differential equations for designing the curving and phasing of continuous line sources with the goal of achieving an adjustable direct sound pressure decay over distance. In addition to defining a curvature without delay, the formalism is also able to propose delays for electronic beamforming (phasing) for either no curving or to facilitate an alternative sound pressure decay with distance. The approach is extended to planar arrays to control the sound also across the width of the audience area with tow-dimensional phasing. For both techniques, simulations and measurements show the applicability in practice.

A 3D printed prototype of a miniature line array is designed and presented as an open design in Publication III and Chapter 3. The practical feasibility is presented in Publication I and Publication III.

These miniature line arrays are used for the simulations in Publication V, where the hybrid approach of curving and phasing of Publication I is realized. Based on these results, a listening experiment is conducted. The results show that a dual-target design of the direct sound should be ideally pursued, cf. Publication VI: 0 dB/dod to preserve the mixing balance of direct sounds and -3 dB/dod to preserve envelopment of diffuse sounds at off-center listening positions. Another experiment focuses on a live sound reinforcement scenario in which direct frontal sounds are complemented with surround reverberation, cf. Publication VII. The results show that single-target designs achieve acceptable playback, even at off-center listening positions. The results also demonstrate that the -1.5 dB/dod configuration achieves sufficiently acceptable playback for the most common cases. More relaxed level decays than 0 dB/dod are preferable, as they perform better in terms of a more consistent frequency response over distance. Furthermore, Publication VIII introduces an approach to use a conventional mixing desk for surround sound reinforcement without the need for a any processor that is more expensive but conventionally employed in such systems.

Further work should focus on the evaluation of the sweet-area size considering mixing balance and envelopment in larger systems using professional line-(source) arrays. On the other hand, planar arrays should be investigated further to find out whether additional optimization can be achieved when the direct sound can also be controlled in width. The formalism of Publication II should be compared with professional systems and their algorithms. Another aspect to be considered is the individual filter design for each array element of line and planar sources to further improve the coverage of the listening area.

References

- [1] W. Ahnert and D. Noy, *Sound Reinforcement for Audio Engineers*. Taylor & Francis Ltd, 2023.
- [2] J. Patterson and H. Lee, Eds., *3D Audio*, 1st ed., ser. Perspective on Music Production. United States: Routledge, Jul. 2021.
- [3] E. Skudrzyk, *The Foundations of Acoustics: Basic Mathematics and Basic Acoustics*. Springer-Verlag, 1971.
- [4] J. McClure and R. Wong, "Multidimensional stationary phase approximation: boundary stationary point," *Journal of Computational and Applied Mathematics*, vol. 30, no. 2, pp. 213–225, 1990. [Online]. Available: <https://www.sciencedirect.com/science/article/pii/037704279090029Y>
- [5] C. Heil and M. Urban, "Sound fields radiated by multiple sound sources arrays," in *Audio Engineering Society Convention 92*, Mar 1992. [Online]. Available: <http://www.aes.org/e-lib/browse.cfm?elib=6864>
- [6] M. Urban, C. Heil, and P. Bauman, "Wavefront sculpture technology," *J. Audio Eng. Soc.*, vol. 51, no. 10, pp. 912–932, 2003. [Online]. Available: <http://www.aes.org/e-lib/browse.cfm?elib=12200>
- [7] J. Ahrens, R. Rabenstein, and S. Spors, "The theory of wave field synthesis revisited," in *Audio Engineering Society Convention 124*, May 2008. [Online]. Available: <https://www.aes.org/e-lib/browse.cfm?elib=14488>
- [8] G. Firtha, "A generalized wave field synthesis framework with application for moving virtual sources," Ph.D. dissertation, Budapest University of Technology and Economics, 2019.
- [9] J. Ahrens and S. Spors, "Reproduction of a plane-wave sound field using planar and linear arrays of loudspeakers," in *2008 3rd International Symposium on Communications, Control and Signal Processing*, 2008, pp. 1486–1491.
- [10] ———, "Sound field reproduction using planar and linear arrays of loudspeakers," *IEEE Transactions on Audio, Speech, and Language Processing*, vol. 18, no. 8, pp. 2038–2050, 2010.

- [11] L. Gölles, “Optimally Curved Arc Source For Sound Reinforcement,” Master’s thesis, University of Music and Performing Arts Graz, Austria, 2021.
- [12] L. Gölles and F. Zotter, “Optimally curved arc source for sound reinforcement,” in *Fortschritte der Akustik (DAGA)*, Vienna, 08 2021.
- [13] S. Riedel and F. Zotter, “Design, control, and evaluation of mixed-order, compact spherical loudspeaker arrays,” *Computer Music Journal*, vol. 44, pp. 60–76, 12 2021.
- [14] T. Mouterde, N. Epain, S. Moulin, and E. Corteel, “On the perception of musical groove in large-scale events with immersive sound,” in *Audio Engineering Society Conference: AES 2023 International Conference on Spatial and Immersive Audio*, Aug 2023. [Online]. Available: <http://www.aes.org/e-lib/browse.cfm?elib=22201>
- [15] —, “On the factors influencing groove fidelity in immersive live music events,” in *Audio Engineering Society Conference: AES 2024 International Acoustics & Sound Reinforcement Conference*, Jan 2024. [Online]. Available: <http://www.aes.org/e-lib/browse.cfm?elib=22367>
- [16] F. Rumsey and J. Berg, “Verification and correlation of attributes used for describing the spatial quality of reproduced sound,” in *Proceedings of the AES 19th International Conference: Surround Sound - Techniques, Technology, and Perception*, vol. Paper Number 1932. Audio Engineering Society, Inc., 2001. [Online]. Available: <https://urn.kb.se/resolve?urn=urn:nbn:se:ltu:diva-27892>
- [17] R. Sazdov, G. Paine, and K. Stevens, “Perceptual investigation into envelopement, spatial clarity, and engulfment in reproduced multi-channel audio,” in *31st AES International Conference: New Directions in High Resolution Audio*. Audio Engineering Society, 2007.
- [18] G. S. Kendall, “Spatial perception and cognition in multichannel audio for electroacoustic music,” *Organised Sound*, vol. 15, no. 3, p. 228–238, 2010.
- [19] S. Riedel and F. Zotter, “Surrounding line sources optimally reproduce diffuse envelopment at off-center listening positions,” *JASA Express Letters*, vol. 2, no. 9, p. 094404, 2022.
- [20] P. Heidegger, B. Brands, L. Langgartner, and M. Frank, “Sweet area using ambisonics with simulated line arrays,” in *Fortschritte der Akustik, DAGA*, Wien, 08 2021.
- [21] F. Zotter, S. Riedel, L. Gölles, and M. Frank, “Acceptable imbalance of sound-object levels for off-center listeners in immersive sound reinforcement,” in *Fortschritte der Akustik, DAGA*, S. Lippert and O. von Estorff, Eds., Hamburg (Deutschland), 03 2023.
- [22] M. A. Gerzon, “General metatheory of auditory localisation,” in *Audio Engineering Society Convention 92*. Audio Engineering Society, 03 1992.

- [23] P. Stitt, S. Bertet, and M. van Walstijn, "Extended energy vector prediction of ambisonically reproduced image direction at off-center listening positions," *J. Audio Eng. Soc.*, vol. 64, no. 5, pp. 299–310, 2016.
- [24] M. Frank, "Localization using different amplitude-panning methods in the frontal horizontal plane," in *Proceedings of the EAA Joint Symposium on Auralization and Ambisonics*, 01 2014.
- [25] E. Kurz and M. Frank, "Prediction of the listening area based on the energy vector," in *International Conference on Spatial Audio*, 09 2017.
- [26] J. Lötsch and A. Ultsch, "A non-parametric effect-size measure capturing changes in central tendency and data distribution shape," *PLoS ONE*, vol. 15, 09 2020.

Publication I

This work was published as:

Lukas Gölles, and Franz Zotter, „Theory of continuously curved and phased line sources for sound reinforcement,“ *Acta Acust.*, vol. 7, p. 52, 2023. [Online].

Available: <https://doi.org/10.1051/aacus/2023045>

Acta Acustica 2023, 7, 52
© The Author(s), Published by EDP Sciences, 2023
<https://doi.org/10.1051/aacus/2023045>



Available online at:
<https://acta-acustica.edpsciences.org>

SCIENTIFIC ARTICLE

OPEN ACCESS

Theory of continuously curved and phased line sources for sound reinforcement

Lukas Göllles* and Franz Zotter

Institute of Electronic Music and Acoustics, University of Music and Performing Arts Graz, 8010 Graz, Austria

Received 24 April 2023, Accepted 6 September 2023

Abstract – To supply large audience areas uniformly with amplified direct sound, large-scale sound reinforcement often employs line-source loudspeaker arrays adapted to the listening area by either adjusting the angles or delays between their individual elements. This paper proposes a model for such or smaller line-source loudspeakers based on a delayed Green's function integrated over an unknown contour. For a broad frequency range, stationary phase approximation yields a differential equation that we utilize to find a curve and delay progression providing direct sound levels rolling off with -6β dB per doubling of the distance; curve and phase designs can also be mixed to meet simultaneous targets using multiple design parameters β . The effectiveness of the formalism is proven by simulations of coverage, directivity, and discretization artifacts. Measurements on a miniature line array prototype that targets medium-scale immersive sound reinforcement applications verify the proposed theory for curvature, delay, and mixed designs.

Keywords: Line source loudspeaker arrays, Sound reinforcement, Stationary phase approximation, Delay beamforming, Curvilinear arrays

1 Introduction

One of the big challenges for sound reinforcement is to provide high-quality sound for the largest parts of a predefined audience area [1]. High-quality, high-power supply of large audience areas with consistently reinforced sound pressure levels has been considering line-source loudspeaker arrays driven by identical signals for several decades, nowadays. The wavefront sculpture technology (WST [2, 3]) as contemporary line-source theory is based on adjusting the length of the most relevant, binary Fresnel zone for all distances from the stage. Despite the simplicity of its model and a handful of criteria it needs, it provides a powerful and practical theory for line-source loudspeaker arrays. Furthermore, Straube et al. [4, 5], Hölter et al. [6] and Thompson et al. [7–9] discuss the modeling and optimization of the line-source array curvature to obtain tilt angles between the discrete elements, adapted to the listening area. Line-source arrays could also be applied in surround sound applications, and for instance Toole [10] of p. 330 describes the application of line sources compared to point-source loudspeaker setups.

As an alternative way to obtain a desired sound level curve over the listening area, beamforming based on constrained least square optimization was suggested by Beuningen et al. [11]. Beamformers can be found in

applications with microphone arrays [12] and with loudspeaker arrays [13–15], and they require individual delays and amplification per transducer, often also filtering.

Moreover, delay and sum beamformers, or phased arrays as they are called when used for narrow-band signals, are also found in antenna theory, radar applications, or optics [16–18]. For a linear antenna array, Shanks [19] applied the stationary phase approximation to determine from the array's radiation integral the phase and amplitude function required to form a cosecant-squared beam. Chiang et al. [20] used the same approximation method to estimate the beam-patterns of in-phase curvilinear arrays, and Chakraborty et al. [21] applied the approximation to a linear array, obtained and solved a first-order differential equation, e.g., to form a cosecant beam. The cosecant beam is equivalent to a 0 dB attenuation target per doubling of the distance, when employing a vertical array below/above a horizontal plane.

Stationary-phase approximation has not only proven to be a powerful tool in antenna beamforming, but it is also used in wave field synthesis [22–24] and yields relatively simple signal processing (gains, delays, common pre-filter). What is more, Schultz [25] suggested the Fourier transform and wave field synthesis as theoretical background for line-source loudspeaker arrays.

In cinema sound practice, SMPTE RP 2096-1 [26] defines a rectangular area of roughly a third of the radius ($\pm 1/5$ times the width by $\pm 1/6$ times the depth of a hall),

*Corresponding author: goelles@iem.at

This is an Open Access article distributed under the terms of the Creative Commons Attribution License (<https://creativecommons.org/licenses/by/4.0/>), which permits unrestricted use, distribution, and reproduction in any medium, provided the original work is properly cited.

in which the loudspeaker sound level should be flat within ± 3 dB. This confines the maximum mixing imbalance of directional sounds to 6 dB in this area and is still soft enough to accept the mixing imbalance at off-center listening positions accomplished by two ideal point source loudspeakers in the free field, at opposite sides. Providing for a more constant coverage with distance, Nettingsmeier et al. [27] demonstrated an enlarged listening area (sweet area), when using eight short line-source arrays for third-order ambisonic surround play-back. Gölles et al. [28] showed that curved line sources designed for a direct-sound coverage of 0 dB attenuation per doubling of the distance potentially improves directional localization in a large listening area, above a length-dependent frequency limit. For less perfect coverage targets, Zotter et al. [29] found that direct sound objects rendered with -1 dB roll-off per doubling of the distance may limit the mixing imbalances acceptably (≤ 3 dB) within 75% of the loudspeaker layout's radius. For a large listening area preserving the envelopment of a diffuse sound scene, by contrast, a substantially different optimal coverage criterion was found by Riedel et al. [30, 31], requiring that horizontally surrounding loudspeakers should exhibit a -3 dB attenuation per doubling of the distance for optimal results.

We propose an extended theoretical basis for the design of line-source curving and phasing. Its result is broadband for line sources that are (i) sufficiently tall, cf. equation (A.1), and (ii) densely spaced, cf. equation (A.2), or waveguided. The target is to support desired sound-pressure roll-off profiles of -6β dB per doubling of distance based on either curvature or delay, or both, and potentially multiple of such profiles, simultaneously, with the design parameter β . The proposed theory employs a stationary-phase-approximated contour integral over delayed Green's functions and yields a second-order nonlinear differential equation. We propose two algorithms to numerically find optimal geometry and delay curves, followed by simulation studies and measurements on a miniature line array prototype as a proof of concept.

2 Continuous curvature and phase

We evaluate the sound pressure p of a curved source fed by a progressive time delay τ given as length $w = c\tau$ by an integral of a Green's function $G(r) = \frac{e^{-ik(r+w)}}{4\pi r}$ over the natural length parameter s of the unknown source contour C ,

$$p = \int_{s \in C} \frac{e^{-ik(r+w)}}{4\pi r} ds. \quad (1)$$

The imaginary unit i yields $i^2 = -1$, the wave number is $k = \frac{2\pi f}{c}$, the speed of sound is $c = 343$ m/s, and f is the regarded frequency.

2.1 Integrals defining contour and delay

We define the convex curve $\mathbf{x}(s) = [x(s) \ 0 \ z(s)]^T$ as parametric curve depending on the inclination angle $\vartheta(s)$ at every length coordinate s on the source, cf. Figure 1,

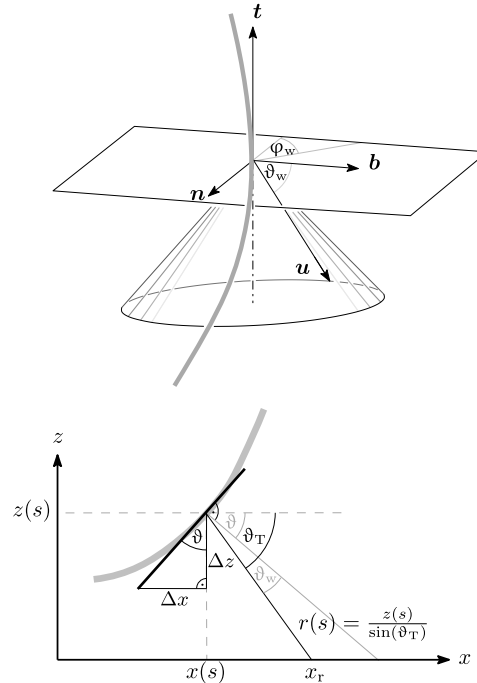


Figure 1. Continuous arc-shaped source (solid grey) with accompanying Frenet trihedron (top) at the point $\mathbf{x}(s) = [x(s) \ 0 \ z(s)]^T$, showing the steering angle ϑ_w and inclination ϑ ; see Sections 2.2–2.4 for total inclination ϑ_T and the stationary-phase cone for ϑ_w containing the direction \mathbf{u} of the polar angle φ_w (bottom: side view).

$$\mathbf{x} = \int_0^s \mathbf{t} ds + \mathbf{x}_0, \quad \mathbf{t} = [\sin \vartheta \ 0 \ \cos \vartheta]^T, \quad (2)$$

and the distance to a receiver at $\mathbf{x}_r = [x_r \ y_r \ 0]^T$ is

$$r = \|\mathbf{x} - \mathbf{x}_r\| = \sqrt{(\mathbf{x} - \mathbf{x}_r)^T (\mathbf{x} - \mathbf{x}_r)}. \quad (3)$$

Moreover, w shall integrate the sine of a local delay-and-sum steering angle ϑ_w measured down from the normal plane of \mathbf{t} , hence with negative sign, cf. Figure 1,

$$w = - \int_0^s \sin \vartheta_w ds. \quad (4)$$

The Frenet–Serret formulas describe $\dot{\mathbf{x}}$ as tangential vector $\mathbf{t} = \dot{\mathbf{x}}$, and $\ddot{\mathbf{x}} = \kappa \mathbf{n}$ as normal vector \mathbf{n} scaled by curvature $\kappa = \dot{\vartheta}$, in our case $\mathbf{n} = [\cos \vartheta \ 0 \ -\sin \vartheta]^T$, and a bi-orthogonal vector $\mathbf{b} = \mathbf{t} \times \mathbf{n} = [0 \ 1 \ 0]^T$, so that $\|\mathbf{t}\| = \|\mathbf{n}\| = \|\mathbf{b}\| = 1$ and $\mathbf{t} \perp \mathbf{n} \perp \mathbf{b}$, cf. equation (2) and Figure 1.

2.2 Stationary-phase approximation

At high frequencies, the integrand of equation (1) oscillates rapidly. Therefore stationary phase approximation is

appropriate, which evaluates the integrand's stationary-phase points $\dot{r} + \dot{w} = 0$; with derivatives abbreviated as $\frac{da}{ds} = \dot{a}$, $\frac{d^2a}{ds^2} = \ddot{a}$. In typical designs, there should only be a single stationary-phase point of minimum delay $(r + w)/c$ to the receiver and therefore the pressure is approximated by,

$$p \approx \frac{e^{-ik(r+w) - i\frac{\pi}{4}}}{\sqrt{8\pi k}} \frac{1}{\sqrt{r^2(\dot{r} + \dot{w})}}, \quad \text{at } \dot{r} = -\dot{w}. \quad (5)$$

2.3 Target coverage

Our goal is to find the curvature and delay length w at each position s on the source such that the sound pressure

$$|p| \propto r^{-\beta} \quad (6)$$

decays by -6β dB per doubling of distance on the listening plane that lies at $z_r = 0$. For an equalized magnitude square, we allow a gain g and desire

$$8\pi k |p|^2 = \frac{1}{r^2(\dot{r} + \dot{w})} = \left(\frac{g}{r^\beta}\right)^2, \quad \text{at } \dot{r} = -\dot{w}. \quad (7)$$

2.4 Stationary-phase direction

We derive $\frac{r^2}{2}$ with regard to s to describe stationary-phase directions $\dot{r} = -\dot{w}$ pointing from the corresponding point on the array emitting the first wave front received to the receiver on the listening plane at $z_r = 0$,

$$\frac{dr^2}{2ds} = r\dot{r} = (\mathbf{x} - \mathbf{x}_r)^T \dot{\mathbf{x}}, \quad \Rightarrow \dot{r} = \frac{(\mathbf{x} - \mathbf{x}_r)^T}{r} \mathbf{t}. \quad (8)$$

We use $\dot{w} = -\sin \vartheta_w$, introduce a unit-length vector $\mathbf{u} = -\frac{\mathbf{x} - \mathbf{x}_r}{r}$ to stationary-phase receivers $\mathbf{x}_r = \mathbf{x} + r\mathbf{u}$ requiring $-\dot{r} = \dot{w}$, so $\mathbf{u}^T \mathbf{t} = -\sin \vartheta_w$, and these stationary-phase receivers lie on a cone of local stationary-phase directions, cf. [Figure 1](#),

$$\begin{aligned} \mathbf{u} &= -\mathbf{t} \sin \vartheta_w + \mathbf{n} \cos \vartheta_w \cos \varphi_w + \mathbf{b} \cos \vartheta_w \sin \varphi_w \\ &= \begin{bmatrix} -\sin \vartheta \sin \vartheta_w + \cos \vartheta \cos \vartheta_w \cos \varphi_w \\ \cos \vartheta \sin \vartheta_w \sin \varphi_w \\ -\cos \vartheta \sin \vartheta_w - \sin \vartheta \cos \vartheta_w \cos \varphi_w \end{bmatrix}. \end{aligned} \quad (9)$$

Below, we design the x -axis sound pressure contour at $y_r = 0$ for receivers at $z_r = 0$, simplifying the direction \mathbf{u} with $\varphi_w = 0$ to

$$\mathbf{u}|_{\varphi_w=0} = \begin{bmatrix} \cos(\vartheta + \vartheta_w) \\ 0 \\ \sin(\vartheta + \vartheta_w) \end{bmatrix}, \quad (10)$$

where the total inclination is gathered as $\vartheta_T = \vartheta + \vartheta_w$.

2.5 Stationary-phase magnitude

We derive $\frac{r^2}{2}$ once more from equation (8) to describe $r\ddot{r}$,

$$\frac{d}{ds} \left(\frac{dr^2}{2ds} \right) = \dot{r}^2 + r\ddot{r} = \dot{\mathbf{x}}^T \dot{\mathbf{x}} + (\mathbf{x} - \mathbf{x}_r)^T \ddot{\mathbf{x}}, \quad (11)$$

and with $\dot{r}^2 = \dot{w}^2 = \sin^2 \vartheta_w$, $\sin^2 \vartheta_w = 1 - \cos^2 \vartheta_w$, $\dot{\mathbf{x}} = \mathbf{t}$, $\|\mathbf{t}\| = 1$, $\mathbf{x} - \mathbf{x}_r = -r\mathbf{u}$, $\ddot{\mathbf{x}} = \dot{\vartheta}_w \mathbf{n}$, $\mathbf{t} \perp \mathbf{n} \perp \mathbf{b}$, as well as $\dot{w} = -\dot{\vartheta}_w \cos \vartheta_w$, we get a part of $|p|^2$ in equation (7)

$$\begin{aligned} r(\dot{r} + \dot{w}) &= \|\mathbf{t}\|^2 - \dot{r}^2 + r\dot{\vartheta}_w \mathbf{u}^T \mathbf{n} + r\dot{w} = 1 - [1 - \cos^2 \vartheta_w] \\ &\quad - r\dot{\vartheta}_w \cos \vartheta_w \cos \varphi_w - r\dot{\vartheta}_w \cos \vartheta_w, \end{aligned} \quad (12)$$

and hereby the equalized magnitude squared

$$8\pi k |p|^2 = \frac{1}{r^2 \frac{\cos^2 \vartheta_w}{r} - (\dot{\vartheta}_w \cos \varphi_w + \dot{\vartheta}_w) \cos \vartheta_w}. \quad (13)$$

We assume receivers at $z = 0$, so $[0 \ 0 \ 1]^T [\mathbf{x} + r\mathbf{u}] = 0$ retrieves r by the contributions of \mathbf{t} , \mathbf{n} to z in equation (9)

$$r = \frac{z}{\cos \vartheta \sin \vartheta_w + \sin \vartheta \cos \vartheta_w \cos \varphi_w}. \quad (14)$$

2.6 Optimum total curving

To design the sound pressure response at $y_r = 0$, we choose $\varphi_w = 0$, yielding with $\vartheta_T = \vartheta + \vartheta_w$

$$\begin{aligned} 8\pi k |p|^2 &= \frac{1}{r \cos^2 \vartheta_w - r^2 \dot{\vartheta}_T \cos \vartheta_w} = \frac{g^2}{r^{2\beta}}, \\ \text{with } r &= \frac{z}{\sin \vartheta_T}. \end{aligned} \quad (15)$$

For the current positions z , total angle ϑ_T , distance r from equation (15), the required angular curvature complies with the constraint equation (7) when it becomes

$$\dot{\vartheta}_T = -\frac{r^{2\beta}}{g^2} \frac{1}{r^2 \cos \vartheta_w} + \frac{\cos \vartheta_w}{r}. \quad (16)$$

Its numerical integration using a phase/geometry split b , gain g^2 , and start inclination ϑ_{offs} defines [Algorithm 1](#), where S denotes the source length and N is the number of discrete elements. The total inclination ϑ_T is split into geometry and delay parts by the factors a , b , linearly, and a constant inclination offset ϑ_{offs} is additionally added to adjust the inclination for a straight line-source with phasing only. Geometry and phase inclination parts become

$$\begin{aligned} \vartheta &= a(\vartheta_T - \vartheta_{\text{offs}}) + \vartheta_{\text{offs}}, \quad \vartheta_w = b(\vartheta_T - \vartheta_{\text{offs}}) \\ \text{with } a + b &= 1. \end{aligned} \quad (17)$$

2.7 Top inclination, gain, curving split

The aiming to the audience area typically lies within $0 \leq \vartheta_T \leq \frac{\pi}{2}$ and reduces from a most horizontal aiming $\frac{\pi}{2}$ thinkable to a most upwards aiming 0 thinkable. For this reason, the total inclination decreases $\vartheta_T \leq 0$ and clarifies the negative sign of $\dot{\vartheta}_T$. We recognize in equation (15) that $\dot{\vartheta}_{T,0} = 0$ yields the loudest sound pressure

$$g^2 = \frac{r_0^{2\beta-1}}{\cos^2(\vartheta_{w,0})}. \quad (18)$$

Algorithm 1. Curving of geometry and/or phase

```

procedure CURVING( $x_{r,0}, z_0, b, \beta, S, N, [g^2, \vartheta_{\text{offs}}]$ )
  constant:
     $\Delta s = -S/N$ 
     $\vartheta_{T,0} = f(x_{r,0}, z_0)$   $\triangleright$  according to eq. (19)
     $a = 1 - b$   $\triangleright$  to ensure  $a + b = 1$ 
     $r_0 = \sqrt{x_{r,0}^2 + z_0^2}$   $\triangleright$  cf. Figure 2
     $[\vartheta_{\text{offs}} = \vartheta_{T,0}]$   $\triangleright$  default inclination offset
     $\left[ g^2 = \frac{r_0^{2\beta-1}}{\cos^2[b(\vartheta_{T,0} - \vartheta_{\text{offs}})]} \right]$   $\triangleright$  default eq. (18)
  initialization:
     $w = \text{zeros}(1, N)$ 
     $x = \text{zeros}(1, N)$ 
     $z = \text{zeros}(1, N)$ 
     $r = r_0, \vartheta_T = \vartheta_{T,0}, z[1] = z_0$ 
    for  $n = 1 \dots N - 1$  do
       $\vartheta = a(\vartheta_T - \vartheta_{\text{offs}}) + \vartheta_{\text{offs}}$   $\triangleright$  cf. eq. (17)
       $\vartheta_w = b(\vartheta_T - \vartheta_{\text{offs}})$   $\triangleright$  cf. eq. (17)
       $x[n+1] \leftarrow x[n] + \sin(\vartheta) \Delta s$   $\triangleright$  num.int. (2)
       $z[n+1] \leftarrow z[n] + \cos(\vartheta) \Delta s$   $\triangleright$  num.int. (2)
       $w[n+1] \leftarrow w[n] - \sin(\vartheta_w) \Delta s$   $\triangleright$  num.int. (4)
       $r \leftarrow \frac{z[n]}{\sin \vartheta_T}$   $\triangleright$  according to eq. (15)
       $\dot{\vartheta}_T \leftarrow f(r, \vartheta_w, g^2, \beta)$   $\triangleright$  according to eq. (16)
       $\vartheta_T \leftarrow \vartheta_T + \dot{\vartheta}_T \Delta s$   $\triangleright$  numerical integration
    end for
  return  $w, x, z$ 
end procedure

```

We need to ensure that the curvature $\dot{\vartheta}_T < 0$ stays negative yielding a convex contour and a single stationary-phase point for each observing point as implied in equation (5). Moreover, a geometrically concave solution with $\dot{\vartheta} > 0$ would be impractical for line-source arrays whose splay angles $\alpha = -\dot{\vartheta} \text{STEP}$ are non-negative. Choosing as a consequence both $\vartheta_{T,0} = 0$ and $\vartheta_0 = 0$ at the top of the source, the beam-steering curvature $\dot{\vartheta}_{w,0} = 0$ must also vanish to preserve $\dot{\vartheta}_T = \dot{\vartheta} + \dot{\vartheta}_w$.

This total inclination $\vartheta_{T,0}$ at the top of the source at $x = x_0 = 0$ and $z = z_0$ should be adjusted to ensure the top is the minimum-distance point supplying the remotest position $x_{r,0}$ in the audience as in Figure 2,

$$\vartheta_{T,0} = \arctan\left(\frac{z_0}{x_{r,0}}\right). \quad (19)$$

The top inclination is suggested to be purely geometrical $\vartheta_{T,0} = \vartheta_{\text{offs}}$ per default, so that its beam steering is neutral and broadside $\vartheta_{w,0} = 0$ for any choice of a, b .

The simplest choices for a and b are: (i) $a = 1, b = 0$ for a line source without phasing $\vartheta_w \equiv 0$ but with curving $\dot{\vartheta} \neq 0$, or (ii) $a = 0, b = 1$ for a straight-line source without curving $\dot{\vartheta} \equiv 0$ but with phasing $\dot{\vartheta}_w \neq 0$. We will also demonstrate the usefulness of mixtures in a later section, targeting the case in which multiple criteria for β should be fulfilled. For instance, the control of the curved array with equal signals fulfills the criterion $\beta_1 = 0$, and $\beta_2 = \frac{1}{2}$ can be accomplished by additional delays.

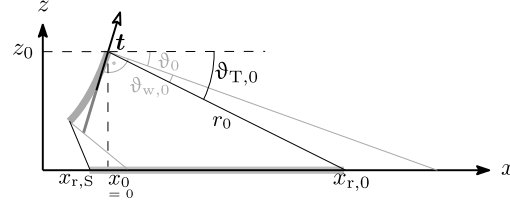


Figure 2. Uniform starting conditions for both curved and phased sources: top end at $x_0 = 0$ at $s = 0$, inclined by ϑ_0 , supplying the most distant listening position at $x_{r,0}$, with the starting value $\vartheta_{T,0} = \vartheta_0 + \vartheta_{w,0}$. The lower end should lie at a length $s = -S$ and supply the closest listeners at $x_{r,S}$. To start at the top point, it is useful to work with a reversed integration direction $-ds$.

3 Simulation studies

In this section, the differential equation will be solved numerically as outlined in Algorithm 1. It applies stepwise updates to ϑ_T based on $\dot{\vartheta}_T$ from equation (16). The algorithm's step size Δs should be appropriately small to solve the problem accurately, by choosing a large N . In default of the optional argument g , Algorithm 1 uses equation (18) to define g^2 .

The simulations below show the result of summing individual point sources described by Green's function positioned along the continuous source contour at 1mm intervals. This summation is performed for frequencies ranging from 20 Hz to 20 kHz with a linear resolution of 248 points, to which and a third-octave band averaging was applied. To show broadband sound pressure curves over the listening area, results were A-weighted [32] and summarized. In addition to the A-weighted on-axis sound pressure curves, a level map of a phased line source with $\beta = 0$ demonstrates the coverage including off-axis listening positions, below. Furthermore the directivity factor is discussed, calculated as result of theoretically simplified considerations, and simulated by (delayed) point sources positioned along the desired contour.

3.1 Curved line source

For curved line sources without phasing ($\vartheta_w \equiv 0$), $a = 1$ and $b = 0$, the design equation (15) simplifies to

$$8\pi k |p|^2 = \frac{1}{r} \frac{1}{1 - r \dot{\vartheta}} = \left(\frac{g}{r^\beta}\right)^2, \quad (20)$$

and the differential equation (16) to

$$\dot{\vartheta} = -\frac{r^{2\beta-2}}{g^2} + \frac{1}{r} \quad \text{with } r = \frac{z}{\sin \vartheta}. \quad (21)$$

3.1.1 Comparison to literature

In a recent paper [28], we presented a second-order differential equation for $\beta = 0$, yielding an optimally curved arc source. While its result is perfectly equivalent for

$\beta = 0$, the main difference lies in the formulation of the integration with regard to the x axis instead of the natural parameter s , which complicates generalization to $\beta > 0$ or comparison to literature. Equation (20) is shown above as it matches the classic equation obtained by Urban et al. [3], which states after re-writing the variables $STEP = \Delta s$, $\alpha = -\Delta\vartheta$, $d = r$, with $I \approx \frac{1}{\rho c} |p|^2$,

$$I \propto \frac{1}{r} \frac{1}{1 - r \frac{\Delta\vartheta}{\Delta s}}. \quad (22)$$

Remarkably, equation (22) resulting from a binary Fresnel-zone-based approach only differs from stationary-phase approximation equation (20) by the missing limit $\Delta s \rightarrow 0$.

A later publication [5] and variable-curvature line-source tutorials [33] chose to show a simplified relation

$$I \propto \frac{1}{r^{2\beta} \Delta s}, \quad (23)$$

which is instructive and intuitively accessible. By letting $I \propto \frac{1}{g^{2+2\beta}}$ and replacing $\frac{\Delta\vartheta}{\Delta s} \approx \dot{\vartheta}$, it implies

$$\dot{\vartheta} \approx -r^{2\beta-2} g^{-2}, \quad (24)$$

and hereby yields the expression

$$r^{2-2\beta} \alpha \approx \text{const.} \quad (25)$$

The equation demands for cabinets pointing at large distances that the splay angle between them must be small so that more cabinets radiate into the same direction. The exponent β defines the desired distance decay. Despite its easier accessibility, however, equation (25) is inaccurate compared to equation (22) whenever $\beta \rightarrow 0$ gets small. While for $\beta = 0.5$ and small Δs , it makes no substantial difference which formula is used for calculation, because either $1 - r \frac{\Delta\vartheta}{\Delta s} = \text{const.}$ or $r \frac{\Delta\vartheta}{\Delta s} = \text{const.}$ approximate $I \propto \frac{1}{r}$, only with a different overall gain.

Without simplification, the equation (22) as defined in [3] yields upon targeting $I \propto \frac{1}{g^{2+2\beta}}$ an approximation

$$\frac{\alpha}{STEP} = g^2 r^{2\beta-2} - \frac{1}{r} \quad (26)$$

of equation (21), as long as $STEP = \Delta s$ stays sufficiently small. In particular, the original paper used the cabinet height for $STEP$ and the splay angles for $\alpha = -\Delta\vartheta$, i.e. a fixed geometric discretization determined by the hardware elements, as opposed to keeping it a free parameter adjusted for fine-enough discretization $\Delta s \rightarrow 0$, when numerically solving a differential equation.

3.1.2 Curved line source: results

The differential equation of equation (21) is solved numerically by the proposed Algorithm 1 with uniform parameters $x_{r,0} = 10$ m, $z_0 = 2.072$ m, $b = 0$ and source length $S = 1.312$ m for all decays, giving the number of discrete elements $N = 1313$ for a step size $\Delta s = 1$ mm. Equation (19) specifies the total inclination on top of the

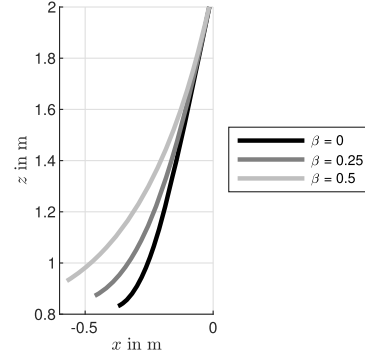


Figure 3. Curved line source contours for different decays β .

source $\vartheta_{T,0} = 11.31^\circ$ and for $\beta = 0$, the gain parameter is calculated by equation (18) yielding a value of $g = \frac{1}{\sqrt{10.2124}}$. For the other decay values, g was set manually to $g = 0.443$ for $\beta = 0.25$ and $g = 0.599$ for $\beta = 0.5$, in order to supply the same listening positions $0 \leq x_r \leq 10$ m with unchanged source length S .

Figure 3 shows the source contour for different decays and Figure 4 the resulting A-weighted sound pressure profiles with dB offsets to make the $\beta = \{0, 0.25, 0.5\}$ curves to go through $\{0, -3.5, -7\}$ dB at the distance of $x_r = 4$ m. The levels do not follow the theoretical roll-off curves -6β dB per doubling of the distance beyond $x_r > 7$ m as stationary phase approximation assumes an infinite line integral although the actual length is finite.

Another parameter to be considered for radiation characteristics is the directivity factor Q . Figure 5 shows the directivity index $DI = 10 \lg Q$ for both cases, curved and phased line source with different decays β . The radiation of the source was calculated at 10 m distance as summation of individual point sources with $\Delta s = 1$ mm. For low frequencies, omnidirectional radiation is seen, which coincides with theoretical considerations for frequencies below 130 Hz ($\frac{c}{\lambda}$). At frequencies above 500 Hz, the curves for different decay values differ, with small decay values leading to higher directivity. With $a \approx \frac{z_0}{r_s}$, Sections A.3 and A.4 we find

$$DI \approx \begin{cases} 10 \lg \left(1 + \frac{kS}{\pi} \right), & \text{for } f < \frac{c}{2\Delta x}, \\ 3 + 10 \lg \frac{a}{\ln a}, & f \rightarrow \infty \text{ for } \beta = \frac{1}{2}, \\ 3 + 10 \lg \frac{a}{1 - a^{-1+2\beta}}, & f \rightarrow \infty \text{ for } \beta \neq \frac{1}{2}. \end{cases} \quad (27)$$

The results are shown as dotted lines in Figure 5 and show the same trends as the simulated solid lines, where $a = 7$ corresponds to the ratio of distances, within which the level curves fulfill the decay profile, cf. Figure 4. The horizontal extent Δx is 9.83 cm for $\beta = 0$, it is 19.82 cm for $\beta = 0.25$, and 32.14 cm for $\beta = 0.5$.

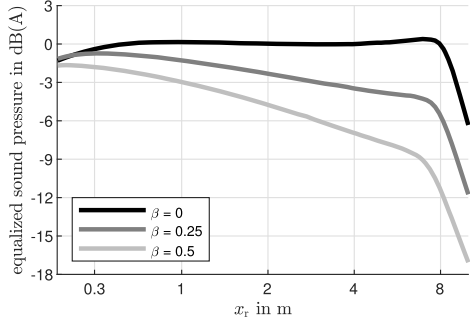


Figure 4. A-weighted sound pressure levels of curved line sources for different decays β with mixed x -axis scaling, linear for $x_r \leq 1$ and logarithmic for $x_r > 1$, with the target range $0 \leq x_r \leq 10$ m.

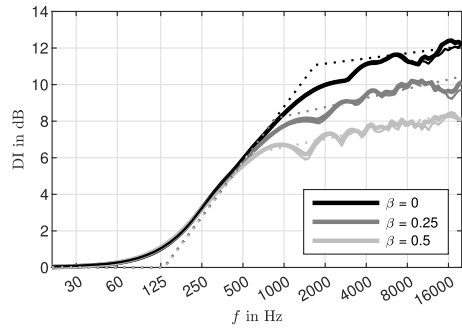


Figure 5. Directivity index for curved (thin) and phased (bold) line sources with different decays β compared to equation (27) (dotted).

Professional line-source array systems typically contain multi-way transducers, of which the larger layout of the low- and mid-frequency transducers is horizontally directional, instead of radiating axisymmetrically. Similarly, their vertical high frequency line-source transducers, e.g. $f > 1$ kHz, are typically equipped with horizontal waveguides or wedge-shaped horns that limit horizontal radiation to 110° , so roughly a third of the 360° panorama, or to 70° which is roughly its fifth. The modeled DI can be adapted correspondingly with an increase by $+5$ dB for 110° or $+7$ dB for 70° horizontal coverage.

3.1.3 Discretization of source and splay angles

Later we will use a prototype of a line array to show the effectiveness of the formalism in practice. Since is solved with the same parameters as in Section 3.1.2 and the resulting continuous source is then composed by point sources that are positioned along the contour, cf. Figure 7A. To simulate a practical device built from discrete elements, the contour was discretized into a polygon of 8.2 cm straight-line segments in Figure 7B. The splay angles are

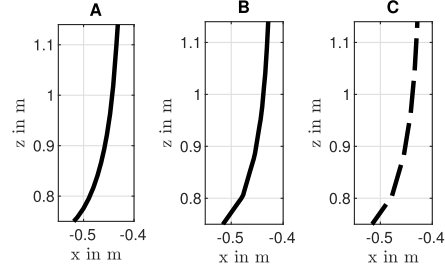


Figure 6. Discretization of a continuously curved line source (A) according to the $\beta = 0$ example from Figure 3 to: a polygon of straight-line sources with splay angles rounded to integer degrees (B) and gaps between these straight-line segments (C); graphs are rotated by ϑ_{offs} and limited to $z < 1.15$ m for easy readability.

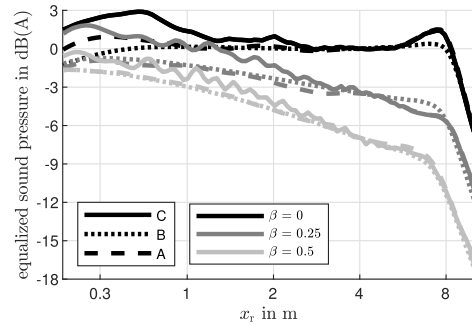


Figure 7. A-weighted sound pressure level for different decays β and different discretization with mixed x -axis scaling, linear for $x_r \leq 1$ and logarithmic for $x_r > 1$, as above; continuous line source (dotted), discrete point sources with 8.2 cm (dashed), straight 6.2 cm line-sources at the same spacing with inclination increments rounded to integer $^\circ$ values (solid).

chosen so that the error made in the total inclination caused by using integer $^\circ$ values for the splay angles is kept minimal. The same procedure is executed for Figure 7C but with shorter 6.2 cm straight-line segments with the same splay angles but leaving gaps in between. Due to discretization with integer-degrees splay angles, the lost control of small curvatures yields a boost of the sound pressure level between 7 m and 8 m for $\beta = 0$ in our example, cf. Figure 7. Gaps between the straight-line source elements weaken the attenuation of spatial aliasing. It occurs at frequencies above $f > \frac{c}{0.082} \approx 4.2$ kHz where the inter-element spacing exceed a wavelength, which causes a noticeable downwards steering $\vartheta_w = 0$.

3.2 Phased straight-line source

With $a = 0$, we get the differential equation for the beamforming angle of a straight-line source from equation (16),

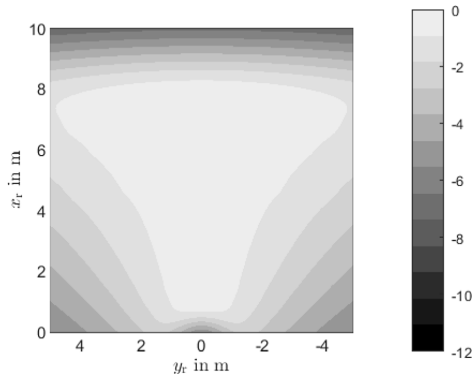


Figure 8. Simulated A weighted sound pressure map of a phased line source for $\beta = 0$ over a listening area of $10\text{ m} \times 10\text{ m}$.

$$\dot{\vartheta}_w = -\frac{r^{2\beta-2}}{g^2 \cos \vartheta_w} + \frac{\cos \vartheta_w}{r} \quad \text{with} \quad r = \frac{z}{\sin \vartheta_T}. \quad (28)$$

3.2.1 Phased straight-line source: results

The differential equation (28) is solved numerically by Algorithm 1 with uniform parameters $x_{r,0} = 10\text{ m}$, $z_0 = 2.117\text{ m}$, $b = 1$, $\vartheta_{w,0} = 0$ and source length $S = 1.312\text{ m}$ for all decay values, resulting in the number of discrete elements $N = 1313$ for a step size $\Delta s = 1\text{ mm}$. Equation (19) defines the inclination on top of the source $\vartheta_{T,0} = \vartheta_{\text{offis}} = 11.365^\circ$ and for $\beta = 0$, the gain parameter is calculated by equation (18) yielding a value of $g = \frac{1}{\sqrt{10.2124}}$. For the other decay values, g was set manually, $g = 0.449$ for $\beta = 0.25$ and $g = 0.614$ for $\beta = 0.5$. Figure 10 shows the delay lengths for different decay values, and Figure 9 describes the resulting A-weighted sound pressure curves for a continuously phased source (dotted lines) compared to direct sound pressures curves of a discrete phased source with enclosure height 8.2 cm , gaps in between and rounded delays being accurate to 1 sample at $f_s = 48\text{ kHz}$. The SPL plots for the continuous source exhibit the same trend as those for the purely curved source. For very close listening positions, the curves differ due to discretization and spatial aliasing. The delays also cause a comb filter, which is greatest at $\beta = 0$ due to the temporal structure of the summed impulse response and has the opposite effect to spatial aliasing. The A-weighted sound pressure for $\beta = 0$ including off-axis listening positions can be found as a level map in Figure 8 over a $10\text{ m} \times 10\text{ m}$ listening area. The coverage for which level changes stays below 1 dB reaches a limit of $|\varphi_w| = 27.5^\circ$ for closer observation points. For farther observation points ($5\text{ m} < x_r < 7.8\text{ m}$) the coverage gets wider up to maximum of $|\varphi_w| = 35^\circ$ for $r = 8.5\text{ m}$.

3.2.2 Comparison to literature

Electronically steered line arrays for sound reinforcement can be found in literature, however not fixed to using

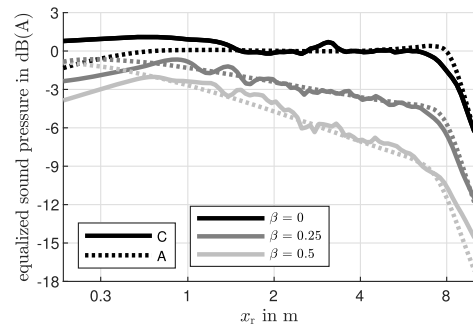


Figure 9. A-weighted sound pressure levels of a phased source with different decays β for a target range $0 \leq x_r \leq 10\text{ m}$, with a continuous source Figure 6A or discrete segments Figure 6C of integer sample delays (48 kHz sample rate); the x -axis is scaled linearly for $x_r \leq 1$ and logarithmically for $x_r > 1$.

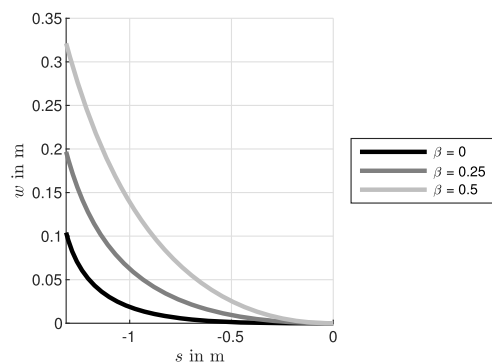


Figure 10. Delay length w for different decays β .

delays, only. Meyer [14, 34] employs individual filters to control each array loudspeaker and proposes to mount the line arrays along the ceiling. Different designs are used with regard to the arrays' throw distance, short-throw vs. long-throw array, and to keep the direct sound coverage of the audience flat. Van der Werff [15] discusses wall-mounted line arrays with non-uniformly spaced transducers, as nested array, with individual filtering with IIR low-pass filter designs. The goal of his work is to increase the direct-to-reverberant ratio in large halls by achieving a flat direct sound pressure level profile of 0 dB per distance doubling, and the design was verified in EASE 1.2. And finally, Duran Audio's Digital Directivity Synthesis is a well-known DSP-assisted method based on least-squares for uniformly spaced line arrays [11]. Its optimization of the desired direct sound pressure level profiles takes transducer directivity into account. The method requires the implementation of FIR filters as signal processing done for each loudspeaker.

Algorithm 2. Two-target curving of geometry and phase

```

procedure TWOBETA( $x_{r,0}, z_0, \beta_1, \beta_2, S, N, g_1^2, g_2^2, \vartheta_{\text{offs}}$ )
  constant:
     $\Delta s = -S/N$ 
     $\vartheta_0 = f(x_{r,0}, z_0)$   $\triangleright$  according to eq. (19)
     $r_0 = \sqrt{x_{r,0}^2 + z_0^2}$   $\triangleright$  cf. Figure 2
  initialization:
     $w = \text{zeros}(1, N)$ 
     $x = \text{zeros}(1, N)$ 
     $z = \text{zeros}(1, N)$ 
     $r_1 = r_2 = r_0, \vartheta[1] = \vartheta_0, z[1] = z_0$ 
    for  $n = 1 \dots N - 1$  do
       $w[n + 1] \leftarrow w[n] - \sin(\vartheta_w) \Delta s$   $\triangleright$  num.int. (4)
       $x[n + 1] \leftarrow x[n] + \sin(\vartheta) \Delta s$   $\triangleright$  num.int. (2)
       $z[n + 1] \leftarrow z[n] + \cos(\vartheta) \Delta s$   $\triangleright$  num.int. (2)
       $r_1 \leftarrow \frac{z[n]}{\sin \vartheta}, r_2 \leftarrow \frac{z[n]}{\sin(\vartheta + \vartheta_w)}$   $\triangleright$  cf. eq. (15)
       $\dot{\vartheta} \leftarrow f(r_1, g_1^2, \beta_1)$   $\triangleright$  according to eq. (21)
       $\vartheta \leftarrow \vartheta + \dot{\vartheta} \Delta s$   $\triangleright$  numerical integration
       $\dot{\vartheta}_w \leftarrow f(r_2, \vartheta_w, \dot{\vartheta}, g_2^2, \beta_2)$   $\triangleright$  acc. to eq. (29)
       $\vartheta_w \leftarrow \vartheta_w + \dot{\vartheta}_w \Delta s$   $\triangleright$  numerical integration
    end for
    return  $w, x, z$ 
end procedure

```

3.3 Curved and phased line source

To support two simultaneous coverage designs (preserving mixing-balance and envelopment) for a large audience area, phasing delays are used in combination with geometrical curving. In addition to a decay β_1 accomplished by driving the cabinets of a curved array with identical signals, delays between individually driven cabinets can be used to satisfy an alternative decay β_2 .

First, equation (21) is solved for a purely curved source ($b = 0$) with β_1 as shown in Algorithm 1, and afterwards the required delay lengths for another choice of β_2 is calculated preserving the geometrical curvature ϑ ,

$$\dot{\vartheta}_w = -\frac{r^{2\beta_2}}{g^2} \frac{1}{r^2 \cos \vartheta_w} + \frac{\cos \vartheta_w}{r} - \dot{\vartheta}, \quad (29)$$

which is summarized in Algorithm 2.

As this design and algorithm will be analyzed in measurements using prototypical hardware in the next section, graphical analysis of the results will be shown below.

4 Experimental setup

To show the effectiveness of the formalism in practice, the reproducible miniature line array presented in [35] was used, cf. Figure 11. The trapezoidal shape was chosen so that a maximum tilt angle of 10 degrees can be set. SB Acoustics SB65WBAC25-4 were used as the 2.5-inch full-range speakers.

For the measurements, 12 enclosures are lined up for which we obtain the continuous source contour and delay



Figure 11. Miniature Line Array of eight 3D printed enclosures (closed 0.4 l boxes).

lengths from Algorithm 1. The measurements took place in an auditorium (30 m \times 9 m \times 3.5 m) with a reverberation time of $T_{60} \approx 0.82$ s. To focus on verifying the direct sound design, the impulse responses were truncated to the first 300 samples (6.25 ms at $f_s = 48$ kHz). The gain values g for $\beta = 0$ are calculated by equation (18), for the other decay values g was set manually, $g = 0.46$ for $\beta = 0.25$ and $g = 0.65$ for $\beta = 0.5$. The solution is then discretized using a step size of 8.2 cm which corresponds to the distance between two neighbouring drivers. In order to record the position-dependent direct sound pressure level curves, impulse responses were measured along 20 positions (on-axis) starting at $x_r = 1$ m and ending at $x_r = 10.5$ m. Pressure zone microphones were positioned on the ground to avoid floor reflections in the measurements. We applied equalization to obtain a flat frequency response between 200 Hz and 20 kHz for the single array element. Moreover, a filter with magnitude increasing by \sqrt{f} until the spatial aliasing frequency was employed to equalize the otherwise pink sound pressure of a linear arrangement of ideal point sources, cf. equation (7). The results are averaged in third octaves and the curves are plotted as A-weighted sum.

4.1 Curved line source

Figure 12 shows the A weighted sum over distance (on-axis) for different decays β compared to the simulated curves with the same discretization as in Figure 6C. The measured results show almost identical curves to the simulation and the artefacts caused by discretization of source and splay angles are observed.

4.2 Phased line source

Figure 14 shows the A-weighted on-axis sound pressure curves in comparison to the simulated for different decays β . Also here, the measured results follow almost

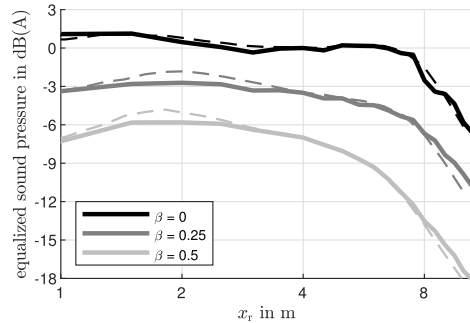


Figure 12. A-weighted measured sound pressure of curved arrays (solid) with different decays over distance compared to the simulated discretized source (dashed) with rounded splay angles keeping the error made in total inclination minimal.

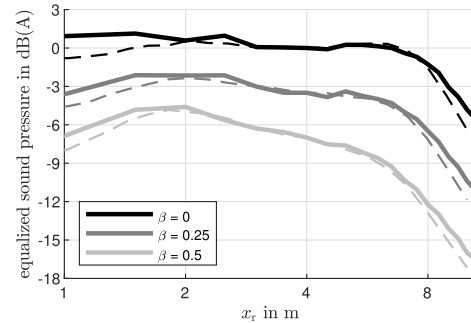


Figure 14. A-weighted measured sound pressure of phased arrays (solid) with different decays over distance compared to the simulated discretized source (dashed) with rounded delays at $f_s = 48$ kHz.

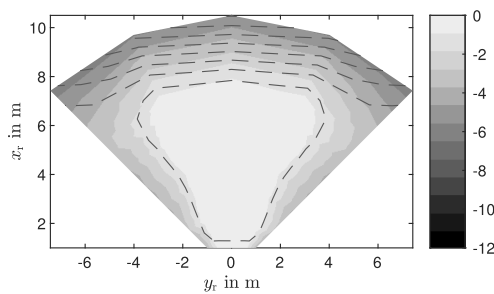


Figure 13. Measured A weighted sound pressure map of a phased array with $\beta = 0$ compared to simulated contours in steps of 1 dB (dashed).

the theoretical simulated based on point source summation. The noticeable differences are close to the source where the beamforming no longer reaches closer listening positions and spatial aliasing affects the results. Figure 13 presents the measured coverage (solid) including off-axis listening positions of a phased array with $\beta = 0$ compared to the simulated (dashed). We observe a lower sound pressure for lateral listening positions because the linearly arranged point sources in the simulation do not take the horizontal directivity of the drivers into account.

4.3 Mixed curve and phase design

For the mixed design, we take the curved line source from Section 4.1 with $\beta_1 = 0$ and use the corresponding time of flight to satisfy $\beta_2 = 0.5$ according to Algorithm 2. The rounded delays at $f_s = 48$ kHz were inserted in the off-line analysis. Figure 15 shows the A-weighted sound pressure profile of a purely curved source with $\beta = 0$ and compares the A-weighted profile of a curved line source with $\beta = 0.5$ with the curve of the mixed design.

The profile for a purely curved source and the one of the mixed design differ in the vicinity of the source only,

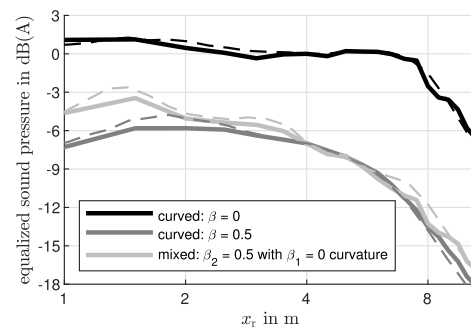


Figure 15. A-weighted measured sound pressure of curved arrays (solid) with decays $\beta = 0$ and $\beta = 0.5$ and mixed array with $\beta_1 = 0$ and $\beta_2 = 0.5$ over distance compared to simulated discretized sources (dashed).

because the impulse responses of the enclosures differ in time structure in this area, yielding a different sum. Nevertheless, both follow the simulated -3 dB per doubling of distance.

5 Conclusion

This paper presented design equations for continuously curved and phased line sources with the target to accomplish desired sound pressure roll-offs. The stationary phase approximation was applied to the contour integral of a Green's function with delay (phasing) to obtain a second-order nonlinear differential equation for curving and phasing. The discretized results are directly applicable to design curvature and phasing of discrete line source arrays. Simulations of the continuous source based on summation of point sources positioned along the line source contour showed the ideal -6β dB profiles per doubling of the distance. Furthermore, the simulations revealed the effects caused by the discretization of the source. The theoretical

results were underlined by measurements of a line array prototype. Moreover, the results showed that a two-target design based on curving and phasing is feasible.

Future work should consider psychoacoustic evaluations of line sources with different β profiles for medium-sized immersive sound reinforcement for 50–250 listeners to assess improvements in envelopment and direct-sound mix. Experiments should also take frequency-response homogeneity into account, which is often optimized as a trade-off with the coverage parameter β , see also [33].

Acknowledgments

Our research was funded by the Austrian Science Fund (FWF): P 35254-N, Envelopment in Immersive Sound Reinforcement (EnImSo). The authors thank Thomas Musil for his design improvements on our miniature line array.

Conflict of interests

The authors declared no conflicts of interests.

Data Availability Statement

The research data associated with this article are included in the supplementary material of this article [36].

References

- W. Ahnert, D. Noy: Sound reinforcement for audio engineers, Taylor & Francis Ltd, 2023.
- C. Heil, M. Urban, Sound fields radiated by multiple sound sources arrays, in: 92nd AES Conv, Vienna, 1992.
- M. Urban, C. Heil, P. Bauman: Wavefront sculpture technology. Journal of the Audio Engineering Society 51, 10 (2003) 912–932.
- F. Straube, F. Schultz, M. Makarski, S. Spors, S. Weinzierl: Evaluation strategies for the optimization of line source arrays, in: 59th AES Conf, Montreal, Canada, 2015.
- F. Straube, F. Schultz, D.A. Bonillo, S. Weinzierl: An analytical approach for optimizing the curving of line source arrays. Journal of the Audio Engineering Society 66, 1/2 (2018) 4–20.
- A. Hölter, F. Straube, F. Schultz, S. Weinzierl: Enhanced polygonal audience line curving for line source arrays, in: 150th AES Conv, 2021.
- A. Thompson: Line array splay angle optimisation, in: Reproduced Sound 22 Conference, Oxford, 2006.
- A. Thompson, Improved methods for controlling touring loudspeaker arrays, in: 127th AES Conv., New York, USA, 2009.
- A. Thompson, J. Baird, B. Webb, Numerically optimized touring loudspeaker arrays – practical applications, in: 131st AES Conv, New York, USA, 2011.
- F. Toole, Sound Reproduction: Loudspeakers and Rooms, in: Audio Engineering Society Presents Series, Elsevier, 2008.
- G. van Beuningen, E. Start: Optimizing directivity properties of DSP controlled loudspeaker arrays, in: Reproduced Sound 16 Conference, Stratford upon Avon, 2000.
- D. Ward, R. Kennedy, R. Williamson: Constant directivity beamforming, in: Microphone Arrays, Springer, Berlin, Heidelberg, 2001, pp. 3–17.
- M. Goodwin, G. Elko: Constant beamwidth beamforming, in: IEEE ICASSP, Vol. 1, Minneapolis, USA, 1993, pp. 169–172.
- D.G. Meyer: Digital control of loudspeaker array directivity. Journal of the Audio Engineering Society 32, 10 (1984) 747–754.
- J. van der Werff, Design and implementation of a sound column with exceptional properties, in: 96th AES Conv, Amsterdam, Netherlands, 1994.
- R. Mailloux: Phased array antenna handbook, 3rd edn., Artech House, 2017.
- T. Taylor: Design of line-source antennas for narrow beamwidth and low side lobes. Transactions of the IRE Professional Group on Antennas and Propagation 3, 1 (1955) 16–28.
- P. McManamon, T. Dorschner, D. Corkum, L. Friedman, D. Hobbs, M. Holz, S. Liberman, H. Nguyen, D. Resler, R. Sharp, E. Watson: Optical phased array technology. Proceedings of the IEEE, 84, 2 (1996) 268–298.
- H. Shanks: A geometrical optics method of pattern synthesis for linear arrays. IRE Transactions on Antennas and Propagation 8, 5 (1960) 485–490.
- B. Chiang, D.H.-S. Cheng: Curvilinear arrays. Radio Science 3, 5 (1968) 405–409.
- A. Chakraborty, B. Das, G. Sanyal: Determination of phase functions for a desired onedimensional pattern. IEEE Transactions on Antennas and Propagation 29, 3 (1981) 502–506.
- E. Start: Direct sound enhancement by wavefield synthesis. Ph.D. dissertation Technical University Delft, 1997.
- G. Firtha: A generalized wave field synthesis framework with application for moving virtual sources. Ph.D. dissertation Budapest University of Technologies and Economics, 2019.
- P. Grandjean, A. Berry, P.-A. Gauthier: Sound field reproduction by combination of circular and spherical higher-order ambisonics: part I — a new 2.5-d driving function for circular arrays. Journal of Audio Engineering Society 69, 3 (2021) 152–165.
- F. Schultz: Sound field synthesis for line source array applications in large-scale sound reinforcement. Ph.D. dissertation University of Rostock, 2016.
- SMPTE RP 2096–1:2017, Recommended practice – cinema sound system baseline setup and calibration, 2017.
- J. Nettingsmeier, D. Dohrmann: Preliminary studies on large-scale higher-order ambisonic sound reinforcement systems, in: Ambisonics Symposium, Lexington, KY, 2011.
- L. Gölles, F. Zotter: Optimally curved arc source for sound reinforcement, in: Fortschritte der Akustik, DAGA, Vienna, 2021.
- F. Zotter, S. Riedel, L. Gölles, M. Frank: Acceptable imbalance of sound-object levels for off-center listeners in immersive sound reinforcement, in: Fortschritte der Akustik, DAGA, Hamburg, 2023.
- S. Riedel, F. Zotter: Surrounding line sources optimally reproduce diffuse envelopment at offcenter listening positions JASA Express Letters 2, 9 (2022) 094404.
- S. Riedel, L. Gölles, F. Zotter, M. Frank: Modeling the listening area of envelopment, in: Fortschritte der Akustik, DAGA, Hamburg, 2023.
- ÖVE/ÖNORM EN 61672–1: Electroacoustics – Sound level meters – Part 1: Specifications, OVE/Austrian Standards Institute, Vienna, AT, Standard, 2015.
- F. Montignies: Understanding line source behaviour – for better optimization, in: VCLS Tutorial, AES, 2020.
- D.G. Meyer: Multiple-beam, electronically steered line-source arrays for sound-reinforcement applications. Journal of the Audio Engineering Society 38, 4 (1990) 237–249.

35. L. Gölles, F. Zotter, L. Merkel: Miniature line array for immersive sound reinforcement, in: Proceedings of AES SIA Conf., Huddersfield, 2023.
36. L. Gölles and F. Zotter: Supplementary material for theory of continuously curved and phased line sources for sound reinforcement. [Online]. Available at <https://phaidra.kug.ac.at/o:129841>.

Appendix

A.1 Line array near field

When observing a line source of the length S at the normal distance r to one of its ends, the distance to its other end is $\sqrt{r^2 + S^2}$. A distance difference $\sqrt{r^2 + S^2} - r$ to both ends that may exceed a $\frac{\pi}{2}$ phase shift towards $r \rightarrow 0$ defines the acoustic near field, within which the distance decay can differ from $\frac{1}{r}$, with $k = \frac{2\pi f}{c}$ and $\sqrt{1+x} \approx 1 + \frac{x}{2}$,

$$kr\sqrt{1 + \frac{S^2}{r^2}} - kr = \frac{\pi}{2}$$

$$k\frac{S^2}{2r} \approx \frac{\pi}{2}, \quad \Rightarrow r = \frac{2fS^2}{c}. \quad (\text{A.1})$$

Example: The near field extends to 10 m for a source of the length 1 m at a frequency of $f = 5 c = 1.7$ kHz.

A.2 Line array aliasing

A line array composed of discrete elements of the height and spacing h driven in phase radiates waves focused to directions perpendicular to the line. It exhibits uncontrolled radiation due to spatial aliasing at and above the frequency at which also waves propagating along the line fit the in-phase control,

$$kh \geq 2\pi, \quad \Rightarrow f \geq \frac{c}{h}. \quad (\text{A.2})$$

Example: The frequency should stay below 3 kHz for $h = \frac{c}{3000} = 11.4$ cm to avoid spatial aliasing.

A.3 Directivity index of a line source

For very low frequencies $f \rightarrow 0$, any phased/curved line source has vanishing extent in terms of wavelengths and the directivity index is zero $\text{DI} \rightarrow 0$ dB.

Any phased/curved line source exhibits a length S as its larger geometric extent. Its directivity index first rises when the length S exceeds half a wavelength $\frac{S}{2} = \frac{1}{2} \frac{c}{f}$

$$f_1 = \frac{c}{2S}. \quad (\text{A.3})$$

Around this frequency, the directivity function is well approximated by a line source of the length S , with $\frac{1}{S} \int_{-\frac{S}{2}}^{\frac{S}{2}} e^{ikz \sin \vartheta} dz = \frac{1}{S} \frac{2 \sin(k \frac{S}{2} \sin \vartheta)}{k \sin \vartheta}$. The directivity factor of an axisymmetric radiation is 2 divided by the

squared directivity pattern integrated along the inclination $d \sin \vartheta$,

$$Q = \frac{2S^2}{4 \int_0^1 \frac{\sin^2(k \frac{S}{2} \sin \vartheta)}{k^2 \sin^2 \vartheta} d \sin \vartheta} \quad (\text{A.4})$$

$$= \frac{k^2 S^2}{kS \text{Si}(kS) + \cos(kS) - 1}, \quad (\text{A.5})$$

and at low frequencies we approximate the sine integral $\text{Si}(kS)$ by kS and cosine $\cos(kS)$ by 1, yielding $Q \approx 1$, and the asymptotic value of $\text{Si}(kS)$ is $\frac{\pi}{2}$ at high frequencies, where we may neglect $\cos(kS) + 1$ and get $Q \approx \frac{kS}{\pi}$, or in total

$$Q \approx 1 + \frac{kS}{\pi}. \quad (\text{A.6})$$

After the linear increase of the directivity factor above $\frac{kS}{\pi} > 1$, a slight saturation will be reached when the second extent of the curved/phased line source $\Delta x = x_s - S \cos \vartheta_0$ or $\Delta x = w_s$ exceeds half a wavelength

$$f_2 = \frac{c}{2\Delta x} = \frac{S}{\Delta x} f_1, \quad (\text{A.7})$$

which is conveniently denoted as frequency f_1 scaled by the approximate aspect ratio $\frac{S}{\Delta x}$ of the source.

A.4 Directivity index of a directional point source with predefined coverage

To estimate the directivity index, we consider the far-field sound pressure of a directional point source,

$$p(r) = \frac{e^{-ikr}}{4\pi r} g(\sin \vartheta) \quad (\text{A.8})$$

mounted at the height z_0 above the audience and exhibiting a roughly axisymmetric directivity function g around the vertical axis. Listeners at ear height are reached if the distance r relates to the variable inclination angle by

$$r = \frac{z_0}{\sin \vartheta}, \quad (\text{A.9})$$

and a correspondingly re-formulated directivity factor depending on this r can be tailored so that listeners receive

$$|p(r)| = \left(\frac{r_0}{r}\right)^\beta, \quad \text{with } g(r) = 4\pi r \left(\frac{r_0}{r}\right)^\beta, \quad (\text{A.10})$$

and hereby a well-controlled direct-sound level decaying with -6β dB per doubling of the distance. To avoid radiation to angles outside $\vartheta_s \leq \vartheta \leq \vartheta_0$, the directivity function must vanish elsewhere, accordingly, and we may substitute $r_s = \frac{r_0}{a}$ and choose $r_s = z_0$ for simplicity,

$$g(r) = 0, \quad \text{for } r < \frac{r_0}{a} \text{ and } r > r_0. \quad (\text{A.11})$$

The characterization of a directivity pattern relies on observation at a direction-independent distance, e.g. r_0 , but we may keep r as unrelated variable defining the directivity function g by the angle-dependent distance to the listeners,

$$|p(r_0)| = \frac{g(r)}{4\pi r_0} = \left(\frac{r_0}{r}\right)^{\beta-1}. \quad (\text{A.12})$$

With the directivity pattern integrated along the inclination $\cos \vartheta \, d\vartheta = -d \sin \vartheta = \frac{r_0}{r^2} dr = \frac{r_0}{a} \frac{dr}{r^2}$ the directivity factor of the axisymmetric radiation is

$$Q = \frac{2}{\int_0^\pi |p|^2 \cos \vartheta \, d\vartheta} = \frac{2ar_0^{1-2\beta}}{\int_{\frac{\vartheta_0}{a}}^{r_0} r^{-2\beta} \, dr} = \begin{cases} \frac{2a(1-2\beta)}{1-a^{-1+2\beta}}, & \beta \neq \frac{1}{2}, \\ \frac{2a}{\ln(a)}, & \beta = \frac{1}{2}. \end{cases} \quad (\text{A.13})$$

For curved/phased line-source arrays, this rough asymptotic approximation can be assumed to hold for high frequencies $f > f_2$, where the directivity function vanishes outside the angular range $\vartheta_s \leq \vartheta \leq \vartheta_0$.

Cite this article as: Gölles L. & Zotter F. 2023. Theory of continuously curved and phased line sources for sound reinforcement. Acta Acustica, 7, 52.

Publication II

This work was published as:

Lukas Gölles and Franz Zotter, „Theory of continuously phased planar sources for sound reinforcement,“ *Acta Acust.*, [Accepted on October 1, 2024]

Acta Acustica 2024, xx, xx
© The Author(s), Published by EDP Sciences, 2024
<https://doi.org/10.1051/aacus/2024070>



Available online at:
<https://acta-acustica.edpsciences.org>

SCIENTIFIC ARTICLE

OPEN ACCESS

Theory of continuously phased planar sources for sound reinforcement

Lukas Göllles* and Franz Zotter

Institute of Electronic Music and Acoustics, University of Music and Performing Arts, Inffeldgasse 10/3, 8010 Graz, Austria

Received 2 July 2024, Accepted 1 October 2024

Abstract – Modern large-scale sound reinforcement systems use line-source loudspeaker arrays with the goal to establish a desired direct sound level decay profile along a line into the audience by adjusting the splay angles or delays between the individual enclosures. To design such a profile not only in the depth but also in the width of the audience area, a two-dimensional source would offer sufficiently many degrees of freedom for adaptation. In practical applications, this task is often accomplished with discrete planar loudspeaker arrays. In this work, we suggest employing the stationary-phase approximation to get a continuous symmetric delay length profile, which is then discretized. The aim of the design is to achieve direct sound levels rolling off by $-6 \cdot \beta$ dB per distance doubling on the listening area. The efficacy of this method is demonstrated by simulations and measurements of coverage with a small planar array confirming the validity of the proposed theory in practice.

Keywords: Planar arrays, Matrix arrays, Sound reinforcement, Stationary phase approximation, Delay beamforming

1 Introduction

Nowadays, modern large-scale sound reinforcement systems often use line-source loudspeaker arrays to provide high-quality sound for the largest parts of the audience area [1]. The optimization of these line sources is a widely discussed topic in the literature [2–11].

For surround sound reinforcement, it has been shown that reproduction at off-center listening positions can be improved by line-source loudspeakers [12–18]. In particular, optimal surround sound reinforcement considers a dual-target design of the direct-sound: 0 dB per distance doubling (dod) to preserve the mixing balance and -3 dB/dod to preserve the envelopment at off-center listening positions. Considering a live concert scenario, single-target line-array designs between 0 dB/dod and -1.5 dB/dod for both, direct sound objects and enveloping parts, achieve similar good results as the proposed dual-target design, also at off-center listening positions [18]. However, the line-array sound pressure design is limited to a line in the audience that lies in the axial direction of the loudspeaker arrangement. By contrast, planar arrays allow the sound pressure to be controlled across the depth and the width of the audience area. Therefore planar arrays should be investigated to find out whether further improvement can be achieved for surround sound reinforcement at off-center listening positions.

Planar arrays are known from antenna theory and telecommunication applications, in which a beam is

electronically formed by applying amplitude and/or phase weights [19–23]. Antennas with co-secant squared patterns are used to track moving targets at constant height, such as airplanes, where the received power should stay independent of the position of the object [24–26]. This design approach is similar to that of loudspeaker arrays that aim for 0 dB/dod.

In acoustics, loudspeaker arrays are often used to reconstruct acoustic wave fields with desired wavefront properties [27, 28]. To control the direct sound, Wave Front Synthesis [29, 30] has been introduced that applies amplitude and phase load (driving function) to linear and planar loudspeaker arrays based on the Kirchhoff-Helmholtz and Rayleigh integrals. While the Rayleigh integral applies as an exact formulation to the planar point-source arrays of three-dimensional Wavefield Synthesis (3D WFS), the stationary-phase approximation of the Kirchhoff-Helmholtz integral is required to obtain the driving function in the case of 2.5D WFS and its linear loudspeaker arrangements [31–36]. Due to practical restrictions, most applications have employed linear loudspeaker arrays as opposed to planar loudspeaker arrays, so far. The WFS theory has been shown to be applicable, more generally, to curved linear arrays in sound reinforcement to design their optimal curvature [37].

Recently, Holoplot¹ has released planar loudspeaker arrays, also referred to as matrix arrays, as commercial products for professional sound reinforcement applications, e.g. targeting 3D audio at live events [38, 39]. In particular,

¹ <https://holoplot.com/>

*Corresponding author: goelles@iem.at

This is an Open Access article distributed under the terms of the Creative Commons Attribution License (<https://creativecommons.org/licenses/by/4.0>), which permits unrestricted use, distribution, and reproduction in any medium, provided the original work is properly cited.

this application relies on FIR filters, gains, and delays to synthesize a virtual source emitting an optimal wavefront.

Although the available array literature in sound reinforcement outlines and summarizes the basic principles of planar arrays, it appears to lack a detailed definition of how to design the delay progression over an ideal continuous planar source in order to produce an adjustable sound pressure level decay across the audience area.

Based on the ideas that have been developed for continuously curved and phased line sources [11], recently, this paper presents a design equation for the continuous delay length profile of a phased planar source. The goal is to obtain an equalized direct-sound pressure level decay of $-6 \cdot \beta$ dB/dod. β is a design parameter whose value ranges typically from 0 and 0.5 yielding sources with distance decays between 0 dB/dod and -3 dB/dod. This essentially yields a (near-field) delay-and-sum beamformer design. Similar to a design based on linear arrays [11], broadband targets can be met when the planar array is tall and wide enough, and its drivers are spaced sufficiently close to each other.

The paper is structured as follows: Section 2.2 utilizes the stationary-phase approximation to get an estimate of the sound pressure level from the two-dimensional integral of the delayed Green's function over a plane. Constrained to target the roll-off $r^{-\beta}$, its result defines a second-order non-linear differential equation describing a continuous phasing across the plane in Section 2.4 that is expressed as a delay length and solved in Algorithms 1–3. Section 3.1 shows simulations of this continuously phased planar source as a proof of concept, and Section 3.3 presents simulations of a discrete source geometry with discrete phase load to discuss the effects of discretization and spatial aliasing. Section 4 presents the applicability to practical applications by comparing the results of the simulations with measurements using on a small prototype array.

2 Continuous phasing

Our objective is to evaluate the sound pressure p of a planar source fed by a progressive time delay τ given as length $w = c\tau$. The integral of a delayed Green's function $G(r) = \frac{e^{-ik(r+w)}}{4\pi r}$ over the horizontal source coordinate h and the vertical source coordinate v describes the resulting sound pressure,

$$p = \iint \frac{e^{-ik(r+w)}}{4\pi r} dh dv. \quad (1)$$

The imaginary unit yields $i^2 = -1$, the wave number is $k = \frac{2\pi f}{c}$, the speed of sound is $c = 343$ m/s, and f denotes the frequency.

2.1 Source geometry

The geometry of the planar source \mathbf{x}_s is described by

$$\mathbf{x}_s = \mathbf{x}_0 + h\mathbf{e}_h + v\mathbf{e}_v, \quad (2)$$

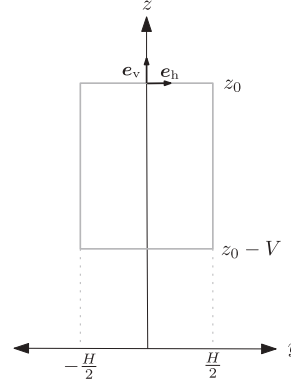


Figure 1. Geometry of a planar source (gray rectangle) with horizontal extent H and vertical extent V showing the unit vectors \mathbf{e}_h in horizontal direction and \mathbf{e}_v in vertical direction.

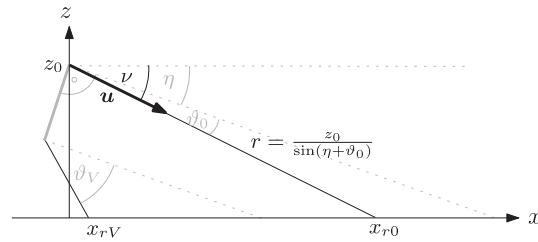


Figure 2. Side view of a planar source (solid gray) inclined by η showing the stationary-phase direction \mathbf{u} , cf. Section 2.3 and the beamforming angles $\vartheta_0 = -\arcsin \frac{\partial w}{\partial h} |_{v=0, h=0}$ on top and $\vartheta_V = -\arcsin \frac{\partial w}{\partial v} |_{v=-V, h=0}$ on the bottom of the source for a desired depth coverage between x_{r0} and x_{rV} , cf. Section 2.3.

where $\mathbf{e}_h = [0 \ 1 \ 0]^T$ is a unit-vector in horizontal direction and the source is symmetrical with regard to the x - z plane, $h \in [-\frac{H}{2}, \frac{H}{2}]$. v defines the source length V in vertical direction, i.e. $v \in [0, -V]$ and η in $\mathbf{e}_v = [\sin \eta \ 0 \ \cos \eta]^T$ is the vertical inclination of the source, cf. Figures 1 and 2. $\mathbf{x}_0 = [0 \ 0 \ z_0]^T$ is a point on the source that defines the height of the source, i.e. the vertical distance z_0 from the highest point of the source to the audience area that is assumed to lie on x - y plane, i.e. $z_r = 0$. The distance to the receiver at $\mathbf{x}_r = [x_r \ y_r \ 0]^T$ is

$$r = \|\mathbf{x}_s - \mathbf{x}_r\| = \sqrt{(\mathbf{x}_s - \mathbf{x}_r)^T (\mathbf{x}_s - \mathbf{x}_r)}. \quad (3)$$

2.2 Stationary-phase approximation

At high frequencies, the integrand of equation (1) oscillates rapidly. Therefore, the stationary-phase approximation is appropriate. Typically, designs should have a single stationary-phase point on the source plane which is characterized by a minimum of delay $\tau = \frac{w}{c}$ plus time of flight to the receiver. Equivalently, the first-order derivatives of the corresponding distances $r + w$ must vanish,

$\frac{\partial r}{\partial h} + \frac{\partial w}{\partial h} = 0$ and $\frac{\partial r}{\partial v} + \frac{\partial w}{\partial v} = 0$. Evaluation at this stationary-phase source point defines the approximate sound pressure

$$p \approx \frac{e^{-ik r - i \frac{\pi}{4} \text{sig}\{\mathbf{H}(r+w)\}}}{2k} \frac{1}{\sqrt{r^2 |\mathbf{H}(r+w)|}}, \quad (4)$$

where $\text{sig}\{\mathbf{H}(\cdot)\}$ denotes the signature of the Hessian matrix and $|\mathbf{H}(\cdot)|$ its determinant,

$$|\mathbf{H}(r+w)| = \begin{vmatrix} \frac{\partial^2 r}{\partial h^2} + \frac{\partial^2 w}{\partial h^2} & \frac{\partial^2 r}{\partial h \partial v} + \frac{\partial^2 w}{\partial h \partial v} \\ \frac{\partial^2 r}{\partial h \partial v} + \frac{\partial^2 w}{\partial h \partial v} & \frac{\partial^2 r}{\partial v^2} + \frac{\partial^2 w}{\partial v^2} \end{vmatrix} \\ = \left(\frac{\partial^2 r}{\partial h^2} + \frac{\partial^2 w}{\partial h^2} \right) \left(\frac{\partial^2 r}{\partial v^2} + \frac{\partial^2 w}{\partial v^2} \right) - \quad (5)$$

$$- \left(\frac{\partial^2 r}{\partial h \partial v} + \frac{\partial^2 w}{\partial h \partial v} \right)^2. \quad (6)$$

The derivatives of the distance are

$$\frac{\partial r}{\partial h} = \frac{\mathbf{e}_h^\top (\mathbf{x}_s - \mathbf{x}_r)}{r} \quad \frac{\partial r}{\partial v} = \frac{\mathbf{e}_v^\top (\mathbf{x}_s - \mathbf{x}_r)}{r}, \quad (7)$$

$$\frac{\partial^2 r}{\partial h^2} = \frac{1 - \left(\frac{\partial r}{\partial h} \right)^2}{r} \quad \frac{\partial^2 r}{\partial v^2} = \frac{1 - \left(\frac{\partial r}{\partial v} \right)^2}{r}, \quad (8)$$

$$\frac{\partial^2 r}{\partial h \partial v} = - \frac{\mathbf{e}_h^\top (\mathbf{x}_s - \mathbf{x}_r) \frac{\partial r}{\partial v}}{r^2} = - \frac{\frac{\partial r}{\partial h} \frac{\partial r}{\partial v}}{r}. \quad (9)$$

2.3 Stationary-phase direction and distance

The direction $\mathbf{u} = -\frac{\mathbf{x}_s - \mathbf{x}_r}{r} = [u_x \ u_y \ u_z]^\top$ points from a position (h, v) on the source to a receiver at $z_r = 0$. With the local coordinates (Eq. (2)) and derivatives (Eq. (7)), we can define its entries using $\frac{\partial r}{\partial h} = -\mathbf{e}_h^\top \mathbf{u} = -u_y$ and $\frac{\partial r}{\partial v} = -\mathbf{e}_v^\top \mathbf{u} = -\sin \eta u_x - \cos \eta u_z$. Furthermore, u_z, u_x follow from the quadratic equation $u_x^2 + u_y^2 + u_z^2 = 1$ as solved in [Appendix A](#),

$$\mathbf{u} = \begin{bmatrix} \sqrt{1 - u_y^2 - u_z^2} \\ -\frac{\partial r}{\partial h} \\ -\frac{\partial r}{\partial v} \cos \eta - \sin \eta \sqrt{1 - \left(\frac{\partial r}{\partial h} \right)^2 - \left(\frac{\partial r}{\partial v} \right)^2} \end{bmatrix}. \quad (10)$$

The stationary-phase conditions $\frac{\partial r}{\partial h} + \frac{\partial w}{\partial h} = 0$ and $\frac{\partial r}{\partial v} + \frac{\partial w}{\partial v} = 0$ yield a stationary-phase direction from (h, v)

$$\mathbf{u} = \begin{bmatrix} \sqrt{1 - u_y^2 - u_z^2} \\ \frac{\partial w}{\partial h} \\ \frac{\partial w}{\partial v} \cos \eta - \sin \eta \sqrt{1 - \left(\frac{\partial w}{\partial h} \right)^2 - \left(\frac{\partial w}{\partial v} \right)^2} \end{bmatrix} \quad (11)$$

targeting a receiver at $z_r = 0$ or $[0 \ 0 \ 1] [\mathbf{x}_s + r \mathbf{u}] = 0$. Therefore, the stationary-phase distance is

$$r = \frac{v \cos \eta + z_0}{-\frac{\partial w}{\partial v} \cos \eta + \sin \eta \sqrt{1 - \left(\frac{\partial w}{\partial h} \right)^2 - \left(\frac{\partial w}{\partial v} \right)^2}}. \quad (12)$$

2.4 Target coverage

Our goal is to find the delay lengths $w = c\tau$ for which the sound pressure

$$|p| \propto r^{-\beta} \quad (13)$$

decays by $-6 \cdot \beta$ dB per doubling to the distance on the audience area that lies at $z_r = 0$. In typical designs, values between 0 and 0.5 are used for the design parameter β . We introduce a gain g and desire for the equalized magnitude square,

$$4k^2 |p|^2 = \frac{1}{r^2 |\mathbf{H}(r+w)|} = \left(\frac{g}{r^\beta} \right)^2 \quad (14)$$

$$\text{with } r = \frac{v \cos \eta + z_0}{-\frac{\partial w}{\partial v} \cos \eta + \sin \eta \sqrt{1 - \left(\frac{\partial w}{\partial h} \right)^2 - \left(\frac{\partial w}{\partial v} \right)^2}}$$

With stationary-phase conditions inserted in equation (6), this yields a design equation for the delay length w ,

$$g^{-2} r^{2\beta} = \left[1 - \left(\frac{\partial w}{\partial h} \right)^2 + r \frac{\partial^2 w}{\partial h^2} \right] \cdot \left[1 - \left(\frac{\partial w}{\partial v} \right)^2 + r \frac{\partial^2 w}{\partial v^2} \right] - \left[-\frac{\partial w}{\partial h} \frac{\partial w}{\partial v} + r \frac{\partial^2 w}{\partial h \partial v} \right]^2. \quad (15)$$

For a given stationary-phase direction and distance specified by $\frac{\partial w}{\partial h}, \frac{\partial w}{\partial v}, r$, this differential equation is a single condition for three curvature parameters $\frac{\partial^2 w}{\partial h^2}, \frac{\partial^2 w}{\partial v^2}, \frac{\partial^2 w}{\partial h \partial v}$. There are many solutions to this underdetermined design equation.

However, it is reasonable to introduce some manual separation and control. The first substitution considers the control of the horizontal coverage. In typical practical applications, w and $\frac{\partial w}{\partial h}$ should be 0 for $h = 0$. At $v = 0$, w must increase to the sides of the source $|h| > 0$ for a convex wave front covering a horizontal target range. Replacing $r \frac{\partial^2 w}{\partial h^2}$ with $\left(\frac{\partial w}{\partial h} \right)^2 + ra$ removes $\frac{\partial^2 w}{\partial h^2}$ from the first bracket of equation (15) and defines a separate equation

$$\frac{\partial^2 w}{\partial h^2} = a + \frac{1}{r} \left(\frac{\partial w}{\partial h} \right)^2, \quad (16)$$

which yields a parabola $w \approx \frac{a^2 h}{2}$ for $\left(\frac{\partial w}{\partial h} \right)^2 \approx 0$. A positive a is used to control the horizontal coverage.

We consider a second substitution for the mixed derivative $\frac{\partial^2 w}{\partial h \partial v}$. It controls the amount by which the vertical

inclination changes up or down or with the lateral coordinate h . Replacing $r \frac{\partial^2 w}{\partial h \partial v}$ with $\frac{\partial w}{\partial h} \frac{\partial w}{\partial v} + r b$ removes $\frac{\partial^2 w}{\partial h \partial v}$ from the third bracket of equation (15) and defines the equation

$$\frac{\partial^2 w}{\partial h \partial v} = b + \frac{1}{r} \frac{\partial w}{\partial h} \frac{\partial w}{\partial v}. \quad (17)$$

Hereby, the off-diagonals of the Hessian are controlled by the parameter b , which influences the twist of the delay profile in the h - v plane. If $b = 0$, the mixed derivative $\frac{\partial^2 r}{\partial h \partial v}$ of equation (9) and $\frac{\partial^2 w}{\partial h \partial v}$ are equal, resulting in observation points for $v = 0$ that build a conical section on the listening area that is close to a circle. For $b > 0$ this arc curves faster towards $x = 0$. For $b < 0$ it curves less towards $x = 0$.

In the design equation (15), these substitutions turn the first bracket into $1 - r a$ and the last one into $r^2 b^2$. In addition to equations (16) and (17) a differential equation for the vertical curvature remains,

$$\frac{\partial^2 w}{\partial v^2} = \frac{1}{r} \left[\frac{g^{-2} r^{2\beta} + r^2 b^2}{1 + r a} + \left(\frac{\partial w}{\partial v} \right)^2 - 1 \right] \quad (18)$$

with $r = \frac{v \cos \eta + z_0}{-\frac{\partial w}{\partial v} \cos \eta + \sin \eta \sqrt{1 - \left(\frac{\partial w}{\partial h} \right)^2 - \left(\frac{\partial w}{\partial v} \right)^2}}$

2.5 Optimal tilting and depth range

Typical applications do not apply horizontal beamforming at $h = 0$ which implies that the first order derivative of w with regard to h must vanish, $\frac{\partial w}{\partial h} \Big|_{h=0} = 0$. The parameters of the horizontal progression are initially defined at this point, so we also specify the initial values for the vertical progression of the delay length here.

By choosing the farthest observation point x_{r0} , i.e. the last seat row, and the height of the source measured from its highest point downwards to the listening area at z_0 , the tilt angle on top of the source is defined by

$$v = \arctan \left(\frac{z_0}{x_{r0}} \right). \quad (19)$$

This tilt angle is composed linearly by the inclination of the source η and a beamforming angle \mathfrak{D}_0 on top of the source, $v = \eta + \mathfrak{D}_0$. The beamforming angle \mathfrak{D}_0 is related to the tangent of the delay length on top of the source via the sine that defines the initial condition for the first derivative of w with regard to v , cf. Figure 2,

$$\frac{\partial w}{\partial v} \Big|_{h=0, v=0} = -\sin(v - \eta). \quad (20)$$

2.6 Start gain parameter

Typical practical applications require a convex progression of the delay length. The zero point of curvature at the highest point of the source determines the maximum value of the gain parameter for a convex delay length profile,

$$g_{\max}^2 = \frac{r^{2\beta}}{\left[1 - \left(\frac{\partial w}{\partial v} \right)^2 \right] (1 + r a) - r^2 b^2}. \quad (21)$$

g defines how straight the starting curvature $\frac{\partial^2 w}{\partial v^2}$ should be. A large parameter yields small curvature and requires a longer curve length to hit the closest observation point x_{rv} . To find this parameter automatically for a given source length V , a fixed-point iteration has already been proposed in [40] to find the gain parameter g for a line source, fitting the curvature between a given nearest x_{rS} and farthest observation point x_{r0} . In our case, we solve the differential equation (18) for $h = 0$ and calculate the x -coordinate of the closest observed point in the audience \hat{x}_{rS} using the stationary-phase direction $\mathbf{x}_r = \mathbf{x}_s + r \mathbf{u}$ evaluated at $h = 0$ and $v = -V$,

$$\hat{x}_{rS} = x_s + r \sqrt{1 - u_z^2} \Big|_{h=0, v=-V}. \quad (22)$$

x_s is the x coordinate of the stationary source and u_z denotes the z coordinate of the stationary-phase direction \mathbf{u} . The algorithm starts with $g^2 = 0.99 g_{\max}^2$ and compares the resulting depth coverage $\hat{X} = x_{r0} - \hat{x}_{rS}$ to the desired depth coverage $X = x_{r0} - x_{rS}$, yielding an exponent parameter $\alpha_1 = \frac{\hat{X}}{X}$ that is used to update the parameter g ,

$$g^2 \leftarrow g_{\max}^2 \left(\frac{g^2}{g_{\max}^2} \right)^{\alpha_1}. \quad (23)$$

Whenever the exponent parameter α_1 is smaller than unity, it increases the gain parameter g resulting in a smaller vertical curvature which happens for an audience range \hat{X} that is too long. α_1 becomes large, if the resulting closest observation point is farther away. Therefore g^2 must be decreased. Furthermore, we introduce κ_1 to accelerate convergence in $\alpha_1 = \left(\frac{\hat{X}}{X} \right)^{\kappa_1}$. We found that $\kappa_1 = 3$ is sufficiently fast to meet X within $\pm 1\%$ in a little number of iterations.

2.7 Horizontal coverage and concaveness parameter

The same fixed-point iteration is applied to find optimal values for the parameters a and b for a desired horizontal coverage, defined by an outermost point with x -coordinate X and y -coordinate Y . Its corresponding stationary-phase point on the source is at $h = \frac{H}{2}$ and $v = 0$. Typical designs require $\frac{\partial w}{\partial h} = 0$ at $h = 0$ defining a positive non-zero value $a > 0$ in $\frac{\partial^2 w}{\partial h^2} = \frac{1}{r} \frac{\partial w}{\partial h} + a$. As the goal is to reach an appropriate horizontal curvature, a_{\min} is set to 0.3. The algorithm starts with $a = 1.2 \cdot a_{\min} = 0.36$ and compares the resulting width \tilde{Y} ,

$$\tilde{Y} = y_s + r \frac{\partial w}{\partial h} \Big|_{h=\frac{H}{2}, v=0}, \quad (24)$$

to the desired width Y , where y_s is the y coordinate of the source. The comparison of the desired width to the observed width yields the parameter $\alpha_2 = \left(\frac{Y}{\tilde{Y}} \right)^{\kappa_2}$ that is used to update the parameter a ,

Algorithm 1. Find parameters a and b .

```

procedure PARAMAB( $x_{r0}$ ,  $z_0$ ,  $H$ ,  $V$ ,  $N$ ,  $\eta$ ,  $Y$ )
constant:
  maxit = 1000
   $\kappa_2 = 0.2$ 
   $\kappa_3 = 0.2$ 
   $\Delta v = -V/N$ 
   $\Delta h = \Delta v$ 
   $v = f(x_{r0}, z_0)$                                 according to Eq. (19)
   $\mathfrak{S}_0 = v - \eta$ 
   $M = -\frac{H}{2\Delta v} + 1$ 
   $r = \frac{z_0}{\sin(\eta + \vartheta_0)}$                                 according to Fig. 2
   $a_{\min} = 0.3$ 
   $b_{\min} = 0.01$ 
initialization:
   $a = 1.2 \cdot a_{\min}$ 
   $b = 1.2 \cdot b_{\min}$ 
   $W = \text{zeros}(M, 1)$ 
   $Wh = \text{zeros}(M, 1)$ 
   $Wv = \text{zeros}(M, 1)$ 
   $Wv[1] = -\sin \mathfrak{S}_0$ 
   $Whh = a$ 
repeat
for  $m = 1 \dots M$  do
   $W[m+1] \leftarrow W[m] + Wh[m] \Delta h$                 num. int.
   $v = n \Delta v$ 
   $r \leftarrow f(v, \eta, Wh[m], Wv[m], z_0)$             cf. Eq. (12)
   $Whh = \frac{Wh[m]^2}{r} + a$                             cf. Eq. (16)

   $Whv = \frac{Wh[m] Wv[m]}{r} + b$                             cf. Eq. (17)
   $Wv[m+1] = Wv[m] + Whv \Delta h$                     num. int.
   $Wh[m+1] = Whh \Delta h$                             num. int.
end for
 $\tilde{Y} \leftarrow \frac{H}{2} - r Wh[m]$ 
 $uz \leftarrow -Wv[m, n] \cos \eta + \sqrt{1 - Wv[m]^2 - Wh[m]^2} \sin \eta$ 
 $\tilde{X} \leftarrow r \sqrt{1 - Wh[m]^2 - uz^2}$ 
 $\alpha_2 \leftarrow \left(\frac{z}{\tilde{Y}}\right)^{\kappa_2}$ 
 $\alpha_3 \leftarrow \left(\frac{z}{\tilde{X}}\right)^{\kappa_3}$ 
 $a \leftarrow a_{\min} \left(\frac{a}{a_{\min}}\right)^{\alpha_2}$ 
 $b \leftarrow b_{\min} \left(\frac{b}{b_{\min}}\right)^{\alpha_3}$ 
until  $0.99 \leq \frac{\tilde{X}}{X} \leq 1.01$  and  $0.99 \leq \frac{\tilde{Y}}{Y} \leq 1.01$  or  $it > \text{maxit}$ 
return  $a, b$ 
end procedure

```

$$a \leftarrow a_{\min} \left(\frac{a}{a_{\min}} \right)^{\alpha_2}. \quad (25)$$

The same procedure is applied to update the parameter b . The observation points build a conical section for $b = 0$. This section gets warped when choosing other values for b or modifying the outermost observation point for $h = \frac{H}{2}$ and $v = 0$. For the fixed-point algorithm, we chose a minimum value of $b_{\min} = 0.01$ and an initial value of $b = 1.2 \cdot b_{\min} = 0.012$. The corresponding x coordinate of the outermost observation point is

$$\tilde{X} = r \sqrt{1 - u_y^2 + u_z^2} \Big|_{h=\frac{H}{2}, v=0}, \quad (26)$$

and the comparison to the desired x coordinate yields $\alpha_3 = \left(\frac{\tilde{X}}{X}\right)^{\kappa_3}$ to update the parameter b ,

Algorithm 2. Find parameter g .

```

procedure PARAMG( $x_{r0}$ ,  $x_{rV}$ ,  $z_0$ ,  $H$ ,  $V$ ,  $N$ ,  $\eta$ ,  $\beta$ ,  $a$ ,  $b$ ,  $X$ )
constant:
   $\kappa_1 = 3$ 
  maxit = 50
   $\Delta v = -V/N$ 
   $v = f(x_{r0}, z_0)$                                 according to Eq. (19)
   $\vartheta_0 = v - \eta$                                     according to Fig. 2
   $r = \frac{z_0}{\sin(\eta + \vartheta_0)}$ 
   $X = x_{r0} - x_{rV}$ 
initialization:
   $W = \text{zeros}(N, 1)$ 
   $Wh = \text{zeros}(N, 1)$ 
   $Wv = \text{zeros}(N, 1)$ 
   $Wv[1] = -\sin \mathfrak{S}_0$ 
   $Whh = a$ 
   $g_{\max} = f(z_0, \eta, Wv[1], Wh[1])$ 
   $g = \sqrt{0.99 g_{\max}^2}$ 
repeat
for  $n = 1 \dots N$  do
   $W[n+1] \leftarrow W[n] + Wv[n] \Delta v$                 num. int.
   $v = n \Delta v$ 
   $r \leftarrow f(v, \eta, Wh[n], Wv[n], z_0)$             cf. Eq. (12)
   $Wv[n] \leftarrow f(r, g, \beta, a, b, Wv[n], Wh[n])$     cf. Eq. (18)
   $Wv[n+1] \leftarrow Wv[n] + Wv[n] \Delta v$             num. int.
end for
 $uz \leftarrow -Wv[n] \cos \eta + \sqrt{1 - Wv[n]^2 - Wh[n]^2} \sin \eta$ 
 $\tilde{X} \leftarrow x_{r0} + V \sin \eta - r \sqrt{1 - Wh[n]^2 - Wv[n]^2}$ 
 $\alpha_1 \leftarrow \left(\frac{X}{\tilde{X}}\right)^{\kappa_1}$ 
 $g \leftarrow \sqrt{g_{\min} \left(\frac{g}{g_{\min}}\right)^{\alpha_1}}$ 
until  $0.99 \leq \frac{\tilde{X}}{X} \leq 1.01$  or  $it > \text{maxit}$ 
return  $g$ 
end procedure

```

$$b \leftarrow b_{\min} \left(\frac{b}{b_{\min}} \right)^{\alpha_3}. \quad (27)$$

Furthermore, we use the constants $\kappa_2 = 0.2$ and $\kappa_3 = 0.2$ to reach convergence in an acceptable number of iterations meeting X and Y within $\pm 1\%$.

3 Simulation study

Similarly to the theory of line sources [11], we apply step-wise updates to solve the differential equation (18) numerically as outlined in Algorithm 3. As we assume symmetry, the procedure is applied for $h \in [0, \frac{H}{2}]$ and the solution is then mirrored. The step sizes Δv and Δh should be appropriately small to solve the differential equation accurately by choosing a large N . Algorithm 1 finds optimal values for the parameters a and b , defining the horizontal coverage, while Algorithm 2 is then used to get an appropriate value for the gain parameter g that fits the desired depth of the audience area.

For our simulation study we assume a listening area of $10 \text{ m} \times 10 \text{ m}$ with the closest observation point at $x_{rV} = 1.5 \text{ m}$. The simulations show the result of summing ideal point sources described by the Green's function, that are positioned at the continuous source in 1 mm intervals. This summation is performed for frequencies ranging from 50 Hz

Algorithm 3. Find delay lengths.

```

procedure CURVING( $x_0, z_0, H, V, N, \eta, \beta, g, a, b$ )
  constant:
     $\Delta v = -V/N$ 
     $\Delta h = \Delta v$ 
     $v = f(x_0, z_0)$  according to Eq. (19)
     $\vartheta_0 = v - \eta$ 
     $M = -\frac{H}{2\Delta v} + 1$ 
     $r = \frac{z_0}{\sin(\eta + \vartheta_0)}$  according to fig. 2
  initialization:
     $W = \text{zeros}(M, N)$ 
     $Wh = \text{zeros}(M, N)$ 
     $Wv = \text{zeros}(M, N)$ 
     $Wv[1] = -\sin\vartheta_0$ 
     $Whh = a$ 
  for  $n = 1 \dots N$  do
     $W[m, n + 1] \leftarrow W[m, n] + Wv[m, n] \Delta v$  num. int.
     $v = n \Delta v$ 
     $r \leftarrow f(v, \eta, Wh[m, n], Wv[m, n], z_0)$  cf. Eq. (12)
     $Wvv \leftarrow f(r, g, \beta, a, b, Wv[m, n])$  cf. Eq. (18)
     $Wv[m, n + 1] \leftarrow Wv[m, n] + Wvv \Delta v$  num. int.
  end for
  for  $m = 1 \dots M$  do
    for  $n = 1 \dots N$  do
       $W[m + 1, n] \leftarrow W[m, n] + Wh[m, n] \Delta h$  num. int.
       $v = n$ 
       $\Delta v \ r \leftarrow f(v, \eta, Wh[m, n], Wv[m, n], z_0)$  cf. Eq. (12)
       $Whh = \frac{Wh[m, n]^2}{r} + a$  cf. Eq. (16)
       $Whv = \frac{Wh[m, n] Wv[m, n]}{r} + b$  cf. Eq. (17)
       $Wv[m + 1, n] \leftarrow Wv[m, n] + Whv \Delta h$  num. int.
       $Wh[m + 1, n] \leftarrow Wh[m, n] + Whh \Delta h$  num. int.
    end for
  end for
  return  $W$ 
end procedure

```

to 20 kHz with a logarithmic third-octave resolution of 27 points. To show broadband sound pressure maps over the listening area, the results are A-weighted [41] and summarized. Since the radiation is symmetrical, the maps are divided into two parts to show the influence of different values of b in a single map.

3.1 Continuously phased planar sources

The differential equation (18) was solved with uniform parameters $z_0 = 1.35$ m, inclination angle $\eta = 0^\circ$ and vertical source length $V = 0.656$ m which yields the number elements $N = 657$ for a step size $\Delta v = 1$ mm. The vertical source length was chosen to fit the length of eight mini line-array elements [42] which are used later in the measurements. For H , we choose 0.572 m so that the total source width corresponds to the length of seven mini line-array elements. The farthest point of observation in y direction is chosen to be at $y_r = 5$ m while in x direction it is $x_r = 10$ m. To show the influence of the parameter b , simulations are performed using $b = 0$ (digonalized Hessian matrix) on the one hand and on the other hand, by using an optimized value of b to reach an outermost observation point at $\mathbf{x}_r = [3.5 \ 5 \ 0]^T$. Applying Algorithm 1 yields $b = 0.2531$.

Figures 8–10 show the delay length profiles $w = c\tau$ using different decay parameters β . Comparing the delay contours for different decay parameters, it is noticeable that higher values of the decay parameter have rounder contours as the outcome of the source has to become more curved. Therefore, higher values of β also require higher delays.

Figure 11–13 show the equalized A-weighted sound pressure maps of the continuously phased planar sources with different decay parameters β . For equalization, we use a filter whose magnitude rises by 6 dB/octave to compensate the red frequency response of a planar source composed by ideal point sources, cf. Appendix B. As the integral of equation (1) and the stationary-phase approximation assume infinite integral bounds, the sound pressure level rolls off by -6 dB/dod for points of observation which lie outside the desired coverage area.

Considering the effect of the parameter b , higher values results in a wider coverage. As mentioned above, the observation points for $b = 0$ build a conical section on the listening area. This section gets warped for higher values of b , which can also be seen in the contours of the maps. Furthermore, higher values of b increase the amount of delay that is necessary.

Ideal phased line sources exhibit a rotationally symmetrical radiation pattern on the listening area without horizontal directivity if they are mounted straight at the wall ($\eta = 0^\circ$). Tilting these optimum phased line sources causes the radiation to become horizontally directional, limiting the horizontal coverage. By contrast, the horizontal range for planar arrays can be set using the parameter a , even for planar arrays mounted on the wall, $\eta = 0^\circ$, cf. Figure 14–16. Unlike phased line sources, the horizontal range is not a direct consequence of the source inclination; rather, it may be adjusted independently of it. In practice, line sources are employed with double bass arrangements and waveguides for higher frequencies to control the horizontal directivity.

3.2 Discretization of geometry

Later, we use the miniature line array [42] with $8.2 \text{ cm} \times 10 \text{ cm} \times 10 \text{ cm}$ 3D-printed enclosures and 2.5 inch broadband drivers to perform a sample measurement. Therefore, we choose the dimensions of the drivers for discretizing the geometry of the planar source. We assume that the planar source is composed by an array of 7×8 elements and simulate a single driver by a circular area with 3 cm radius leaving gaps in between the elements, cf. Figure 3. To comply with our simulations done in [11, 42, 43], the radius of these discrete elements gets shorter by the fifth power of the simulated frequency. For 50 Hz the radius is 3 cm, for 20 kHz it is 1.8 cm.

Figures 17–19 show the equalized A-weighted sound pressure maps over the desired area. For equalization, we use the filter that compensates the red frequency response, cf. Appendix B, but keep the magnitude constant above the spatial aliasing frequency for which endfire-radiation occurs whenever $\lambda < 8.2$ cm, i.e. $f_{\text{pat.al.}} = 4.2$ kHz. In comparison to the results of the continuous source, the main difference

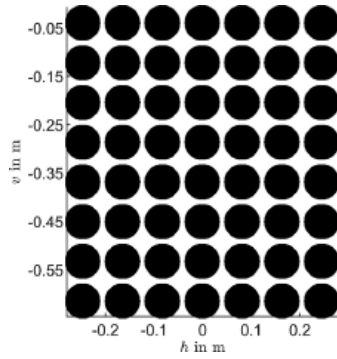


Figure 3. Discretization of geometry of a phased planar source.

lies in the vicinity of the source where spatial aliasing has a high influence on the sound pressure. We denote that the contours are little narrower compared to those of the continuous source. Due to spatial aliasing, higher sound pressures are also to be expected for observation points which lie outside the desired coverage area. [Figure 4](#) compares the radiation of a planar source with discretized geometry in 0 dB/dod configuration for 1 kHz and 6 kHz. Considering the maps for 1 kHz, it is noticeable that also for the continuous source grating lobes are observed. However, the maps of the continuous source and the discretized source are comparable. For 6 kHz, where spatial aliasing occurs for the discrete source, it is seen that the grating lobes, that lie outside the desired coverage area, are more pronounced and therefore higher sound pressure levels for close observation points $x_r < 0.5$ m are denoted.

3.3 Discretization of phase

Both the phase load and the source geometry are typically discrete in practical applications. Just like a smoothing filter in image processing [44], we apply a Gaussian filter as discretization kernel, to get an appropriate delay length w for a single element,

$$K[m, n] = e^{-\frac{m^2 + n^2}{2\sigma^2}}. \quad (28)$$

σ^2 denotes the standard deviation and determines the width of the Gaussian kernel. An average value for the delay length that is employed as a discrete value is obtained by summing the continuous delay length values w_d belonging to a discrete loudspeaker element, weighted by the discretization kernel $H[h, v]$,

$$\tilde{w}_d = \text{rd} \left\{ \frac{\sum_m \sum_n w_d[m, n] K[m, n]}{\sum_m \sum_n K[m, n]} \frac{f_s}{c} \right\} \frac{c}{f_s}, \quad (29)$$

whereby $c = 343$ m/s denotes the speed of sound. For our simulations, the discrete delay length is rounded to be realized with integer samples at $f_s = 48$ kHz. Normalization is

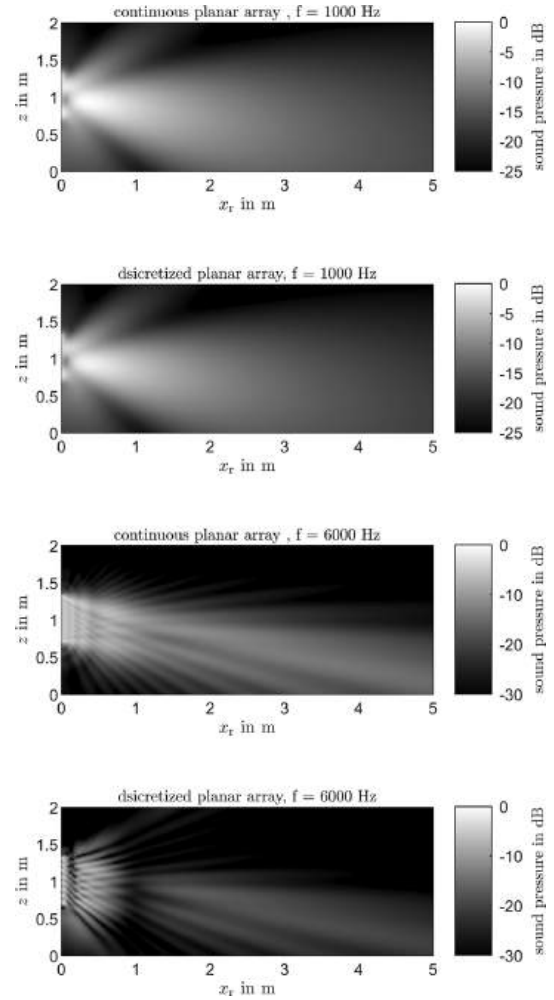


Figure 4. Side view of simulated sound pressure level maps at $y=0$ for phased planar arrays in 0 dB/dod configuration comparing the continuous source to a source with discretized geometry for $f = 1$ kHz and $f = 6$ kHz.

necessary to prevent the delay length from being distorted whenever $\sum_m \sum_n K[m, n] \neq 1$. In our case the diameter of a discrete element is 0.082 m with a resolution of 1mm which requires a discretization kernel of size 82×82 . $\sigma = 0.025$ is found to be a useful value that lets the kernel fade out sufficiently towards the outside of a discrete element.

[Figure 17–19](#) show the A-weighted measured level maps of the planar source with discrete geometry and phase load. Compared to the simulations before, the results for $b = 0$ differ in that lower sound pressure values are denoted for more distant and more outlying observation points, as well as that the contours are narrower. The results for the optimized value of b indicate that the curvature of the delay

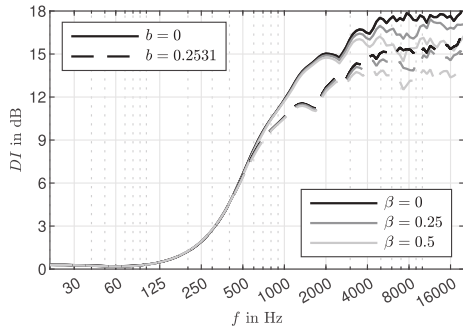


Figure 5. Directivity index of phased planar sources with $b = 0$ (solid lines) and $b = 0.2531$ (dashed lines) for different decay parameters β .

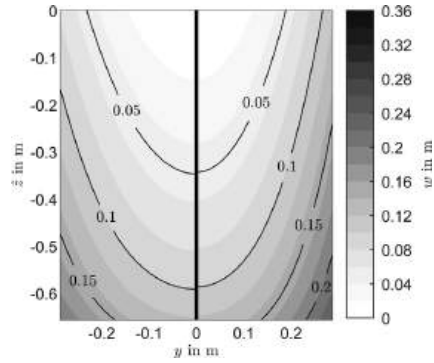


Figure 8. Delay lengths for a continuously phased planar source ($\eta = 0^\circ$), $b = 0$ (left) and $b = 0.2531$ (right) for $\beta = 0$ (0 dB/dod).

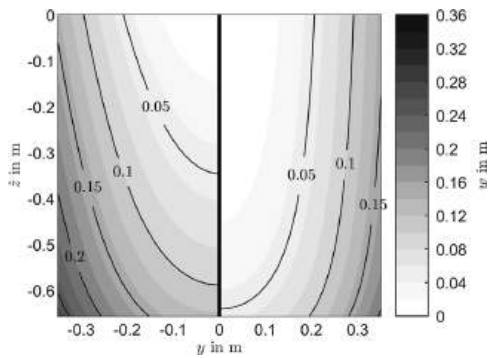


Figure 6. Delay lengths of a continuous phased planar source mounted straight on the wall (left, $\eta = 0^\circ$) compared to the delay lengths of a continuous phase planar source inclined by $\eta = 6.5^\circ$ with $\beta = 0$ and $b = 0.3324$.

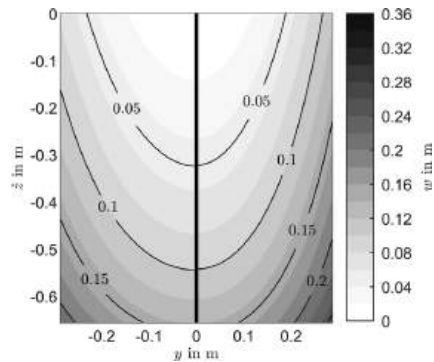


Figure 9. Delay lengths for a continuously phased planar source ($\eta = 0^\circ$), $b = 0$ (left) and $b = 0.2531$ (right) for $\beta = 0.25$ (-1.5 dB/dod).

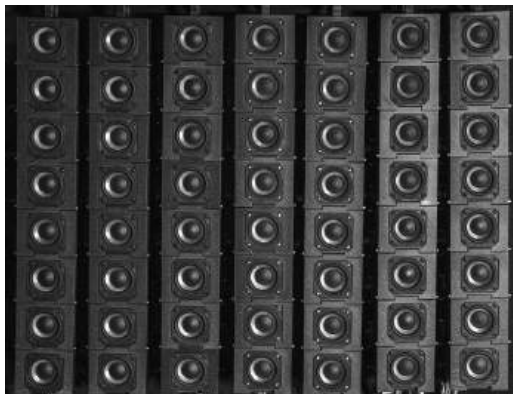


Figure 7. Experimental setup using line array enclosures of [42] mounted as 7×8 element planar array.

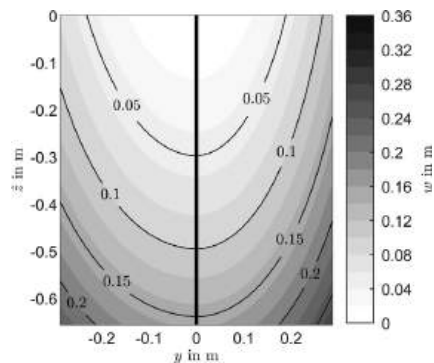


Figure 10. Delay lengths for a continuously phased planar source ($\eta = 0^\circ$), $b = 0$ (left) and $b = 0.2531$ (right) for $\beta = 0.5$ (-3 dB/dod).

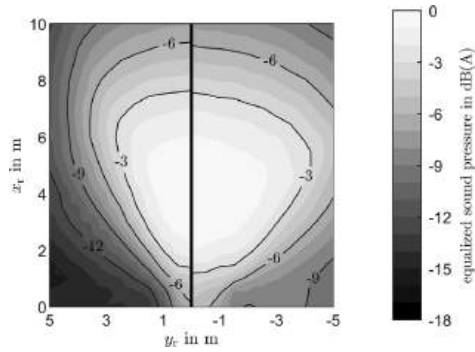


Figure 11. Map and contours of the simulated A-weighted sum of a continuous phased planar source ($\eta = 0^\circ$), $b = 0$ (left) and $b = 0.2531$ (right) for $\beta = 0$ (0 dB/dod).

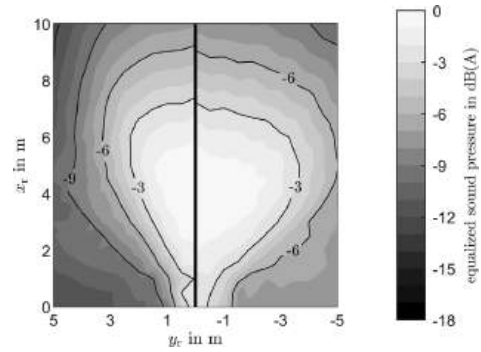


Figure 14. Map and contours of the simulated A-weighted sum of a discrete phased planar source ($\eta = 0^\circ$) with continuous delay profile, $b = 0$ (left) and $b = 0.2531$ (right) for $\beta = 0$ (0 dB/dod).

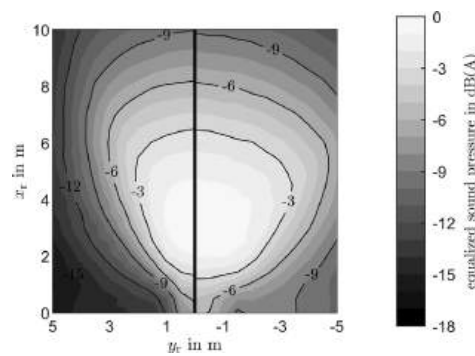


Figure 12. Map and contours of the simulated A-weighted sum of a continuous phased planar source ($\eta = 0^\circ$), $b = 0$ (left) and $b = 0.2531$ (right) for $\beta = 0.25$ (-1.5 dB/dod).

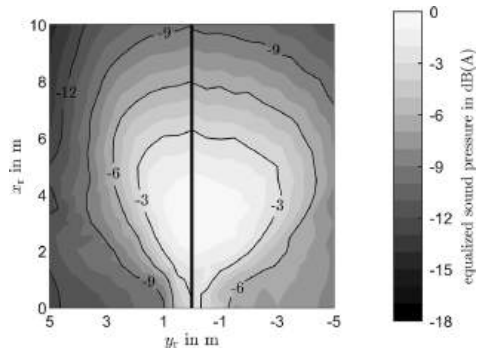


Figure 15. Map and contours of the simulated A-weighted sum of a discrete phased planar source ($\eta = 0^\circ$) with continuous delay profile, $b = 0$ (left) and $b = 0.2531$ (right) for $\beta = 0.25$ (-1.5 dB/dod).

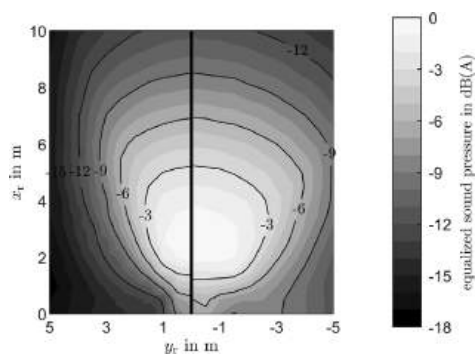


Figure 13. Map and contours of the simulated A-weighted sum of a continuous phased planar source ($\eta = 0^\circ$), $b = 0$ (left) and $b = 0.2531$ (right) for $\beta = 0.5$ (-3 dB/dod).

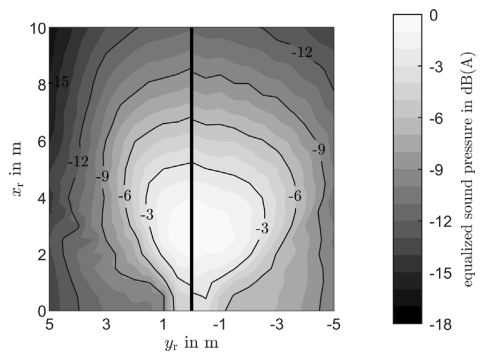


Figure 16. Map and contours of the simulated A-weighted sum of a discrete phased planar source ($\eta = 0^\circ$) with continuous delay profile, $b = 0$ (left) and $b = 0.2531$ (right) for $\beta = 0.5$ (-3 dB/dod).

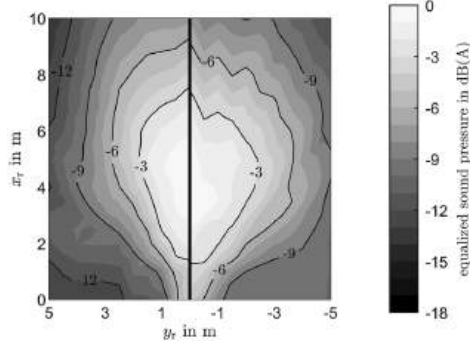


Figure 17. Map and contours of the simulated A-weighted sum of a discrete phased planar source ($\eta = 0^\circ$) with discretized delay profile, $b = 0$ (left) and $b = 0.2531$ (right) for $\beta = 0$ (0 dB/dod).

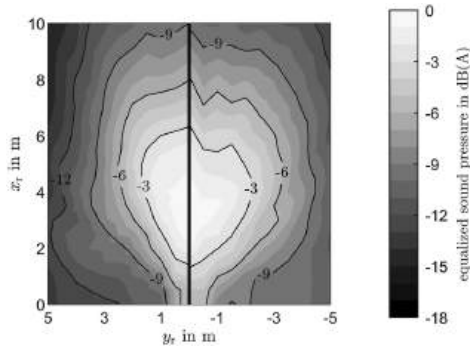


Figure 18. Map and contours of the simulated A-weighted sum of a discrete phased planar source ($\eta = 0^\circ$) with discretized delay profile, $b = 0$ (left) and $b = 0.2531$ (right) for $\beta = 0.25$ (-1.5 dB/dod).

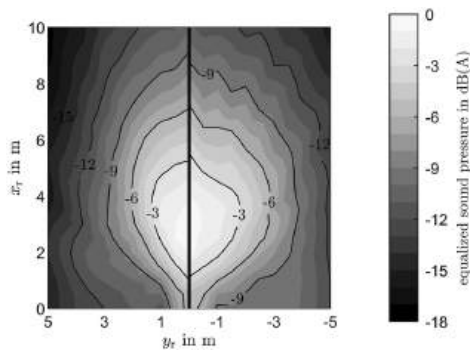


Figure 19. Map and contours of the simulated A-weighted sum of a discrete phased planar source ($\eta = 0^\circ$) with discretized delay profile, $b = 0$ (left) and $b = 0.2531$ (right) for $\beta = 0.5$ (-3 dB/dod).

length cannot be achieved with the coarse discretization. The continuous delay lengths of the outermost element on the bottom of the source lie in a range between 0.156 m and 0.24 m for $\beta = 0$. The discrete delay length, 0.2 m, represents the curvature in this area very poorly, resulting in highly pronounced discretization effects. These effects could be minimized by using smaller drivers and smaller driver spacing correspondingly which would require a two-way system in practice. Figures 20–22 show the results of a simulation using half driver spacing, i.e. 0.041 m. These are comparable to the results of the simulation with discrete geometry only. For the majority of the listening area, only minor differences to the simulation with discrete geometry can be noted.

A simpler solution is achieved by tilting the source which also results in smaller delay lengths to be realised, as performed later for the sample measurement. Furthermore, a tilt is preferable in practice because better coverage can be expected in high frequencies if the source is tilted towards the audience area, due to the directivity of the drivers.

3.4 Directivity

Another parameter to be considered beside the coverage, is the frequency-dependent directivity ratio $Q(f)$ and the frequency-dependent directivity index $DI(f) = 10 \lg Q(f)$,

$$Q(f) = \frac{\max\{|p(f, \theta, \phi)|^2\}}{\frac{1}{4\pi} \int_0^{2\pi} \int_0^\pi |p(f, \theta, \phi)|^2 \sin \theta \, d\theta \, d\phi}. \quad (30)$$

$\max\{|p(f, \theta, \phi)|^2\}$ denotes the maximum squared sound pressure for the observed frequency evaluated at azimuth ϕ and elevation θ . Figure 5 shows the directivity index of phased planar sources for both values of b . As before, the simulation is based on summing the sound pressure of ideal point sources placed in 1 mm intervals on the continuous planar source. To comply with previous work [11], the simulation was done in 10 m distance to the source. It is noticeable that for frequencies below 500 Hz the radiation of the source is independent of any settings of β and b . For frequencies below 250 Hz the radiation gets omnidirectional as the dimensions are too small. Above 500 Hz, the curves for different values of b run differently. Higher values of b result in lower values of the directivity index as the beam gets broader to cover a larger area.

4 Sample measurement

4.1 Experimental setup

To verify the theory in practice, impulse response measurements of a planar array consisting of 7×8 elements were taken using the miniature line-array enclosures presented in [42], cf. Figure 7. By contrast to the simulations before, the array elements cannot be placed as dense horizontally as

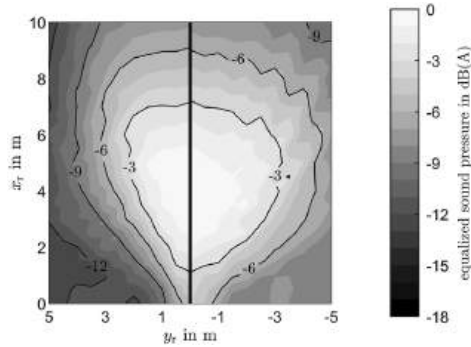


Figure 20. Map and contours of the simulated A-weighted sum of a discrete phased planar source ($\eta = 0^\circ$) with discretized delay profile, $\beta = 0$ (0 dB/dod), $b = 0$ (left) and $b = 0.2531$ (right) using a smaller discretization.

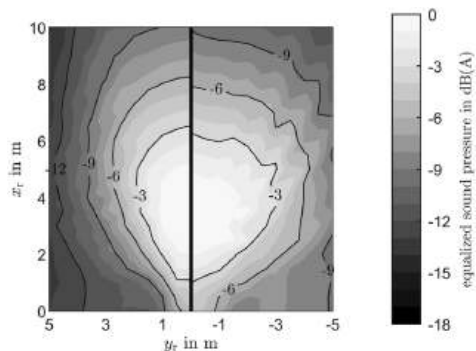


Figure 21. Map and contours of the simulated A-weighted sum of a discrete phased planar source ($\eta = 0^\circ$) with discretized delay profile, $\beta = 0.25$ (-1.5 dB/dod), $b = 0$ (left) and $b = 0.2531$ (right) using a smaller discretization.

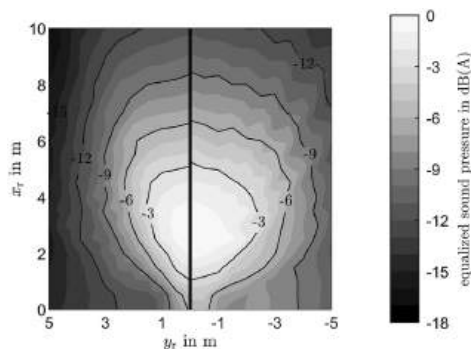


Figure 22. Map and contours of the simulated A-weighted sum of a discrete phased planar source ($\eta = 0^\circ$) with discretized delay profile, $\beta = 0.5$ (-3 dB/dod), $b = 0$ (left) and $b = 0.2531$ (right) using a smaller discretization.

they are vertically because the enclosures are wider and there are additional screws on the sides that are used for adjusting the line-array splay angles. In order to reduce the amount of required delay, an inclination of $\eta = 6.5^\circ$ was applied. Figure 6 shows the comparison of the continuous delay lengths between a source that is mounted flat on the wall and a source that is inclined by $\eta = 6.5^\circ$. The inclination significantly decreases the delays in vertical direction. At the lower end of the source, this results in a 6.85 cm shorter delay length, which corresponds to approximately 10 samples at a sampling rate of $f_s = 48$ kHz.

The measurements were conducted at the IEM CUBE, a 10.2 m \times 12 m studio with $T_{30} \approx 0.5$ s. To focus on the direct sound behavior, the impulse responses were truncated to the first 300 samples (6.25 ms at $f_s = 48$ kHz).

We recorded the responses of a 2 s sweep over a grid of 9 m \times 6 m with a resolution of 0.5 m in order to capture the position-dependent direct sound radiation of the planar array. Each element was measured individually to allow the possibility of adding delays later in the analysis. To avoid floor reflections influencing the measurements, we used pressure zone microphones, AKG PZM 30D, which were positioned on the floor. For each element, we applied the filter proposed in [42], in order to make the frequency response of a single element flat. Furthermore, we used the filter that compensates the red frequency response of a planar source composed by point sources until the frequency for which endfire radiation occurs, $f_{\text{spat.al.}} = 3.1$ kHz. The results are averaged in third octaves and the curves are plotted as A-weighted sum.

4.2 Results

Figures 23–25 show the measured equalized A-weighted sound pressure level maps for the phased planar sources with different decay parameters β . As in the simulation, the results for $b = 0$ are shown on the left while the results for the optimized value of b to reach the outermost observation point at $\mathbf{x}_r = [3.5 \ 5 \ 0]^T$ are shown on the right ($b = 0.3324$).

Considering the plots for $b = 0$, the width of the contours are similar to those of the simulations of the planar sources with discrete geometry only. The main difference lies in farther points of observation where jagged contours are visible. These are an effect of the discretization of geometry and phase as well as the directivity of the used drivers. Nevertheless, it can be seen that the desired level distribution is achieved with the coarse discretization when applying an inclination.

For $b = 0.3324$, similar discretization effects can be seen. Comparing to the simulation results of discrete geometry and phase load, it should be noted that the measurements results come closer to the simulation results of discrete geometry only. Also here, the advantage of the tilted source becomes apparent, as it requires less delay to achieve the desired level supply. However, further improvements can be expected by using a multi-way system, where smaller tweeters can be used and placed closer together.

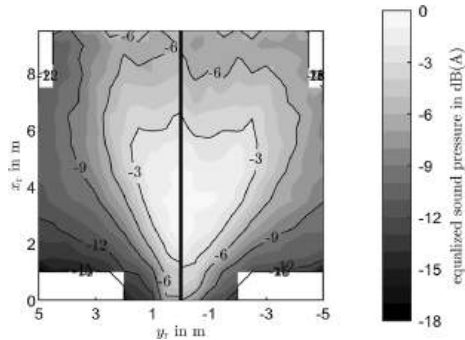


Figure 23. Map and contours of the measured A-weighted sum of a discrete phased planar source ($\eta = 6.5^\circ$) with $\beta = 0$ (0 dB/dod) using $b = 0$ (left) and $b = 0.3324$ (right).

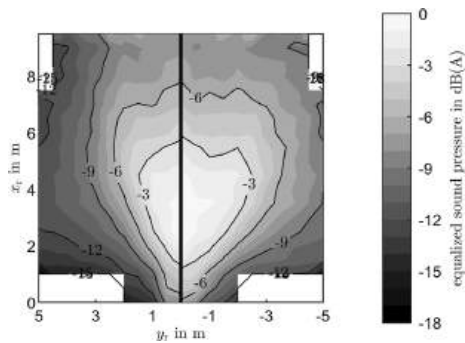


Figure 24. Map and contours of the measured A-weighted sum of a discrete phased planar source ($\eta = 6.5^\circ$) with $\beta = 0.25$ (−1.5 dB/dod) using $b = 0$ (left) and $b = 0.3324$ (right).

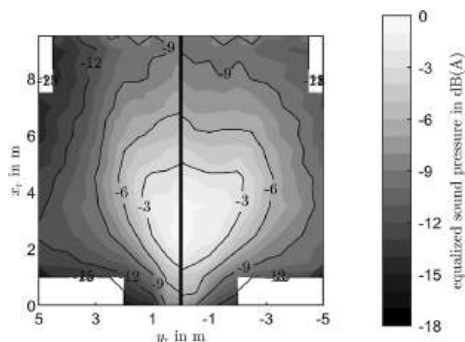


Figure 25. Map and contours of the measured A-weighted sum of a discrete phased planar ($\eta = 6.5^\circ$) source with $\beta = 0.5$ (−3 dB/dod) using $b = 0$ (left) and $b = 0.3324$ (right).

5 Conclusion

With the aim of achieving sound pressure levels on the listening plane rolling-off by $6 \cdot \beta$ dB/dod, this paper proposed a design method for the delay load of phased planar sources. In contrast to a vertical phased line, another objective was to be able to variably adjust the horizontal coverage of the source. Starting from the integral of a Green's function along two dimensions, stationary-phase approximation was applied to obtain a second-order non-linear differential equation of the delay length profile. This equation is under-determined in terms of the three curvature parameters. To solve it, a manual separation into three design equations is proposed.

Simulations of the continuous source based on the summation of point sources showed the optimal $-6 \cdot \beta$ dB/dod maps. Furthermore, the simulation shows the effects caused by discretization of the geometry and also by discretization of the phase load that is necessary in practice but also outlined the limits of a coarse discretization. The simulations therefore indicate that acceptable broadband results can be achieved with smaller drivers and smaller driver spacing. It has been shown that an inclined source will reduce the amount of delay for easier practical applicability. Measurements of a prototypical setup showed the practical feasibility.

Future work should consider (virtual) listening experiments with different β profiles that compare the phased planar arrays with line arrays for medium-sized surround sound reinforcement for 50–250 listeners. Moreover, waveguide solutions should be investigated to improve radiation with reduced spatial aliasing. In order to reduce the spatial aliasing even further, multi-way systems could be investigated in which the smaller tweeters are spaced more closely. Furthermore, the impact of equalizing strategies for individual elements have to be considered.

Funding

Our research was funded by the Austrian Science Fund (FWF) under project number P 35254-N, Envelopment in Immersive Sound Reinforcement (EnImSo).

Conflicts of interest

The authors declared no conflicts of interests.

Data availability statement

The research data associated with this article are included in the supplementary material of this article [45].

References

1. W. Ahnert, D. Noy: Sound reinforcement for audio engineers, Taylor Francis Ltd, London, 2023.
2. C. Heil, M. Urban: Sound fields radiated by multiple sound sources arrays, in: 92nd AES Convention, Vienna, Austria, 24–27 March, 1992.
3. D.L. Smith: Discrete-element line arrays—their modeling and optimization, Journal of the Audio Engineering Society 45, 11 (1997) 949–964.

4. M. Urban, C. Heil, P. Bauman: Wavefront sculpture technology, *Journal of the Audio Engineering Society* 51, 10 (2003) 912–932.
5. M.S. Ureda: Analysis of loudspeaker line arrays, *Journal of the Audio Engineering Society* 52, 5 (2004) 467–495.
6. A. Thompson: Line array splay angle optimisation, in: *Reproduced Sound 22 Conference*, Oxford, 3–4 November, 2006.
7. A. Thompson, J. Baird, B. Webb: Numerically optimized touring loudspeaker arrays – practical applications, in: *131st AES Convention*, New York, USA, 20–23 October, 2011.
8. F. Straube, F. Schultz, M. Makarski, S. Spors, S. Weinzierl: Evaluation strategies for the optimization of line source arrays, in: *59th AES Conference*, Montreal, Canada, 15–17 July, 2015.
9. F. Straube, F. Schultz, D.A. Bonillo, S. Weinzierl: An analytical approach for optimizing the curving of line source arrays, *Journal of the Audio Engineering Society* 66, 1/2 (2018) 4–20.
10. A. Hölter, F. Straube, F. Schultz, S. Weinzierl: Enhanced polygonal audience line curving for line source arrays, in: *150th AES Convention*, Virtual, 25–28 May, 2021.
11. L. Gölles, F. Zotter: Theory of continuously curved and phased line sources for sound reinforcement, *Acta Acustica* 7 (2023) 52.
12. P. Heidegger, B. Brands, L. Langgartner, M. Frank: Sweet area using ambisonics with simulated line arrays, in: *Fortschritte der Akustik, DAGA*, Vienna, Austria, 15–18 August, 2021.
13. L. Gölles, F. Zotter: Optimally curved arc source for sound reinforcement, in: *Fortschritte der Akustik, DAGA*, Vienna, Austria, 15–18 August, 2021.
14. S. Riedel, F. Zotter: Surrounding line sources optimally reproduce diffuse envelopment at off-center listening positions, *JASA Express Letters* 2, 9 (2022) 094404.
15. S. Riedel, L. Gölles, F. Zotter, M. Frank: Modeling the listening area of envelopment, in: *Fortschritte der Akustik, DAGA*, Hamburg, 6–9 March, 2023.
16. L. Gölles, M. Frank, F. Zotter: Simulating the sweet area of immersive sound reinforcement with surrounding mini line arrays, in: *Fortschritte der Akustik, DAGA*, Hannover, 18–21 March, 2024.
17. L. Gölles, M. Frank, F. Zotter: Improving surround sound reinforcement at off-center listening positions with miniature line arrays, in: *Audio Engineering Society Convention 156*, Madrid, 15–17 June, 2024.
18. L. Gölles, M. Frank, F. Zotter: Evaluating a dual-target line-array design for medium-scale surround sound reinforcement, in: *Audio Engineering Society Convention 156*, Madrid, 15–17 June, 2024.
19. O. Bucci, G. Mazzarella, G. Panariello: Reconfigurable arrays by phase-only control, *IEEE Transactions on Antennas and Propagation* 39, 7 (1991) 919–925.
20. C.A. Balanis: *Antenna theory: analysis and design*, 2nd edn, Wiley-Interscience, Hoboken, NJ, 1997.
21. A. Reyna, M.A. Panduro: Optimization of a scannable pattern for uniform planar antenna arrays to minimize the side lobe level, *Journal of Electromagnetic Waves and Applications* 22, 16 (2008) 2241–2250.
22. T. Sallam: Different array synthesis techniques for planar antenna array, *Applied Computational Electromagnetics Society Journal* 34, 05 (2019) 716–723.
23. N. Ghattas, A.M. Ghuniem, A.A. Abdelsalam, A. Magdy: Planar antenna arrays beamforming using various optimization algorithms, *IEEE Access* 11 (2023) 68486–68500.
24. Z.-C. Hao, M. He: Developing millimeter-wave planar antenna with a cosecant squared pattern, *IEEE Transactions on Antennas and Propagation* 65, 10 (2017) 5565–5570.
25. T. Sallam, A.M. Attiya: Low sidelobe cosecant-squared pattern synthesis for large planar array using genetic algorithm, *Progress in Electromagnetics Research M* 93 (2020) 23–34.
26. J. Puskely, T. Mikulasek, Y. Aslan, A. Roederer, A. Yarovoy: 5g siw-based phased antenna array with cosecant-squared shaped pattern, *IEEE Transactions on Antennas and Propagation* 70, 1 (2022) 250–259.
27. A.J. Berkhout: A holographic approach to acoustic control, *Journal of the Audio Engineering Society* 36, 12 (1988) 977–995.
28. A.J. Berkhout, D. de Vries: Acoustic holography for sound control, in: *Audio Engineering Society Convention* 86, Hamburg, 7–10 March, 1989. Available at <https://www.aes.org/e-lib/browse.cfm?elib=5893>.
29. A.J. Berkhout, D. de Vries, P. Vogel: Wave front synthesis: a new direction in electroacoustics, in: *Audio Engineering Society Convention* 93, San Francisco, CA, USA, 1–4 October, 1992.
30. A.J. Berkhout, D. de Vries, P. Vogel: Acoustic control by wave field synthesis, *Journal of the Acoustical Society of America* 93, 5 (1993) 2764–2778.
31. E. Start: Direct sound enhancement by wavefield synthesis, PhD dissertation, Delft University of Technology, Technical University Delft, 1997.
32. G. Firtha: A generalized wave field synthesis framework with application for moving virtual sources, PhD dissertation, Budapest University of Technology and Economics, Budapest University of Technologies and Economics, 2019.
33. P. Grandjean, A. Berry, P.-A. Gauthier: Sound field reproduction by combination of circular and spherical higher-order ambisonics: Part I – a new 2.5-d driving function for circular arrays, *Journal of the Audio Engineering Society* 69, 3 (2021) 152–165.
34. J. Ahrens, R. Rabenstein, S. Spors: The theory of wave field synthesis revisited, in: *Audio Engineering Society Convention* 124, Amsterdam, The Netherlands, 17–20 May, 2008. Available at <https://www.aes.org/e-lib/browse.cfm?elib=14488>.
35. J. Ahrens, S. Spors: Reproduction of a plane-wave sound field using planar and linear arrays of loudspeakers, in: *2008 3rd International Symposium on Communications, Control and Signal Processing*, Saint Julian’s, Malta, 12–14 March, IEEE, 2008, pp. 1486–1491.
36. J. Ahrens, S. Spors: Sound field reproduction using planar and linear arrays of loudspeakers, *IEEE Transactions on Audio, Speech, and Language Processing* 18, 8 (2010) 2038–2050.
37. F. Schultz: Sound field synthesis for line source array applications in large-scale sound reinforcement, PhD dissertation, University of Rostock, 2016.
38. E. El-Saghir: Deployment of two-dimensional loudspeaker arrays in worship spaces – new application concepts and a real-world case study, in: *Audio Engineering Society Conference: AES 2024 International Conference on Acoustics & Sound Reinforcement*, Le Mans, France, 23–26 January, 2024. Available at <https://www.aes.org/e-lib/browse.cfm?elib=22353>.
39. E. Start: Loudspeaker matrix arrays: challenging the way we create and control sound, in: *Audio Engineering Society Conference: AES 2024 International Conference on Acoustics & Sound Reinforcement*, Le Mans, France, 23–26 January, 2024. Available at <https://www.aes.org/e-lib/browse.cfm?elib=22351>.

40. F. Zotter, L. Gölles: Curvature and delay-based line-array design, in: Fortschritte der Akustik, DAGA, Hannover, 18–21 March, 2024.
41. ÖVE/ÖNORM EN 61672-1: Electroacoustics – sound level meters – part 1: specifications, ÖVE/Austrian Standards Institute, Vienna, AT, Standard, 2015.
42. L. Gölles, F. Zotter, L. Merkel: Miniature line array for immersive sound reinforcement, in: Proceedings of AES SIA Conference, Huddersfield, UK, August 23–25, 2023.
43. L. Gölles, F. Zotter: Dual-target design for large-scale sound reinforcement: Simulation and evaluation, in: Audio Engineering Society Conference: AES 2024 International Conference on Acoustics & Sound Reinforcement, Le Mans, France, 23–26 January, 2024.
44. B.M. Romeny: The Gaussian kernel, in: Front-end vision and multi-scale image analysis, Springer Netherlands, Dordrecht, 2003, pp. 37–51. https://doi.org/10.1007/978-1-4020-8840-7_3.
45. L. Gölles, F. Zotter: Impulse responses of a planar array, 2024. Available at <https://phaidra.kug.ac.at/o:133794>.

Cite this article as: Gölles L. & Zotter F. 2024. Theory of continuously phased planar sources for sound reinforcement. Acta Acustica, xx, xx. <https://doi.org/10.1051/aacus/2024070>.

Appendix A

Deriving the z-component of the stationary-phase direction

From the derivatives of r in equation (7) and the definition of the direction $\mathbf{u} = [u_x \ u_y \ u_z]^T$, we know that $\frac{\partial r}{\partial v} = -\sin \eta u_x - \cos \eta u_z$. The stationary-phase direction \mathbf{u} must be a unit vector. We may replace u_x by $\sqrt{1 - u_y^2 - u_z^2}$ to get,

$$\frac{\partial r}{\partial v} + \cos \eta u_z = -\sin \eta \sqrt{1 - u_y^2 - u_z^2}. \quad (\text{A1})$$

Taking the square of both sides yields a quadratic equation for u_z ,

$$u_z^2 + 2 \frac{\partial r}{\partial v} \cos \eta u_z + \left(\frac{\partial r}{\partial v}\right)^2 + \sin^2 \eta (u_y^2 - 1) = 0, \quad (\text{A2})$$

and by applying $\sin^2 \eta + \cos^2 \eta = 1$, the z component of the direction gets

$$u_z = -\frac{\partial r}{\partial v} \cos \eta (\pm) \sin \eta \sqrt{1 - \left(\frac{\partial r}{\partial v}\right)^2 - u_y^2}. \quad (\text{A3})$$

Because we are only interested in a stationary-phase direction pointing downwards on the listening area, the negative sign must be selected.

Appendix B

Equalization of a planar source

We consider a phased planar source of infinite length and width that is expanded over the vertical axis z and the horizontal axis y . Integration the Green's function over y and z yields its sound pressure,

$$p = \int_{-\infty}^{\infty} \int_{-\infty}^{\infty} \frac{e^{-ik(r+w)}}{4\pi r} dy dz. \quad (\text{B1})$$

i denotes the imaginary unit, k the wave number, r the distance between source and receiver and w the delay expressed as delay length. By applying the stationary-phase approximation, we get

$$p \approx \frac{e^{-ik(r+w)_* - i\frac{\pi}{4} \text{sig}\{\mathbf{H}(r+w)_*\}}}{2kr_*\sqrt{|\mathbf{H}(r+w)_*|}} \Big|_{w=0} = \frac{e^{-ik|x|}}{2ik}, \quad (\text{B2})$$

where $|\mathbf{H}(\cdot)|$ is the determinant of the Hessian and $\text{sig}\{\mathbf{H}(\cdot)\}$ its signature. * is used here as explicit indicator for the evaluation at the stationary-phase point. For zero phasing $w \equiv 0$, the stationary-phase distance is the normal distance $r_* = |x|$ to the y - z plane and the exact result of equation (B1) is obtained: the one-dimensional Green's function $\frac{e^{-ik|x|}}{2ik}$. In any case, the resulting sound pressure is proportional to $\frac{1}{k}$. So, its frequency response can be said to be colored red, in analogy to the colors of noise (red, pink, white). For a neutral frequency response, a filter proportional to $k = \frac{\omega}{c}$ is required, i.e. introducing a 6 dB/octave increase.

Publication III

This work was published as:

Lukas Gölles, Franz Zotter, and Leon Merkel, “Miniature line array for immersive sound reinforcement,” in Proceedings of AES SIA Conf., Huddersfield, 08 2023. [Online]. Available: <https://aes2.org/publications/elibrary-page/?id=22156>



Audio Engineering Society Conference Paper 62

Presented at the International Conference on Spatial and Immersive Audio
2023 August 23–25, Huddersfield, UK

This conference paper was selected based on a submitted abstract and 750-word precis that have been peer reviewed by at least two qualified anonymous reviewers. The complete manuscript was not peer reviewed. This conference paper has been reproduced from the author's advance manuscript without editing, corrections, or consideration by the Review Board. The AES takes no responsibility for the contents. This paper is available in the AES E-Library (<http://www.aes.org/e-lib>), all rights reserved. Reproduction of this paper, or any portion thereof, is not permitted without direct permission from the Journal of the Audio Engineering Society.

Miniature Line Array for Immersive Sound Reinforcement

Lukas Gölles^{1,2}, Franz Zotter^{1,2}, and Leon Merkel^{2,3}

¹*Institute of Electronic Music and Acoustics, Graz, Austria*

²*University of Music and Performing Arts, Graz, Austria*

³*Graz, University of Technology, Austria*

Correspondence should be addressed to Lukas Gölles (goelles@iem.at)

ABSTRACT

Progressively curved line-source arrays became state of the art in large-scale sound reinforcement as they are flexibly adapted to the listening area by well-chosen splay angles between individual elements in the chain of line-source loudspeakers. In cinema-sized sound reinforcement, point-source loudspeaker setups are still common, despite maybe difficult to adjust to designs targets suggested by current literature: 0 dB per doubling of the distance for ideally preserved direct sound mix, -3 dB per doubling of the distance for ideally preserved envelopment. To explore how much practical benefit lies in pursuing these targets with smaller line arrays, this paper presents the open design for a miniature line array with 3D printed enclosure. Moreover, measured free field frequency responses, distortion, and directivity are discussed for an individual prototype element, and of the entire line array the coverage over distance is discussed for two target designs using a purely curved or curved and delayed array.

1 Introduction

One of the big challenges for sound reinforcement in concerts, cinema, or speech events is to provide high-quality sound for the largest parts of a predefined audience area [1]. For immersive sound reinforcement, Zotter et. al [2] showed that acceptable mixing balance of direct sound objects is achieved when rendered with -1 dB roll-off per doubling of the distance and Gölles et. al [3] showed that loudspeakers, designed for a direct-sound coverage of 0 dB attenuation per doubling of the distance, could potentially improve directional localisation in a large listening area, above a length-dependent frequency. Considering envelopment

of a diffuse scene, Riedel et al. [4, 5] purposes to use horizontally surround loudspeakers whose sound level decrease with -3 dB per doubling of the distance.

Variable curvature line arrays seem to be suitable to implement these designs in practise. For example, the Wavefront Sculpture Technology [6, 7] defines the curvature of line source arrays to adjust the direct sound level for a predefined listening area. Furthermore, a Straube et al define an algorithm to optimize the tilt angles between the individual elements of a line source array [8]. What literature has in common is that only one target design is pursued.

Considering optimal mixing balance and optimally pre-

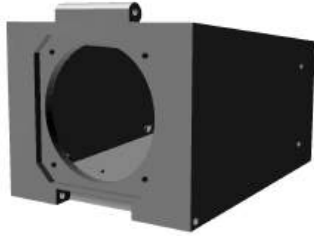


Fig. 1: CAD model of a single cabinet.

serving the envelopment for off-center listening positions, current knowledge suggests a two-target design. The practical goal is to use only one loudspeaker array to satisfy both targets.

This paper presents the open design of a 3D printed miniature line array element that joins with others and permits to adjust a splay angles in between. The primary target is to implement an experimental setup to accomplish multiple target designs for cinema-sized sound reinforcement. The primary target is reached by adjusting the splay angles between the individual elements which are driven in phase. Individual delays added in each loudspeaker feed of the array allow other targets to be met on another signal bus. Beside the open design, impulse response measurements are presented to show the practical performance of the prototype.

2 Design of the loudspeaker element

The line array should be small enough to reach a high spatial aliasing limit, and it should be able to cover a wide frequency range. To accomplish this while keeping the technical effort manageable, a solution of broad-band loudspeakers (1-way system) of small size is preferable. We chose SB acoustics SB65WBAC25-4¹ as wide-band transducer as implemented by the 3913 loudspeaker [9] because of their ability to reproduce low frequencies from 115 Hz on and to perform with high quality also at high frequencies.

The resonance frequency is calculated by the compliance $C_{ms} = 0.77 \frac{\text{mm}}{\text{N}}$ and the moving mass $M_{ms} = 2.5 \text{ g}$,

$$f_s = \frac{1}{2\pi} \frac{1}{\sqrt{C_{ms} M_{ms}}} = 115 \text{ Hz}. \quad (1)$$

¹<https://sbacoustics.com/product/2-5in-sb65wbac25-4/>



Fig. 2: Miniature line array with 3D printed cabinets, fully assembled, 8-element example.

We allow a shift of the resonance frequency by $\sqrt{2}$, so that the resonance frequency of the closed box is $f_{cb} = 162 \text{ Hz}$ yielding the compliance ratio $\alpha = \frac{f_{cb}^2}{f_s^2} - 1 = 1$. This defines the volume of the closed box to be equal to the equivalent volume of the driver suspension $V_{as} = 0.431$. As the interior of our real box is loosely filled with Visaton Damping Material, the goal is to reach a volume of approximately $V_{as} = 0.41$.

To minimise the effect of spatial aliasing, the drivers have to be placed as closely together as possible, yielding a minimum feasible inside front cabinet height $h_{f,i} = 6.4 \text{ cm}$. 8 mm thick walls have to be added to ensure stability and to enable linking of the cabinet fronts. This results in an outside front cabinet height of $h_{f,o} = 8 \text{ cm}$. Furthermore, the cabinet side profile must be trapezoidal to permit angular range of motion required to adjust the inclination between the line array elements, cf. Figs. 1 and 2. Setting the maximum adjustable splay angle to 10° , as common in professional sound reinforcement systems, and a cabinet depth of $d_i = 10 \text{ cm}$, yields as back height of the cabinet

$$h_{b,i} = h_{f,i} - 2d_i \tan\left(\frac{10^\circ}{2} \frac{\pi}{180^\circ}\right) = 4.65 \text{ cm}, \quad (2)$$

or $h_{b,o} = 6.25 \text{ cm}$ on the outside. We choose $w_i = 8.4 \text{ cm}$ or $w_o = 10 \text{ cm}$ for the width of the cabinets to provide enough space for cabling. With these dimensions and the volume that is occupied by the driver V_d ,

the interior volume of this trapezoidal prism is

$$V_b = \frac{h_{f,i} + h_{b,i}}{2} w_i d_i - V_d = 404.1 \text{ cm}^3. \quad (3)$$

From measurements, we get a resonance frequency of 161 Hz, matching the theoretical considerations.

Figure 1 shows the CAD model of a single enclosure and Figure 2 presents the 3D printed prototype with mounted drivers as exemplary setup with 8 enclosures.

3 Design of line array curvature

Typically, the sound pressure of a linear arrangement of ideal point sources decreases with $1/\sqrt{r}$, cf. Appendix A. The goal in line array curvature design is to reach an equalised magnitude square $8\pi k|p|^2 = \left(\frac{g}{r\beta}\right)^2$ with adjustable $-6 \cdot \beta$ dB per doubling of the distance r between the point on the array emitting the first wave front received and the receiver; $k = \frac{2\pi f}{c}$ is the wave number and $c = 343$ m/s the speed of sound.

The theory of adjusting the splay angles in the chain of line-source loudspeaker arrays is known from the Wavefront Sculpture Technology [6, 7]. In [10], the stationary-phase approximated integral of a Green's function over an unknown contour was used to obtain a more generic differential equation for a total curvature

$$\dot{\vartheta}_T = -\frac{r^{2\beta}}{g^2} \frac{1}{r^2 \cos \vartheta_w} + \frac{\cos \vartheta_w}{r} \quad r = \frac{z}{\sin \vartheta_T}, \quad (4)$$

which corresponds to the design equation for line source array curvature of the Wavefront Sculpture Technology without beamforming when $\vartheta_w = 0$ as presented in [6]. Here, the total inclination $\vartheta_T = a\vartheta + (1-a)\vartheta_w$ at any point of the array is linearly composed of the physical inclination ϑ of the curved array contour and a local delay-and-sum beamformer's steering angle ϑ_w . The total curvature $\dot{\vartheta}_T$ is the total inclination change over the natural length parameter s of the contour. The gain parameter g sets the initial curvature at the highest point of the source. Defining the tangent vector $\mathbf{t} = [\sin \vartheta \quad 0 \quad \cos \vartheta]^T$, we get the source contour by integration over the natural length parameter $\mathbf{x} = \int_0^s \mathbf{t} ds$.

To simulate a real case scenario, 12 enclosures are lined up, for which we obtain the continuous source contour

enclosure	Tilt angle	delay
1	11.3°	0
2	0°	0
3	0°	1
4	1°	1
5	0°	2
6	1°	3
7	1°	4
8	1°	6
9	2°	8
10	3°	10
11	4°	13
12	10°	15

Table 1: Tilt angles for the curved array and delays in samples at $f_s = 48$ kHz for the mixed array

from eq. (4). A web-based tool² is used to solve the differential equation with low effort yielding discrete splay angles and delays. For simulation, we use the following parameters: The mounting height was set to $z(s=0) = 2$ m and the farthest observation point to $x_{r,0} = 10$ m, which defines the gain parameter $g = 0.27$. The solution is then discretized using a step size of 8.2 cm, which corresponds to the distance between two neighbouring drivers when mounted in the chain. For broadside beamforming, this yielding the spatial aliasing frequency for which endfire radiation occurs whenever $\lambda < 8.2$ cm,

$$f_{\text{spat. al.}} = 4.2 \text{ kHz}. \quad (5)$$

The discretized solution yields integer splay angles which are summarised in Table 1.

To include effects caused by source discretization, the simulated continuous contour was discretized into a polygon of 6.2 cm straight-line segments leaving gaps in between, as done in [10]. On these polygons, same-delay point sources are positioned and the sound pressures of all point sources are summed up. The dashed lines in Figure 7 show the results for the curved line source without beamforming and $\beta = 0$ as well as the result of the mixed design by adding delays to reach -3 dB per doubling of the distance where a second gain parameter $g = 0.567$ was used for the mixed design.

²<https://enimso.iem.sh/post/line-array-designer-two-target/>

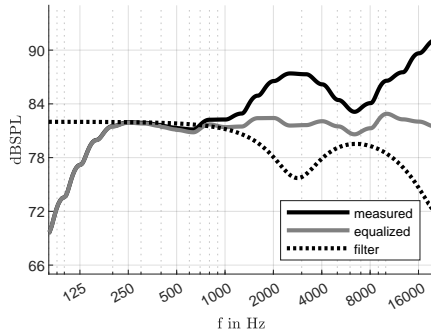


Fig. 3: Third-octave averaged frequency response of one element.

4 Measurements

To measure the frequency response and distortion, a single array element was mounted on a cord in a largely anechoic room (5 m × 4.2 m × 3 m). Measurements were done with an NTI M2230 microphone. Directivity measurements with the same microphones covered an angular grid of 10° × 10°, for line arrays suspended from a stand. Measurements concerning coverage over distance also used a suspended line array, and were done in larger lecture hall i9 (17.25 m × 9.5 m × 3.90 m) of Graz University of Technology, with pressure-zone microphones on the floor to avoid floor reflections.

4.1 Single-element frequency response

As it is not possible to record the free field frequency response directly due to the room dimensions, impulse responses were taken at different distances, 4 cm and 0.5 m. Afterwards, the frequency responses were matched between 400 Hz and 500 Hz. Figure 3 shows the third-octave averaged frequency responses for a single enclosure. Compared to the free field measurement in the data sheet [11], an amplitude boost around 2.5 kHz sticks out. The increase in high frequencies coincides with the on-axis data provided in the data sheet. For equalization, two peak filters were used, $f_{EQ,1} = 2.8 \text{ kHz}$, $g_{EQ,1} = -6 \text{ dB}$, $Q_{EQ,1} = 0.8$ and $f_{EQ,2} = 22 \text{ kHz}$, $g_{EQ,2} = -10.5 \text{ dB}$, $Q_{EQ,3} = 1.69$. After equalization, the direct sound pressure level stays between ±3 dB for frequencies between 142 Hz and 22 kHz. A stricter limit, ±1.2 dB, increases the lower frequency to 175 Hz.

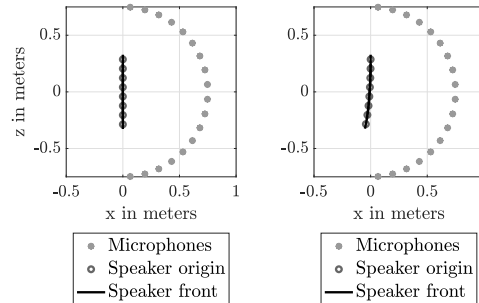


Fig. 4: Setup for directivity data of $\varphi = 0^\circ$, straight array with no angles (left), array optimized for 3 dB per doubling of distance with $\beta = 1/2$ and $g = 0.666$ (right).

4.2 Single-element distortion

To measure distortion of a single element, Room Equalization Wizard³ was used and the results were exported as text file afterwards for further work. For a single enclosure, Figure 5 shows the fundamental-frequency response to a sinusoid, and the second and the third harmonics as well as total harmonic distortion are shown for a frequency range of 150 Hz to 1.5 kHz, measured at 0.5 m distance to the driver. The results are only shown up to 1.5 kHz, as total harmonic distortion does not increase for higher frequencies and remains negligibly small. For an A-weighted sound pressure level of 87 dB(A) (left plot), total harmonic distortion rises for low frequencies up to approximately 2%. For frequencies above 250 Hz, it stays below 1%. There is a noticeable peak at 755 Hz, for which mainly the second harmonic distortion of the driver itself contributes to the result. Increasing the volume to 93 dB(A) yields a strong boost in distortion for low frequencies reaching 7%. By contrast, the peak at mid frequencies caused by the driver itself increases only little.

4.3 Single-element directivity

The vertical and horizontal directivity patterns were measured in the acoustically treated measurement chamber of IEM. Four different array configurations (straight; 0 dB/distance doubling, $g = 0.315$, $\beta =$

³<https://www.roomeqwizard.com/>

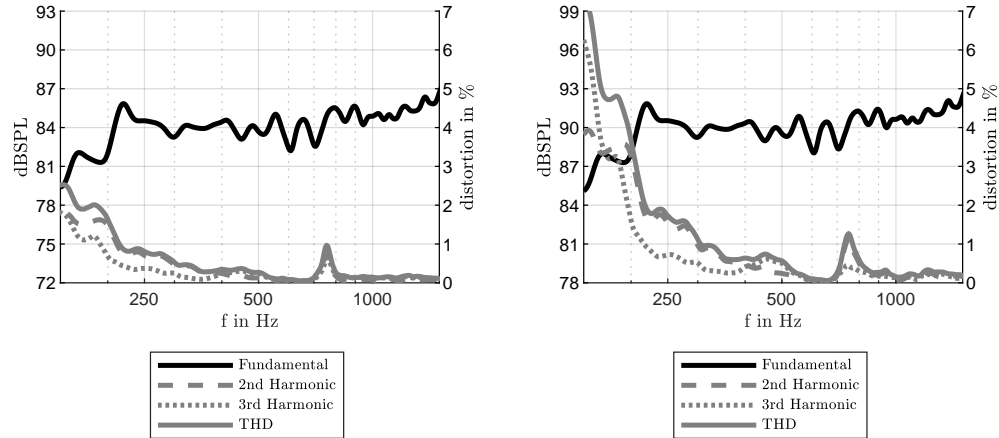


Fig. 5: Fundamental frequency, second, third, and total harmonic distortion of a single enclosure for different sound pressure levels, 87 dB(A) (left) and 93 dB(A) (right).

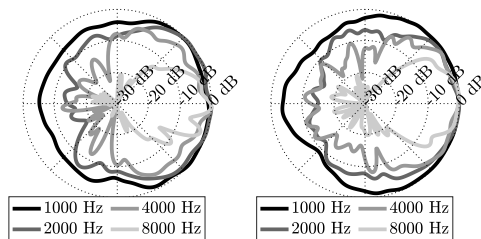


Fig. 6: Directivity pattern of the 5th top element of the straight array, vertical (left), horizontal (right)

0; 1.5 dB/distance doubling, $g = 0.466$, $\beta = 1/4$; 3 dB/distance doubling, $g = 0.666$, $\beta = 1/2$) the array of $N_{ls} = 8$ elements was set up on a remote-controlled turntable, and the top elements of the line array were aligned with the turntable rotation axis. In a radius of $r_{meas} = 0.75$ m a total of 18 NTI M2230 measurement microphones are located in a semi-circle from the zenith $\theta = 5^\circ$ in equi-angle spacing of 10° to 175° . The 10° were also chosen as the resolution for the rotation steps of the turntable from an azimuth $\varphi = 0^\circ$ to 350° . By feeding the speakers sequentially using mul-

tiple sinusoidal sweeps, $18 \times 36 \times 8$ impulse responses were obtained by the microphones via deconvolution, and truncation to 170 samples at 48 kHz sampling frequency, for brevity of the dataset. This removes reflections from the turntable on the lowest microphone (approx. 60 cm smallest distance between turntable and microphone). For the resulting directivity dataset, Figure 4 sketches the measurement setup for a straight (left) and a curved array for $\beta = 1/2$ and $g = 0.666$.

For interpolated directivity plots of the 5th array element, the measured impulse responses were decomposed into circular harmonics, after removing the linear phase and $1/r$ propagation attenuation in the frequency domain to center the slight off-center location of the element. Figure 6 shows the directivity patterns of this array element interpolated in 1° steps for 4 frequencies. The vertical directivity plot contains the influence of the vertical array extent as slight ripple and increase of the front-to-back ratio, but is otherwise similar to the horizontal directivity, so that we can assume largely axisymmetric loudspeaker directivities. The loudspeakers begin to be directional at 2 kHz and above, and cover a -6 dB angle of about $\pm 30^\circ$ at 8 kHz.

Our paper does not pursue analyzing the $10^\circ \times 10^\circ$ directivity data of 3 arrays designs measured further, but datasets are openly accessible, cf. section 7.

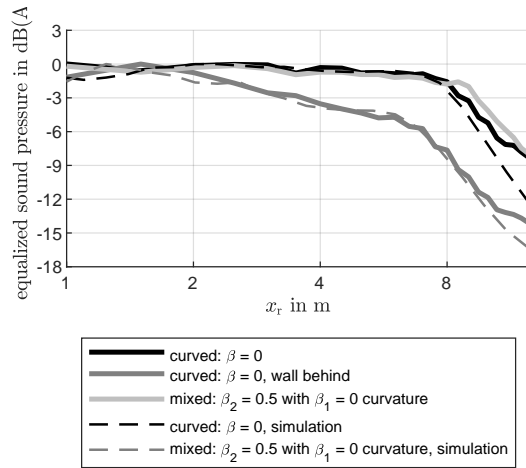


Fig. 7: A-weighted measured sound pressure of a curved array with $\beta = 0$ (solid black) compared to simulation (dashed) as well as the same array mounted in front of a reflecting wall (solid light grey) and mixed array with $\beta_1 = 0$ and $\beta_2 = 0.5$: (dashed dark grey) simulation and measurement (solid dark grey).

4.4 Line array: coverage over distance

In order to record the position-dependent direct sound pressure levels in a room, impulse responses were measured along 22 positions (away from the array, on-axis) starting at $x_r = 1$ m and ending at $x_r = 12.5$ m. Pressure zone microphones were positioned on the ground to prevent floor reflections influencing the measurement. The first 250 samples of the impulse responses (5.2 ms at $f_s = 48$ kHz) were evaluated in a frequency range between 20 Hz and 20 kHz. The impulse responses of the individual loudspeakers are equalized according to the filter presented in Figure 3. Furthermore, for frequencies below the spatial aliasing frequency $f < 4.2$ kHz eq. (5), we applied the typical \sqrt{f} filter required to equalize any line source, cf. Appendix A. The results are averaged in third octaves and the curves are plotted as A-weighted sum.

Figure 7 shows the A-weighted on-axis sound pressure curve for a curved line source with $\beta = 0$ (black solid) compared to the simulation of a discrete source composed of straight-line source polygons of length 6.2 cm

with splay angles rounded to integer degrees and leaving gaps in between the discrete elements (black dotted). Furthermore, the results for the same source but mounted in front of a reflecting wall is presented (light grey). The distance between wall and top enclosure was 86 cm and the distance on the bottom was 62 cm.

For the curved arrays with $\beta = 0$ (solid black and solid light grey in Figure 7), the direct sound pressure level remains almost constant until 8 m. Due to the finite length and the fact that the differential equation assumes an infinitely long source, the sound pressure level decreases for farther observation points. It is noticeable, that the reflecting wall behind the source does not influence the A-weighted curve of the direct sound level. For the mixed design with $\beta_1 = 0$ for the curvature and $\beta_2 = 0.5$ (solid dark grey in Figure 7), the direct sound level decreases by -3 dB from 1.75 m to 3.5 m, and from 3.5 m to 7 m. For farther observation points, the direct sound level decreases by 6 dB as observed for the curved arrays with $\beta = 0$. Moreover, the measured results almost coincide with the simulated results. The result show that the mixed design is feasible in practise.

5 Conclusion

This paper presented the open design of a miniature line array with 3D-printed enclosures with the practical goal to apply to cinema-sized electroacoustic-music immersive sound reinforcement. Measurements in an anechoic environment showed that the frequency response of the direct sound may be equalized by two simple peak filters and measurements concerning distortion showed that a maximum level of 93 dB(A) can be reached by a single loudspeaker keeping THD below 10%. The results also show the increasing directivity of a single loudspeaker at higher frequencies. Moreover, we could present that a two-target design based on curving and phasing is feasible in practise.

We plan to undertake psychoacoustic experiments using 8 of the 8-element line arrays surrounding the audience, as a first target application of the hardware presented here. The investigations shall clarify whether mixing balance or envelopment rendering can be improved for an extended audience area in medium-sized immersive sound reinforcement for 50-250 listeners.

6 Acknowledgement

Our research was funded by the Austrian Science Fund (FWF) under project number P 35254-N, Envelopment in Immersive Sound Reinforcement (EnImSo). The authors thank Thomas Musil for his design improvements on our miniature line array, Garcia-Leticia Gabriel, Gregor Schmidt, Niklas Urban, and Chonglian Yu for joint efforts in measuring the coverage over distance (sound reinforcement lab exercise), and Alexander Mülleder and Nico Seddiki for measuring the directivity together (acoustic holography and holophony lab exercise).

7 Data availability

The CAD model of the miniature line array enclosure as well as the measurement data is provided under <https://phaidra.kug.ac.at/o:130608> for download.

References

- [1] Ahnert, W. and Noy, D., *Sound Reinforcement for Audio Engineers*, Taylor & Francis Ltd, 2023, ISBN 978-1-032-11518-4.
- [2] Zotter, F., Riedel, S., Gölles, L., and Frank, M., “Acceptable Imbalance of Sound-Object Levels for Off-Center Listeners in Immersive Sound Reinforcement,” in *Fortschritte der Akustik, DAGA*, Hamburg, 2023.
- [3] Gölles, L. and Zotter, F., “Optimally Curved Arc Source for Sound Reinforcement,” in *Fortschritte der Akustik, DAGA*, Vienna, 2021.
- [4] Riedel, S. and Zotter, F., “Surrounding line sources optimally reproduce diffuse envelopment at off-center listening positions,” *JASA Express Letters*, 2(9), p. 094404, 2022, doi:10.1121/10.0014168.
- [5] Riedel, S., Gölles, L., Zotter, F., and Frank, M., “Modeling the Listening Area of Envelopment,” in *Fortschritte der Akustik, DAGA*, Hamburg, 2023.
- [6] Heil, C. and Urban, M., “Sound Fields Radiated by Multiple Sound Sources Arrays,” in *92nd AES Conv.*, Vienna, 1992.
- [7] Urban, M., Heil, C., and Bauman, P., “Wavefront Sculpture Technology,” *J. Audio Eng. Soc.*, 51(10), pp. 912–932, 2003.
- [8] Straube, F., Schultz, F., Bonillo, D. A., and Weinzierl, S., “An Analytical Approach for Optimizing the Curving of Line Source Arrays,” *J. Audio Eng. Soc.*, 66(1/2), pp. 4–20, 2018.
- [9] Riedel, S. and Zotter, F., “Design, Control, and Evaluation of Mixed-Order, Compact Spherical Loudspeaker Arrays,” *Computer Music Journal*, 44, pp. 60–76, 2021, doi:10.1162/comj_a_00581.
- [10] Gölles, L. and Zotter, F., “Theory of Continuously Curved and Phased Line Sources for Sound Reinforcement,” *Acta Acustica*, accepted 2023.
- [11] Acoustics, S., “Product Overview: SB Acoustics 2,5” SB65WBAC25-4 / Aluminum,” <https://sbacoustics.com/product/2-5in-sb65wbac25-4/>, 2023.
- [12] Skudrzyk, E., *The Foundations of Acoustics: Basic Mathematics and Basic Acoustics*, Springer Link, 1971, ISBN 978-3-7091-8257-4.

A Equalization of an ideal line source

We consider a line source of infinite length that is expanded over the vertical axis z and get its sound pressure by integrating the Green’s function over z ,

$$p = \int_{-\infty}^{\infty} \frac{e^{-ikr}}{4\pi r} dz \quad (6)$$

where i denotes the imaginary unit, k the wavenumber and r the distance between source and receiver. By using the Sommerfeld integral for the Hankel function of zero order of the second kind $H_0^{(2)}(kr)$ [12], the pressure becomes

$$p = -\frac{i}{4} H_0^{(2)}(kr). \quad (7)$$

The asymptotic representation for $H_0^{(2)}(kr)$ yields,

$$p \approx \frac{1}{\sqrt{8\pi k}} \frac{e^{-i(kr + \frac{\pi}{4})}}{\sqrt{r}}. \quad (8)$$

To equalize the pressure magnitude, the magnitude of the filter has to increase by \sqrt{f} .

Publication IV

This work was published as:

Lukas Gölles, and Franz Zotter, “Dual-target design for large-scale sound reinforcement: Simulation and evaluation,” in Audio Engineering Society Conference: AES 2024 International Conference on Acoustics & Sound Reinforcement, Jan 2024. [Online]. Available: <https://aes2.org/publications/elibrary-page/?id=22369>



Audio Engineering Society Conference Paper 5

Presented at the International Conference on Acoustics & Sound
Reinforcement
2024 January 23–26, Le Mans, France

This paper was peer-reviewed as a complete manuscript for presentation at this conference. This paper is available in the AES E-Library (<http://www.aes.org/e-lib>), all rights reserved. Reproduction of this paper, or any portion thereof, is not permitted without direct permission from the Journal of the Audio Engineering Society.

Dual-Target Design for Large-Scale Sound Reinforcement: Simulation and Evaluation

Lukas Göllés^{1,2} and Franz Zotter^{1,2}

¹*Institute of Electronic Music and Acoustics, 8010 Graz, Austria*

²*University of Music and Performing Arts Graz, 8010 Graz, Austria*

Correspondence should be addressed to Lukas Göllés (goelles@iem.at)

ABSTRACT

Progressively curved line-source arrays became state of the art in large-scale sound reinforcement as they are flexibly adapted to the listening area by well-chosen splay angles between individual elements in the chain of line-source loudspeakers. Recent perceptual studies suggest using a dual-target design to meet contradictory goals in immersive sound reinforcement: 0 dB per doubling of the distance to preserve the direct sound mix, and -3 dB per doubling of the distance to preserve the envelopment at off-center listening positions. A practical implementation has been proposed to achieve both objectives simultaneously by driving the transducers of a curved array either in phase or with individual delays. Its feasibility was verified using measurements on a miniature line array that works for small audiences, but not specifically for large arrays and audiences that would be typically found in live events. To check the applicability of the dual-target approach to large-scale sound reinforcement systems, this contribution presents a simulation study with various professional line-source arrays and a sample measurement.

1 Introduction

Providing high-quality sound for the largest parts of a predefined audience area is one of the big challenges for sound reinforcement in concerts, cinema, or speech events [1]. In the typical professional sector, large-area sound systems consider the supply with almost single-channel sound material fed to multiple line-source loudspeaker arrays. The Wavefront Sculpture Technology [2, 3] is considered a fundamental work on line array curvature design and beyond purely geometric calculation methods, Polygonal Audience Line Curving (PALC) [4, 5, 6] offers an algorithm for shaping line array contours.

As an alternative to adapting the source geometry to the listening area accordingly, beamforming-based approaches are used to obtain a desired sound level curve over the listening area, but electronically. Beamformers known from phased arrays in antenna theory, radar applications, or optics are already found in microphone arrays [7] and loudspeaker arrays [8, 9, 10]. Beamforming is typically implemented by individual delays per transducer and often with additional filtering.

Considering surround sound applications, recent research suggests a dual-target design for optimal immersive sound reinforcement, 0 dB attenuation per doubling of the distance to preserve the mixing balance of direct sound objects at off-center listening positions

[11, 12] and -3 dB per doubling of the distance to preserve the envelopment [13, 14]. Therefore, optimal immersive sound reinforcement requires a dual-target design with two individual mix buses. One contains the direct sound objects and, e.g., drives the elements of a line array in phase, assuming its curvature is designed for 0 dB per distance doubling. The other one is used for the diffuse and enveloping parts, which, e.g., require additional individual delays for each line array element to achieve -3 dB per distance doubling. Such a dual-target design was already evaluated by simulations and measurements using a miniature line array [15, 16].

To study the applicability of such a dual-target approach to professional large-scale systems, this paper presents and discusses simulations of professional line-source arrays. Simulations are done in EASE using the speaker data (.gll) provided by the manufacturers and compared to a simpler and loudspeaker-independent simulation based on point-source interference. Furthermore, the results of impulse response measurements are presented to verify the practical performance of one exemplary professional system.

2 Design of Line Array Curvature and Delay Loading (Phasing)

Considering a multi-target design, [15] presents a non-linear differential equation that defines line array curving and phasing to achieve a $-6 \cdot \beta$ dB attenuation of the direct sound,

$$\dot{\vartheta}_T = -\frac{r^{2\beta}}{g^2} \frac{1}{r^2 \cos \vartheta_w} + \frac{\cos \vartheta_w}{r} \quad (1)$$

with $r = \frac{z}{\sin \vartheta_T}$.

g is a gain parameter and r denotes the distance for which acoustic plus electronic delay to the source is minimal, for a receiver in the xy plane. At this z coordinate of the source, ϑ_T denotes the total inclination composed of a geometric part ϑ and a delay-beamforming part ϑ_w ,

$$\vartheta = a(\vartheta_T - \vartheta_{\text{offs}}) + \vartheta_{\text{offs}}, \quad \vartheta_w = b(\vartheta_T - \vartheta_{\text{offs}}) \quad (2)$$

with $a + b = 1$,

where ϑ_{offs} is the inclination at the top coordinate \mathbf{x}_0 of the source. The convex curve geometry results from integrating over the natural length parameter s ,

$$\mathbf{x} = \int \mathbf{t} ds + \mathbf{x}_0, \quad \mathbf{t} = [\sin \vartheta \quad 0 \quad \cos \vartheta]^T, \quad (3)$$

Line Array Designer considering Two Targets

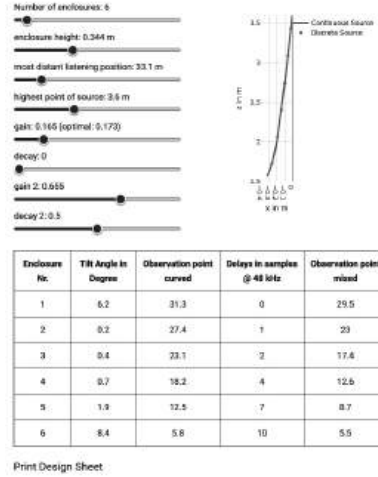


Fig. 1: Line Array Designer

and the delay length $w = c \tau$ is calculated correspondingly,

$$w = -\int_0^s \sin \vartheta_w ds. \quad (4)$$

The algorithm outlined in [15, Alg.2] proposes a numerical solution of Equations 1, 3 and 4 for a mixed design of a continuous source that is discretized afterward. This algorithm is implemented in a web-based solver written in Javascript [17], cf. figure 1 that is used for line array curving and phasing in this contribution. Since this solver is capable of taking URL parameters into account, links to this tool are given in the footnote with the necessary parameters.

3 EASE and MATLAB Simulation Study

For the simulation study, we assume a listening area of 30 m depth. We use line-source arrays from different manufacturers and limit the source length to a range of 2.0 m to 2.2 m. To simulate a real-case scenario, we choose ‘single motor’ as rigging mode and use a single pickup point. This yields a discretization of the offset angle ϑ_{offs} , i.e. the inclination of the whole source. In addition, the resulting forces should also be within the permitted range, fulfilling the requirements for practical usage.

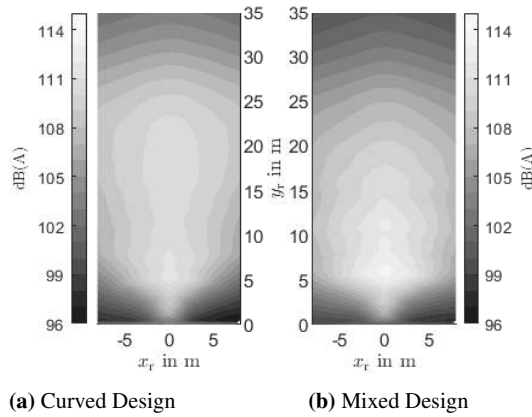


Fig. 2: GEO S12: Simulated A-weighted sound pressure over the listening area for the curved design with $\beta = 0$ and the mixed design with $\beta_2 = 0.5$ and $\beta_1 = 0$ curvature.

Simulations shown here are mainly done in EASE 4.4 using the corresponding speaker data provided by the manufacturers. The simulated results of the direct sound level are exported as text files to be graphically represented using MATLAB which is also used as an alternative simulation tool. To this end, the regarded line arrays are modeled as multiple point sources. These point sources are placed along the contour that is discretized into a polygon of straight-line segments with small gaps in between with the same splay-angle configurations as in EASE. The activate length around the center of each straight-line segment is simulated to get shorter by the fifth power of the frequency, i.e. for 20 Hz the length of the straight line corresponds to 90% of the discrete line-source element length and for 20 Hz it is 60%.

3.1 Nexo GEO S1210

For our requirements, six Nexo GEO S1210 elements ($N = 6$, $h = 0.344$ m) are suitable yielding a total source length of 2.06 m. The online solver¹ outputs the splay and delay parameters with farthest observation point $x_{r,0} = 33.1$ m, highest point of the source $z_0 = 3.6$ m

¹<https://enimso.iem.sh/post/line-array-designer-two-target//?N=6&h=0.344&xr0=33.1&y0=3.6&g=0.165&beta=0&g2=0.655&beta2=0.5>

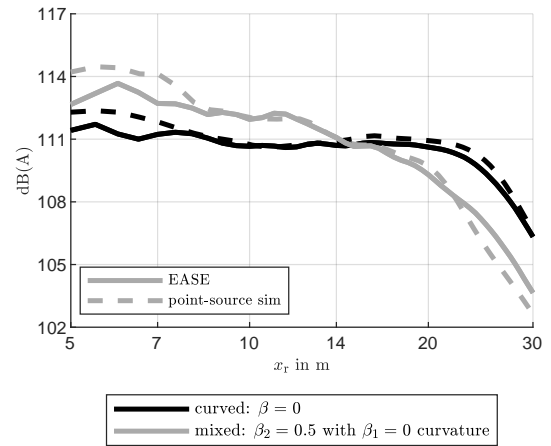


Fig. 3: GEO S12: A-weighted simulated on-axis sound pressure of curved array (black) with decay $\beta = 0$ and mixed array (grey) with $\beta_1 = 0$ and $\beta_2 = 0$ over distance compared to simulations based on point sources (dashed).

and gain parameter $g_1 = 0.165$ for the physical curvature with design parameter $\beta_1 = 0$. For the mixed design, the second gain is $g_2 = 0.655$ to reach a -3 dB attenuation of the direct sound level when doubling the distance ($\beta_2 = 0.5$). Considering the rigging point, NS-1 predicts a negligible bumper angle error of -0.04° when using pick-up position -5. Furthermore, the software reports a force on the bumper rigging point of 2.15 kN, which is well below the permitted limit of 6.8 kN. The safety factor considering all forces and moments of the entire array is 12.5.

Figure 2 presets the simulated A-weighted sound pressure over the listening area compared to a simulation based on point sources. In the majority of the listening area, the target of the curved source $\beta = 0$ is reached, cf. Figure 2a. For near observation points, we denote higher levels because the outlet of the lowest cabinet is not curved enough compared to the ideal requirement. At distant points of observation $x_r > 22$ m, there is a level drop because the stationary phase approximation assumes an infinitely extended symmetric Fresnel integral along the line source, which however only extends downwards from the top end of the line source, yielding a loss of 6 dB. Figure 2b shows the simulated level map with added delays of the mixed design. For more

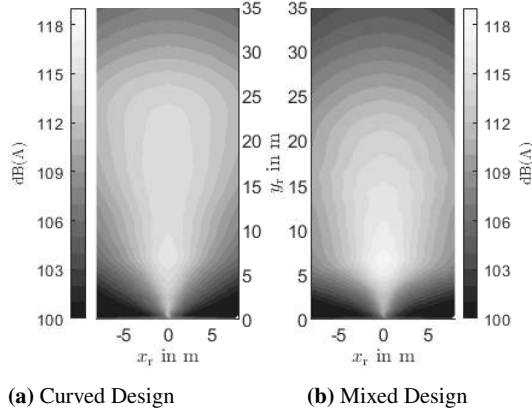


Fig. 4: KARAII: Simulated A-weighted sound pressure over the listening area for the curved design with $\beta = 0$ and the mixed design with $\beta_2 = 0.5$ and $\beta_1 = 0$ curvature.

detailed considerations, Figure 3 shows the on-axis level curves for both design targets. While the level stays almost constant for the $\beta = 0$ array, the results show that the target of the mixed design $\beta_2 = 0.5$ is reached when comparing the EASE simulation to the simulation based on point sources.

3.2 L’Acoustics KARAII

Next, we use eight L’Acoustics KARAII elements ($N = 8$, $h = 0.252$ m) with a total source length of 2.02 m to simulate both designs. The highest point of the source and farthest listening point remain the same as before. Due to a different source length, the gain values have to be modified², $g_1 = 0.165$ and $g_2 = 0.649$. The simulation in Soundvision yields a bumper error of 0.2° when using M-BUMP + M-BAR hole A at rigging hole 6. Although the error is small, it is taken into account in the simulations below to check the impact of this small error. Forces of 2.3 kN act at the rigging point which yields a safety factor of 11.9.

Figure 4 shows the maps of the curved design as well as the mixed design and Figure 5 presents the A-weighted direct sound curve when observing the on-axis direction. Again, the simulations show that the calculated

²<https://enimso.iem.sh/post/line-array-designer-two-target/?N=8&h=0.252&xr0=33.1&y0=3.6&g=0.165&beta=0&g2=0.649&beta2=0.5>

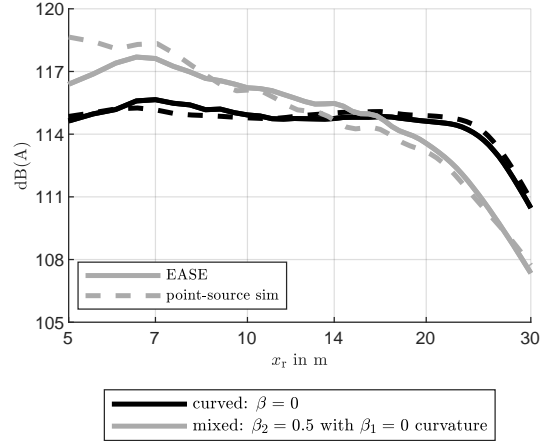


Fig. 5: KARAII: A-weighted simulated on-axis sound pressure of curved array (black) with decay $\beta = 0$ and mixed array (grey) with $\beta_1 = 0$ and $\beta_2 = 0$ over distance compared to simulations based on point sources (dashed).

source geometry reaches in the desired 0 dB target and that additional delays yield the desired attenuation of -3 dB per distance doubling. For both cases, we denote that the small bumper error does not have any crucial impact on the results. Furthermore, it is particularly noteworthy that the point source-based simulation mainly corresponds to the EASE simulation when considering the on-axis levels. For predicting the on-axis direct sound level, the point-source-based simulation is suitable as the deviations in more effortful EASE simulations stay reasonably low.

3.3 d&b V8

A third simulation is performed using seven d&b V8 elements ($N = 7$, $h = 0.31$ m) yielding a total source length of 2.17 m. The highest point of the source and farthest observation point remain the same as chosen for the Nexo array. Due to other enclosure dimensions, the gain values have to be modified again³, $g_1 = 0.165$ and $g_2 = 0.655$. Using pick-up hole 19 at V flying

³<https://enimso.iem.sh/post/line-array-designer-two-target/?N=6&h=0.344&xr0=33.1&y0=3.6&g=0.165&beta=0&g2=0.655&beta2=0.5>

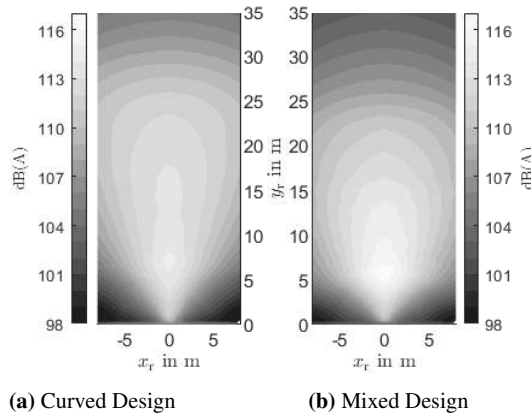


Fig. 6: V8: Simulated A-weighted sound pressure over the listening area for the curved design with $\beta = 0$ and the mixed design with $\beta_2 = 0.5$ and $\beta_1 = 0$ curvature.

frame results in a bumper error of 0.2° that is also incorporated in the simulations. ArrayCalc does not provide any information on the safety factor, only that 28 % of the load limit is reached.

Figure 6 shows the maps of the curved design as well as the mixed design and Figure 7 shows the A-weighted direct sound curve in on-axis direction. Compared to the previous results, it is noticeable that for more distant observation points lower sound pressure values are calculated in EASE for the $\beta = 0$ array than those obtained in the point source-based simulation. For the mixed array, the EASE simulation corresponds to the point-source-based simulation.

4 Measurement Study: Nexo Sample

For measurement, six Nexo GEO S1210 elements are lined up for which we calculated the source contour and simulated the direct sound levels in subsection 3.1. To record the position-dependent direct sound level curves, impulse response measurements were taken along 26 positions (on-axis) starting at $x_r = 5$ m and ending at $x_r = 30$ m. Pressure zone microphones, AKG PZM30 D, were positioned on the ground to avoid floor reflections in the measurements. We evaluated the first 300 samples of the impulse responses (6.25 ms at $f_s = 48$ kHz). Figure 8 shows the measurement setup.

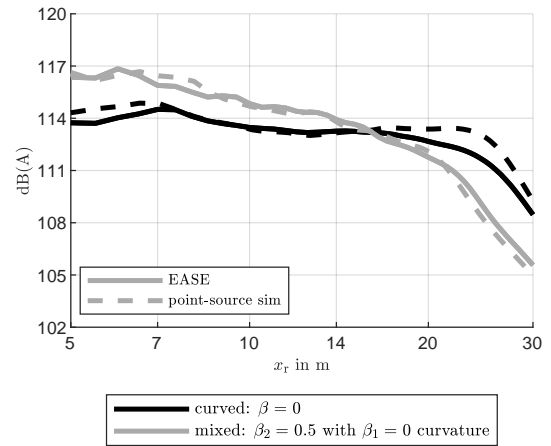


Fig. 7: V8: A-weighted simulated on-axis sound pressure of curved array (black) with decay $\beta = 0$ and mixed array (grey) with $\beta_1 = 0$ and $\beta_2 = 0$ over distance compared to simulations based on point sources (dashed).

Filter nr.	Frequency	Gain	Quality
1	386 Hz	-3.6 dB	1.004
2	539 Hz	2.7 dB	3.092
3	1203 Hz	-0.2 dB	5.738
4	3278 Hz	3.3 dB	1.417
5	8628 Hz	4.5 dB	1.118

Table 1: Filter settings for equalizing the RMS averaged response.

4.1 Equalizer

For equalization, we took the root mean squared average of the third octave averaged frequency responses of all positions. Table 1 shows the filter settings and Figure 9 presents the original averaged frequency response compared to the equalized as well as the frequency response of the proposed filter. It is noticeable that especially for higher frequency significant corrections are necessary to achieve a flat frequency response. Although it is common in practice to let the frequency response rise to low frequencies, we use a flat frequency response for broadband evaluation using A weighted sum. This makes only little difference to our analysis, as the A-filter is insensitive to low frequencies.



Fig. 8: Picture of the measurement setup: Nexo GEO S12 line-source array with pressure zone microphones on the floor.

4.2 Coverage over distance

Figure 10 shows the A-weighted on-axis sound pressure curve for the curved line-source array with $\beta = 0$ (black solid) compared to the simulation in EASE (black dotted) and the simulation of a discrete source composed of straight-line source polygons with splay angles rounded to integer degrees and leaving gaps in between the discrete elements (black dashed). For the measured level of the curved array, it sticks out that there is a boost between $x_r = 7$ m and $x_r = 10$ m and also around $x_r = 20$ m. This is most likely caused by the non-flat measurement plane which sags a little and reaches the lowest point at $x_r = 18$ m.

For analyzing the mixed design, the impulse response of each enclosure is shifted in time (sample-wise) as calculated by the online solver in section 3.1. Although the cabinet height of the line-source elements seems to be obstructive for the mixed design that is based on a delay and sum beamformer, the results show that the mixed design is also feasible in practice. The trend of the measured level (solid grey) coincides with the simulated one (dashed and dotted grey). The curves of both arrays were separated in the graphical representation for easier readability.

4.3 Frequency dependent radiation

Figure 11a shows the third octave averaged coverage of the $\beta = 0$ array over distance for different frequencies.

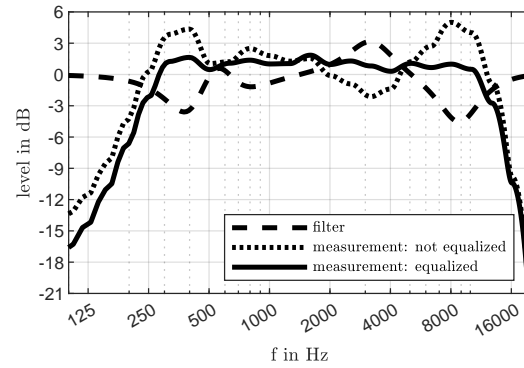


Fig. 9: GEO S12: Frequency response third octave averaged and root mean square averaged over the positions with the proposed filter.

To compare the results to the theoretical, Figure 11b shows the coverage of a continuous source using the point-source-based simulation. It sticks out that for low frequencies, the radiation gets point-source-like. For example, the transition radius between the far and near field is 6.2 m for 250 Hz, which is approximated by

$$r = \frac{2fS^2}{c}, \quad (5)$$

where S denotes the source length, f the frequency and c the speed of sound [15]. For both, measurement and simulation, point-source-like radiation for all presented frequencies is seen above $x_r = 18$ m due to finite source length. It is noticeable that the mid frequencies 500 Hz and 1000 Hz are more pronounced for farther points of observation in the measurement as in the simulation. This behavior is also seen as a small deviation in Figure 12a that presents the frequency response for different points of observation. In addition to the rather flat frequency responses for the mid-frequency range for distances above 10 m, the comb filter for the response at 7 m is striking which is also visible in the results of the point source based simulation, cf. Figure 12b that is caused by different times of arrival between the enclosures of the array and the observation point. This effect is more pronounced for closer points of observation as the difference in arrival times is larger than for farther points. For frequencies above 4 kHz, the results of simulation and measurement differ because the point-source-based simulation does not incorporate behavior of the HRW (Hyperbolic Reflective Waveguide).

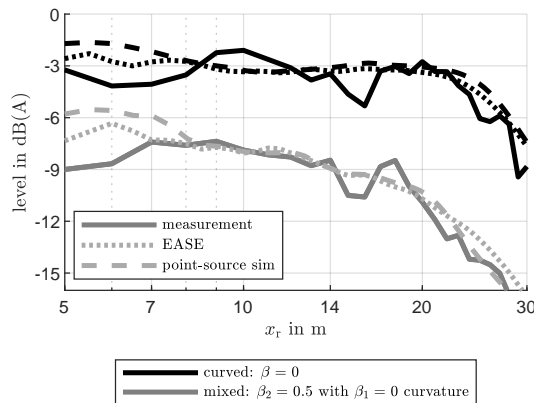


Fig. 10: GEO S12: A-weighted measured sound pressure of a curved array with decay $\beta = 0$ and mixed array with $\beta_1 = 0$ and $\beta_2 = 0$ over distance compared to simulated discretized sources.

By contrast, Figure 13a presents the third-octave averaged frequency responses of the mixed array with $\beta_2 = 0.5$ and $\beta_1 = 0$ curvature. The same filter from Figure 9 is used. The added delays lead to a position-dependent change in the impulse response of the entire array, which would require another equalization for this case, which is not implemented in our analysis. To match the frequency response of the mixed array to the response of the curved array, position-dependent filters would be necessary that are not feasible in practice. Figure 13b shows the sound level profile over distance for different frequencies of the mixed array. Compared to the purely curved array it is visible that all frequencies follow nearly the same trend. Therefore, it should be noted that design targets $\beta > 0$ are more relaxed and realistic and also more common in practical line-source array implementations.

5 Conclusion

This paper presented simulations of line-source arrays from different manufacturers considering a two-target design for immersive sound reinforcement. These showed that a mixture of curved and phased designs yields the desired targets and measurements of one system verified the simulated results in practice. Furthermore, we could show that a simplistic point-source-

based simulation suitably predicts the A-weighted sum of the azimuthally on-axis direct SPL.

We plan to undertake psychoacoustic experiments using miniature line arrays surrounding the audience in medium-sized immersive sound reinforcement for 50-250 listeners. Then experiments on bigger systems using conventional line-source arrays should be conducted to implement the idea of the two-target design for larger audience areas.

6 Acknowledgment

Our research was funded by the Austrian Science Fund (FWF): P 35254-N (Envelopment in Immersive Sound Reinforcement, EnImSo). We thank Scherrer Audio Veranstaltungstechnik for their help and for letting us measure the coverage of one of their Nexo line-source arrays at their facilities in Graz.

7 Data Availability

To support reproducible research, the simulation results and the impulse responses are available in [18] for download.

References

- [1] Ahnert, W. and Noy, D., *Sound Reinforcement for Audio Engineers*, Taylor & Francis Ltd, 2023, ISBN 978-1-032-11518-4.
- [2] Heil, C. and Urban, M., “Sound Fields Radiated by Multiple Sound Sources Arrays,” in *92nd AES Conv.*, Vienna, 1992.
- [3] Urban, M., Heil, C., and Bauman, P., “Wavefront Sculpture Technology,” *J. Audio Eng. Soc.*, 51(10), pp. 912–932, 2003.
- [4] Straube, F., Schultz, F., Makarski, M., Spors, S., and Weinzierl, S., “Evaluation Strategies for the Optimization of Line Source Arrays,” in *59th AES Conf.*, Montreal, Canada, 2015.
- [5] Straube, F., Schultz, F., Bonillo, D. A., and Weinzierl, S., “An Analytical Approach for Optimizing the Curving of Line Source Arrays,” *J. Audio Eng. Soc.*, 66(1/2), pp. 4–20, 2018.
- [6] Hölter, A., Straube, F., Schultz, F., and Weinzierl, S., “Enhanced Polygonal Audience Line Curving for Line Source Arrays,” in *150th AES Conv.*, 2021.

- [7] Ward, D., Kennedy, R., and Williamson, R., *Microphone Arrays*, chapter Constant Directivity Beamforming, pp. 3–17, Springer Berlin, Heidelberg, 2001, ISBN 978-3-642-07547-6, doi: 10.1007/978-3-662-04619-7.
- [8] Goodwin, M. and Elko, G., “Constant beamwidth beamforming,” in *IEEE ICASSP*, volume 1, pp. 169–172 vol.1, Minneapolis, USA, 1993, doi: 10.1109/ICASSP.1993.319082.
- [9] Meyer, D. G., “Digital Control of Loudspeaker Array Directivity,” *J. Audio Eng. Soc.*, 32(10), pp. 747–754, 1984.
- [10] van der Werff, J., “Design and Implementation of a Sound Column with Exceptional Properties,” in *96th AES Conv.*, Amsterdam, Netherlands, 1994.
- [11] Gölles, L. and Zotter, F., “Optimally Curved Arc Source for Sound Reinforcement,” in *Fortschritte der Akustik, DAGA*, Vienna, 2021.
- [12] Zotter, F., Riedel, S., Gölles, L., and Frank, M., “Acceptable Imbalance of Sound-Object Levels for Off-Center Listeners in Immersive Sound Reinforcement,” in *Fortschritte der Akustik, DAGA*, Hamburg, 2023.
- [13] Riedel, S. and Zotter, F., “Surrounding line sources optimally reproduce diffuse envelopment at off-center listening positions,” *JASA Express Letters*, 2(9), p. 094404, 2022, doi: 10.1121/10.0014168.
- [14] Riedel, S., Gölles, L., Zotter, F., and Frank, M., “Modeling the Listening Area of Envelopment,” in *Fortschritte der Akustik, DAGA*, Hamburg, 2023.
- [15] Gölles, Lukas and Zotter, Franz, “Theory of continuously curved and phased line sources for sound reinforcement,” *Acta Acust.*, 7, p. 52, 2023, doi: 10.1051/aacus/2023045.
- [16] Gölles, L., Zotter, F., and Merkel, L., “Miniature Line Array for Immersive Sound Reinforcement,” in *Proceedings of AES SIA Conf.*, Huddersfield, 2023.
- [17] Lukas Gölles, “Line Array Designer considering Two Targets,” <https://enimso.iem.sh/post/line-array-designer-two-target/>, 2023.
- [18] Lukas Gölles and Franz Zotter, “Supplementary Data for Dual-Target Design for Large-Scale Sound Reinforcement: Simulation and Evaluation,” <https://phaidra.kug.ac.at/o:131670>, 2023.

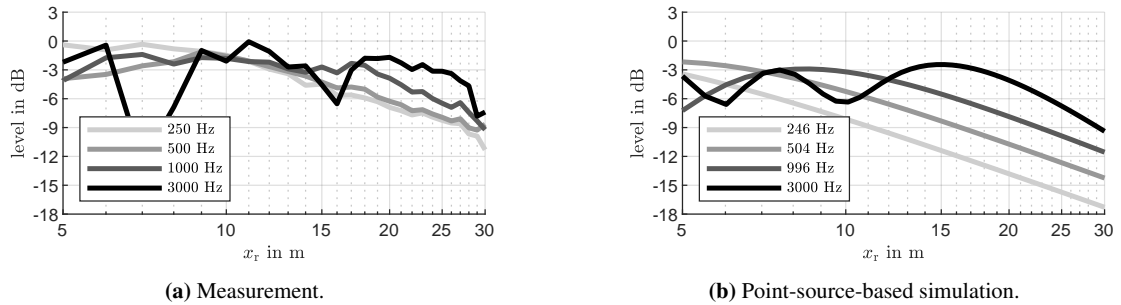


Fig. 11: GEO S12: Measured and simulated sound pressure of a curved array with decay $\beta = 0$ over distance for different frequencies.

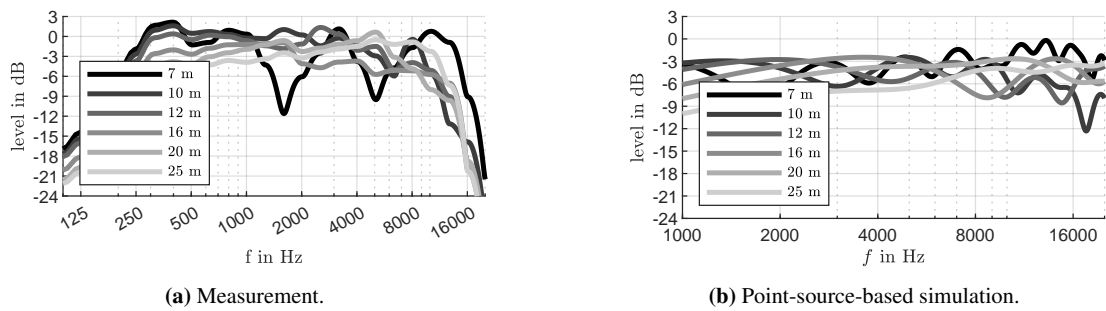


Fig. 12: GEO S12: Third octave averaged frequency response of $\beta = 0$ array for different positions.

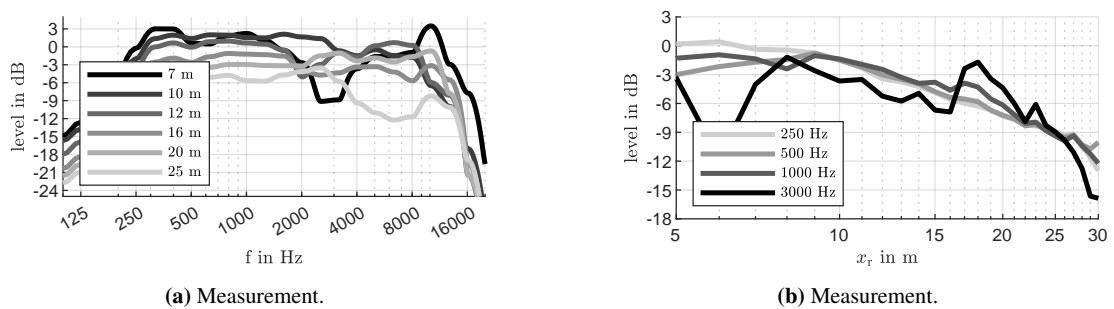


Fig. 13: GEO S12: Third octave averaged frequency response for different positions (left) and sound pressure profile for different frequencies (right) of a mixed array with $\beta_1 = 0$ curvature and $\beta_2 = 0.5$ target.

Publication V

This work was published as:

Lukas Gölles, Matthias Frank, and Franz Zotter, "Simulating the sweet area of immersive sound reinforcement with surrounding mini line arrays," in Fortschritte der Akustik, DAGA, Hannover, March 2024. [Online].

Available: https://pub.dega-akustik.de/DAGA_2024/files/upload/paper/188.pdf

DAGA 2024 Hannover

Simulating the Sweet Area of Immersive Sound Reinforcement with Surrounding Mini Line Arrays

Lukas Göllés¹, Matthias Frank¹, Franz Zotter¹¹ University of Music and Performing Arts, Institute of Electronic Music and Acoustics, 8010 Graz, Austria

Email: goelles@iem.at, frank@iem.at, zotter@iem.at

Introduction

The recent success in commercializing immersive music productions for home consumers boosts the urge to create surround audio experiences in concerts. Success requires a large sweet area in which the audience is presented with a balanced spatial audio reproduction. The sweet area needs to become larger than what point-source loudspeakers can achieve. Recent studies [1, 2, 3, 4] indicated that two design targets of the direct sound level should be pursued: 0 dB per doubling of the distance (dod) to preserve the mixing balance, and -3 dB/dod to preserve the envelopment at off-center listening positions.

The extended \mathbf{r}_E vector model [5, 6, 7] has already been used to predict the position-dependent localization error of an Ambisonic playback system [8]. This contribution deals employs this model to predict the mean absolute localization error of an arrangement of eight surrounding miniature line arrays with different distance decay settings in a 10 m \times 12 m room. In terms of direct-sound mixing balance, we use the maximum deviation from the median of all direct sound levels to estimate the area for plausible reproduction. To verify previous findings from listening experiments about envelopment [3, 4], we assume playback of decorrelated signals from all eight loudspeakers and use the length of the energy vector to predict diffuseness.

Line Array Curving and Phasing

To achieve an equalized on-axis direct sound level roll-off by $-6 \cdot \beta$ dB/dod, [9] presents a differential equation for a total inclination, composed linearly from a physical inclination / curvature and an electronic beamforming angle using delays. A mixed design implements two targets in a single system, e.g. the curvature is designed for 0 dB/dod and additional delays for each enclosure achieve -3 dB/dod. An online tool¹ solves this differential equation for a continuous source, discretizes the solution afterwards, and proposes tilt angles and delays for each enclosure in the chain of a line array. For practical reasons, we use mixed line array designs so that they may be compared to the results of listening experiments later. To support reproducible research, links to the online tool are provided with the parameters used.

Room and Source Geometry

The listening area is evaluated at the IEM CUBE, a 10 m \times 12 m studio with a reverberation time of 500 ms. We use a setup of eight surrounding line arrays that are equally spaced in the azimuth and positioned as close to

ear height (1.2 m for seated audience) as possible. The number of loudspeakers determines the optimal Ambisonic playback order $N = 3$ [10]. To simulate a real case scenario, we consider the dimensions of our miniature line array with eight enclosures. Each enclosure has a height of $h = 8.2$ cm [11]. For the sources positioned near the corners, we choose the farthest observation point of 12 m, the other sources were designed for 10 m. With these parameters, the online solver^{2,3,4,5} is used to set up the tilt angles for a purely curved line source with $\beta = 0$ and to propose delays to achieve $\beta_2 = 0.5$ or $\beta_2 = 1$ with the $\beta_1 = 0$ curvature, cf. [9]. Note that the line array solver assumes that the listener's ears are located in the x-y plane ($z = 0$).

Simulating the sound pressure of a discrete line source

The continuous source contour is discretized into a polygon of frequency-dependent straight-line elements of 7.38 cm length with gaps in between [9]. The length of these segments gets shorter by the fifth power of the frequency, i.e. for 20 Hz the length of the straight line corresponds to 90% of the height $h = 8.2$ cm and for 20 kHz it is 60%. The sound pressure is evaluated on a grid of 5 cm space for a frequency range between 20 Hz and 20 kHz with a linear resolution of 128 points. The results were A-weighted and summarized for broadband analysis. Figure 1 shows the simulated A-weighted direct sound pressure levels for different distance decay settings of the center loudspeaker in the front, 0 dB/dod, -3 dB/dod, and -6 dB/dod. These results are used as damping weights $w_{d,1}$ for calculating the energy vector below.

Energy vector

The normalized energy vector is calculated as the sum of the weighted unity vectors $\boldsymbol{\theta}_1$ [5, 6, 7],

$$\mathbf{r}_E = \frac{\sum_L (w_{\tau,1} \cdot w_{d,1} \cdot g_1)^2 \boldsymbol{\theta}_1}{\sum_L (w_{\tau,1} \cdot w_{d,1} \cdot g_1)^2}. \quad (1)$$

²<https://enimso.iem.sh/post/line-array-designer-two-target/?N=8&h=0.082&xr0=10&y0=1.1&g=0.312&beta=0&beta2=0.5&g2=0.683>

³<https://enimso.iem.sh/post/line-array-designer-two-target/?N=8&h=0.082&xr0=12&y0=1.1&g=0.282&beta=0&beta2=0.5&g2=0.657>

⁴<https://enimso.iem.sh/post/line-array-designer-two-target/?N=8&h=0.082&xr0=10&y0=1.1&g=0.312&beta=0&beta2=1&g2=1>

⁵<https://enimso.iem.sh/post/line-array-designer-two-target/?N=8&h=0.082&xr0=12&y0=1.1&g=0.282&beta=0&beta2=1&g2=1>

θ_l denotes the unity vector pointing from the listening position to the l -th loudspeaker, g_l the gain weight of the l -th loudspeaker, $w_{\tau,l}$ is the time weight and $w_{d,l}$ denotes the damping weight that we get from direct sound level simulations. For N -th order Ambisonic encoding and decoding to L loudspeakers, these gains $\mathbf{g} = [g_1 \ g_2 \ \dots \ g_L]^\top$ are

$$\mathbf{g} = \mathbf{D} \operatorname{diag}\{\mathbf{a}\} \mathbf{y}_N(\boldsymbol{\theta}_s). \quad (2)$$

\mathbf{D} is the decoder matrix calculated by the AllRAD approach [12], the diagonal matrix $\operatorname{diag}\{\mathbf{a}\}$ is used to apply max- r_E weights [13] and \mathbf{y}_N is the column vector containing the spherical harmonics up to order N evaluated at the desired normalized source direction $\boldsymbol{\theta}_s$. The time weights are $w_{\tau,l} = 10^{\frac{w_{\tau,l} - \tau_l}{1000}}$, where τ_l denotes the acoustic delay of the l -th loudspeaker to the listening position. $w_{\tau} = -1 \frac{\text{dB}}{\text{ms}}$ is a multiplication factor that is known from the echo threshold and chosen as trade-off between transient and stationary signals [14, 15, 16, 17, 18].

Localization error

The localization error is the horizontal difference between the predicted direction of the energy vector and the desired panning direction relative to the listening position. Figure 2 shows the root mean square of the localization error for panning around the horizon in steps of 1° with applied max- r_E weights for all three line array configurations, 0 dB/dod, -3 dB/dod, and -6 dB/dod. For excellent localization, the error should stay below 10° [13]. The area that is enclosed by the 10° contour is 61 m^2 for 0 dB/dod, 58 m^2 for -3 dB/dod and 49 m^2 for -6 dB/dod. The main difference between 0 dB/dod and -3 dB/dod lies in the areas near the loudspeakers located at $\varphi \in \{0^\circ, 90^\circ, 180^\circ, 270^\circ\}$. Furthermore, the area for 0 dB/dod is elliptical while it is square to rectangular for the other configurations.

Mixing balance

While the localization results show only weak differences between the different distance decay settings, we should also consider the mixing balance for surround sound applications. Optimally, direct sound objects should reach all positions in the audience with the same level, regardless of their panning direction. It has been shown that listeners tolerate a mixing imbalance of ± 3 dB with regard to the optimal mix [19]. We define the maximum absolute deviation from the median \tilde{w}_d as mixing balance,

$$\text{MB} = \max(|20 \lg w_d - 20 \lg \tilde{w}_d|). \quad (3)$$

Figure 3 shows the mixing balance for all three distance decay settings, 0 dB/dod, -3 dB/dod, and -6 dB/dod. In contrast to the results of the localization error, the results are clearly different from each other because the localization error only takes the direction of the energy vector into account which neglects the actual level of the phantom source. The area that is enclosed by the ± 3 dB limit is 65 m^2 for 0 dB/dod, 19 m^2 for -3 dB/dod, and 4 m^2 for -6 dB/dod.

Envelopment

So far, our simulations took the localization and mixing balance into account and thus only considered the behavior of direct sound objects of an immersive mix. However, immersive sound reinforcement has also to face surround effects, such as reverberation. Riedel et al. [3, 4] showed that loudspeakers, which direct sound level rolls off by -3 dB/dod, would be optimal to preserve the envelopment at off-center listening positions for a horizontal loudspeaker arrangement. Here, we use the length of the energy vector to predict the diffuseness, $1 - \|\mathbf{r}_E\|$. The diffuseness has to stay above 80 % to achieve plausible reproduction [20]. Figure 4 shows the results for eight surrounding line arrays with different distance decays assuming uncorrelated noise with unit variance from all arrays. It can be clearly seen that -3 dB/dod yields the largest area of 78 m^2 that is enclosed by the 80 % limit. By contrast, the areas of 0 dB/dod and -6 dB/dod are smaller with 12 m^2 and 4 m^2 , respectively.

Furthermore, the directions of the energy vectors for 0 dB/dod show an interesting behavior, cf. Figure 5. They point in the opposite direction when moving from the central listening position. At off-center positions, the number of closer loudspeakers decreases while the number of farther loudspeakers increases. As there are more distant loudspeakers of (nearly) equal level, the direction of the energy vector is dominated by the more distant loudspeakers. We may compensate that effect for many listening positions when using -3 dB/dod. For -6 dB/dod, the closer loudspeakers dominate the direction of the energy vector.

Optimal Targets

Optimal surround sound reinforcement should consider 0 dB/dod for direct sound objects and -3 dB/dod for the diffuse parts of an audio scene. To use both targets with a single system, mixed line array designs have to be pursued [9]. For a setup with eight surrounding line arrays with eight enclosures each, this requires a mixing desk with two individual eight-channel mix buses. The output of both buses must be fed into a processor that distributes the signal to 64 channels while adding delays to the envelopment bus for each enclosure individually. Furthermore, 64 amplifiers are necessary to drive the enclosures individually.

Conclusion

The simulations using the extended vector models could indicate that optimal immersive sound reinforcement must pursue two targets, 0 dB/dod for the direct sound and -3 dB/dod for the diffuse part to create maximum sweet areas for mixing balance and envelopment. Further listening experiments have to be conducted to verify the results of the simulations in practice. Moreover, such experiments should investigate whether the hardware effort could be decreased by a single design target with 0 dB/dod, -1.5 dB/dod or -3 dB/dod instead of the two targets while still providing plausible reproduction of audio scenes with both direct sound objects and enveloping diffuse sound.

DAGA 2024 Hannover

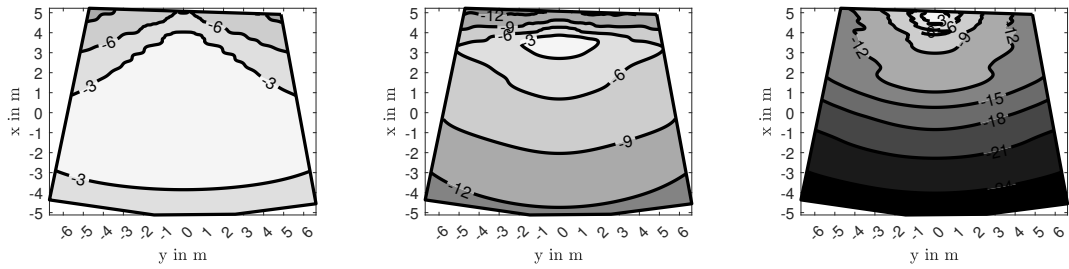


Figure 1: Simulated A-weighted direct sound level of the center line array with different distance decays: 0 dB/dod (left), -3 dB/dod (center) and -6 dB/dod (right).

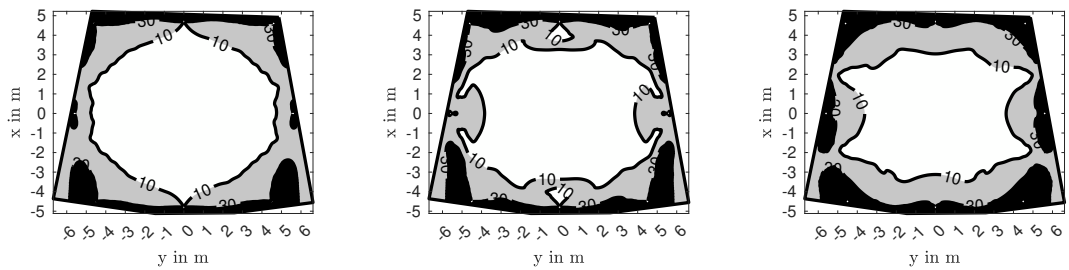


Figure 2: Simulations of the mean absolute localization error using the r_E vector model for third order Ambisonic encoding and decoding for panning on the horizon with applied max r_E weights: 0 dB/dod (left), -3 dB/dod (center) and -6 dB/dod (right).

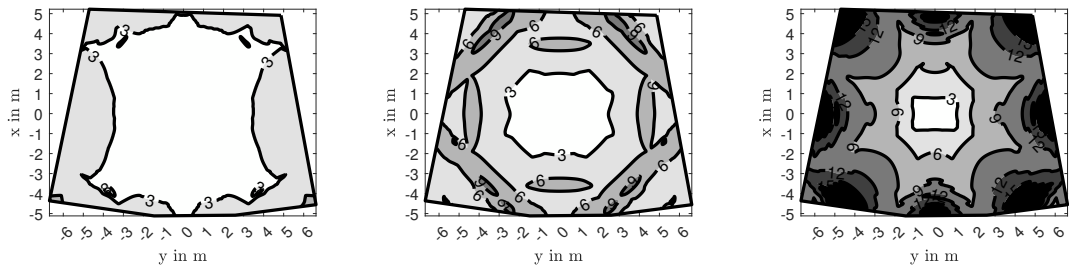


Figure 3: Simulated mixing balance for a setup of eight surrounding line arrays: 0 dB/dod (left), -3 dB/dod (center) and -6 dB/dod (right).

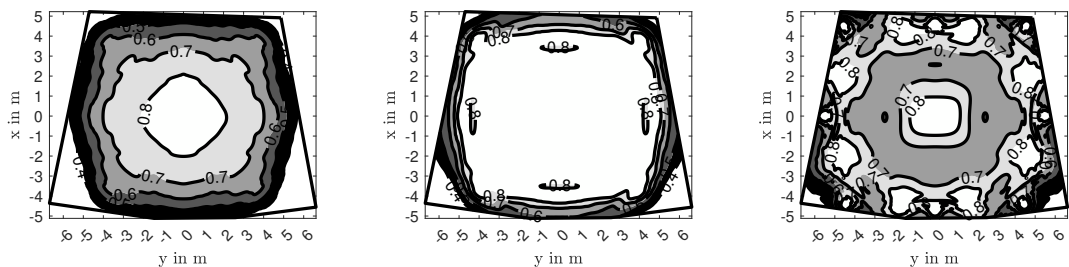


Figure 4: Simulated diffuseness of different line array settings for a setup of eight surrounding line arrays: 0 dB/dod (left), -3 dB/dod (center) and -6 dB/dod (right).

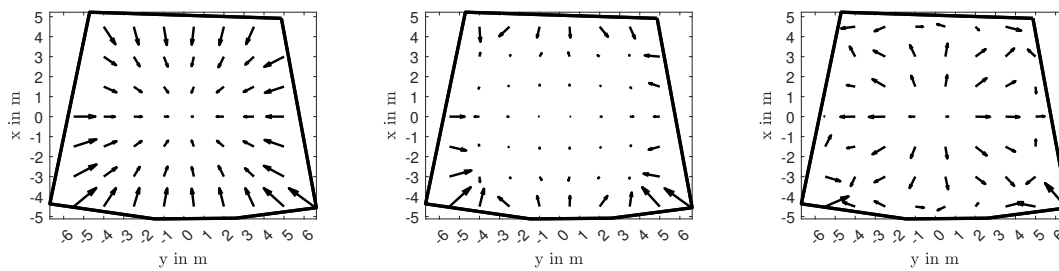


Figure 5: Simulated r_E vectors assuming decorrelated noise is played back by the line arrays: 0 dB/dod (left), -3 dB/dod (center) and -6 dB/dod (right).

Acknowledgment

Our research was funded by the Austrian Science Fund (FWF): P 35254-N, Envelopment in Immersive Sound Reinforcement (EnImSo).

Data Availability

In order to provide reproducible research, the direct sound level simulations are made available under [21].

References

- [1] P. Heidegger, B. Brands, L. Langgartner, and M. Frank, “Sweet area using ambisonics with simulated line arrays,” in *Fortschritte der Akustik, DAGA*, Wien, 08 2021.
- [2] L. Gölles and F. Zotter, “Optimally curved arc source for sound reinforcement,” in *Fortschritte der Akustik, DAGA*, Wien, 08 2021.
- [3] S. Riedel and F. Zotter, “Surrounding line sources optimally reproduce diffuse envelopment at off-center listening positions,” *JASA Express Letters*, vol. 2, no. 9, p. 094404, 09 2022.
- [4] S. Riedel, L. Gölles, F. Zotter, and M. Frank, “Modeling the listening area of envelopment,” in *Fortschritte der Akustik, DAGA*, 03 2023.
- [5] M. A. Gerzon, “General metatheory of auditory localisation,” in *Audio Engineering Society Convention 92*. Audio Engineering Society, 03 1992.
- [6] P. Stitt, S. Bertet, and M. van Walstijn, “Extended energy vector prediction of ambisonically reproduced image direction at off-center listening positions,” *J. Audio Eng. Soc.*, vol. 64, no. 5, pp. 299–310, 2016.
- [7] E. Kurz and M. Frank, “Prediction of the listening area based on the energy vector,” in *International Conference on Spatial Audio*, 09 2017.
- [8] M. Frank, “Localization using different amplitude-panning methods in the frontal horizontal plane,” in *Proceedings of the EAA Joint Symposium on Auralization and Ambisonics*, 01 2014.
- [9] L. Gölles and F. Zotter, “Theory of continuously curved and phased line sources for sound reinforcement,” *Acta Acust.*, vol. 7, p. 52, 2023.
- [10] M. Frank, L. Gölles, S. Riedel, and F. Zotter, “Equalizing the coloration of different ambisonic order weightings,” in *Fortschritte der Akustik, DAGA*, Hamburg, 03 2023.
- [11] L. Gölles, F. Zotter, and L. Merkel, “Miniature line array for immersive sound reinforcement,” in *Audio Engineering Society Conference: AES 2023 International Conference on Spatial and Immersive Audio*, Aug 2023.
- [12] F. Zotter and M. Frank, “All-round ambisonic panning and decoding,” *J. Audio Eng. Soc.*, vol. 60, no. 10, pp. 807–820, 2012.
- [13] —, *Ambisonics*. Springer, 04 2019.
- [14] H. Seraphim, “Über die Wahrnehmbarkeit mehrerer Rückwürfe von Sprachschall,” *Acta Acustica united with Acustica*, vol. 11, no. 2, pp. 80–91(12), 1961.
- [15] Rakerd, Hartmann, and Hsu, “Echo suppression in the horizontal and median sagittal planes,” *The Journal of the Acoustical Society of America*, vol. 107 2, pp. 1061–4, 2000.
- [16] P. Robinson, A. Walther, C. Faller, and J. Braasch, “Echo thresholds for reflections from acoustically diffusive architectural surfaces,” *The Journal of the Acoustical Society of America*, vol. 134, pp. 2755–2764, 10 2013.
- [17] E. Kurz, “Efficient prediction of the listening area for plausible reproduction,” Master’s thesis, University of Music and Performing Arts, Nov. 2018.
- [18] M. Frank and J. Kristl, “Perceptual sweet area of 2-channel stereo playback,” in *VDT International Convention*, 03 2024.
- [19] F. Zotter, S. Riedel, L. Gölles, and M. Frank, “Acceptable imbalance of sound-object levels for off-center listeners in immersive sound reinforcement,” in *Fortschritte der Akustik, DAGA*, 03 2023.
- [20] —, “Diffuse sound field synthesis,” 2024.
- [21] L. Gölles, “Simulated A weighted direct sound pressure levels of line arrays at the IEM CUBE,” 2024. [Online]. Available: <https://phaidra.kug.ac.at/o:133064>

Publication VI

This work was published as:

Lukas Gölles, Matthias Frank, and Franz Zotter, “Improving surround sound reinforcement at off-center listening positions with miniature line arrays,” in Audio Engineering Society Convention 156, Madrid, June 2024. [Online]. Available: <https://aes2.org/publications/elibrary-page/?id=22504>



Audio Engineering Society Convention Paper

Presented at the AES 156th Convention
2024 June 15–17, Madrid, Spain

This paper was peer-reviewed as a complete manuscript for presentation at this convention. This paper is available in the AES E-Library (<http://www.aes.org/e-lib>), all rights reserved. Reproduction of this paper, or any portion thereof, is not permitted without direct permission from the Journal of the Audio Engineering Society.

Improving Surround Sound Reinforcement at Off-center Listening Positions with Miniature Line Arrays

Lukas Göllés^{1,2}, Matthias Frank^{1,2}, and Franz Zotter^{1,2}

¹*Institute of Electronic Music and Acoustics, 8010 Graz, Austria*

²*University of Music and Performing Arts Graz, 8010 Graz, Austria*

Correspondence should be addressed to Lukas Göllés (goelles@iem.at)

ABSTRACT

Successful immersive sound reinforcement requires a large sweet area in which the audience is presented with a balanced sound. In smaller venues, state-of-the-art surround sound reinforcement employs point-source loudspeakers producing direct sounds that decays at a rate of 6 dB per distance doubling. In contrast, simulation studies and listening experiments using simulated line arrays have shown that a dual-target design of the direct sound has to be pursued: 0 dB per distance doubling to preserve the mixing balance and -3 dB to preserve the envelopment at off-center listening positions. This contribution presents a listening experiment comparing different distance decay settings of eight surrounding miniature line arrays of 65 cm total length in a 10.3 m × 12 m room. The experimental results can verify the findings of previous, more theoretical studies.

1 Introduction

Spatial audio, principally known from cinema and games, is gaining in importance, which also increases the interest in using such technology at live events. There are already several commercial solutions for large-scale sound reinforcement considering line arrays [1, Ch. 2, p. 24ff] which primarily concentrate on frontally positioned direct sound objects supplemented by surrounding effects to maintain the time-alignment of spatialized objects, particularly percussion elements, at off-center listening positions [2, 3].

However, direct sound objects can be positioned also around the listeners at venues with smaller listening areas for up to 250 people. These mid-scale surround sound applications still employ point-source loudspeakers in many cases. Experiments showed that a maximum mixing imbalance of ± 3 dB is acceptable for

surround sound reproduction [4]. In these experiments, listeners had to balance a mix of two sound objects and then find an upper and lower level difference at which playback is still acceptable. Considering two opposing point-sources, a level difference of 3 dB is reached, when moving approximately $\frac{1}{6}$ the setup radius away from the central listening position, strongly limiting the sweet area for mixing balance. By contrast, it has already been shown that sound reinforcement using surrounding line-source arrays increases the sweet area [5]. Furthermore, listening experiments with simulated line arrays (done by a half or full compensation of the $\frac{1}{r}$ direct sound level decay of physical point sources) revealed similar results for an Ambisonic playback system [6]. Simulations using the A-weighted direct sound level of curved line-source loudspeakers predicted an enlarged listening area compared to a setup with conventional point-source loudspeakers [7]. Considering



Fig. 1: IEM CUBE with miniature line arrays.

the diffuse surrounding sound, experiments showed that a setup of point sources is also not able to reproduce a fully enveloping scene at off-center listening positions [8]. Simulations and listening experiments with simulated line arrays showed that a -3 dB decay per distance doubling (dod) has to be pursued for preserving envelopment at off-center listening positions [6, 9, 10].

These simulated line arrays with point-source loudspeakers were able to compensate the level balances of the direct sound, but they neglected details that real line-source arrays exhibit: their directivity and frequency-dependent radiation.

This contribution presents a listening experiment using a surrounding ring of eight real miniature line arrays applying the theory proposed in [11]. We use a dual-target line-array design, which is a combination of curving and phasing/beamforming of line arrays. The listening experiment is split into two individual parts to find optimal array design targets for preserving the mixing balance on the one hand and to preserve the envelopment on the other at three off-center listening positions.

2 Preparation of the Experiment

2.1 Room and Source Setup

The listening experiment was conducted at the IEM CUBE, a $10.3\text{ m} \times 12\text{ m} \times 4.8\text{ m}$ studio with a reverberation time of 0.5 s . We used eight miniature line arrays with eight enclosures each in a circular layout, cf. Figure 1 and Figure 2. The $10\text{ cm} \times 10\text{ cm} \times 8.2\text{ cm}$ 3D printed enclosures of the line arrays are equipped with

2.5 inch broadband drivers, cf. [12]. In this experiment, three distance decay configurations were investigated: 0 dB/dod (constant source), -3 dB/dod (line source) and -6 dB/dod (point source). For the 0 dB/dod configuration, the position-dependent frequency responses of the small line arrays follow the desired target for frequencies above 1 kHz , while the radiation for lower frequencies tends towards -3 dB/dod . Furthermore, we added a special configuration which reduces the level of the center loudspeaker of the point-source setup by 9 dB . To preserve the signal components from the center, the signal was distributed to adjacent loudspeakers. This configuration was included to investigate the benefit of a center loudspeaker.

To enable seamless switching between the different configurations, we use mixed line array designs, a combination of curving and phasing/beamforming as described and evaluated in [11]. The curvature was designed to achieve 0 dB/dod when the line array elements were driven in phase. For the other configurations, delays were added to each enclosure to achieve -3 dB/dod and -6 dB/dod [13]. The nonlinear differential equation to design curving and phasing for a $-6 \cdot \beta$ dB direct sound level decay per distance doubling was presented in [11] and is implemented in an online solver [14]. This tool was used to calculate tilt angles and delays for the discrete line arrays, to which links are given in the footnote with the used parameters. Our setup required two different line array designs as the throw distances of odd-numbered loudspeakers^{1,2} differ from the throw distances of even numbered loudspeakers^{3,4}. We choose a rigging height of 2.3 m for which we assumed seated audiences (ear height: 1.2 m). The additional delays change the frequency response of the loudspeakers for each listening position individually. For example, Figure 6 shows the frequency responses of loudspeaker 1, 4, 7 and 8 for all positions

¹<https://enimso.iem.sh/post/line-array-designer-two-target/?N=8&h=0.082&xr0=10&y0=1.1&q=0.31&beta=0&beta2=0.5&g2=0.693>

²<https://enimso.iem.sh/post/line-array-designer-two-target/?N=8&h=0.082&xr0=10&y0=1.1&q=0.31&beta=0&beta2=0.5&g2=0.693>

³<https://enimso.iem.sh/post/line-array-designer-two-target/?N=8&h=0.082&xr0=12&y0=1.1&q=0.283&beta=0&beta2=0.5&g2=0.668>

⁴<https://enimso.iem.sh/post/line-array-designer-two-target/?N=8&h=0.082&xr0=12&y0=1.1&q=0.283&beta=0&beta2=1&g2=1>

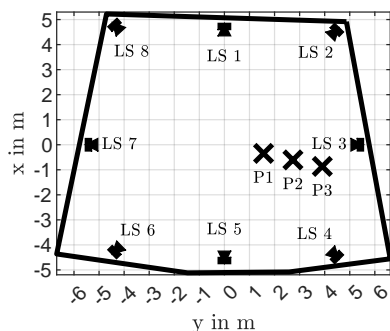


Fig. 2: Loudspeaker setup at the IEM CUBE with positions for the listening experiments marked as crosses.

with different distance decay settings. The graphs were separated for easier readability. As there are only slight differences in the responses, we omitted any position-dependent equalizing in detail, as it is not feasible in practice.

The three off-center listening positions were chosen to be on a straight line and that the level difference of two opposing sources that contains direct sound objects in the listening experiments, LS 3 and LS 7, is included. However, we have placed the line at a slight angle to the rear so that LS 3 does not take on an overriding role in the listening experiment because the results in the off-axis direction are representative of a larger number of listeners.

The listening test was split into two parts to find the optimum distance decays for two different tasks: preservation of the mixing balance at off-center listening positions and preservation of the envelopment at off-center listening positions.

2.2 Stimuli

In the first part, three music excerpts were played back in the following sequence with increasing complexity of the scene:

- (i) a 12.09 s loop from Clara Berry and Wooldog's *Waltz For My Victims* from MUSDB18 [15] where the drums are panned to $\varphi = -90^\circ$, the bass and the singing voice are placed to the frontal center, $\varphi = 0^\circ$, and the piano is panned to $\varphi = 90^\circ$. The spatial placement where chosen to enable clear separation of the instruments in the first track to be rated.
- (ii) a 4.56 s loop from the live-concert recording

The Magical Music of Disney played by Bergkapelle Leoben-Seegraben, a wind orchestra consisting of 63 musicians with a choir consisting of 10 singers. We spatialized the recordings of 41 spot microphones in the frontal semicircle using the `MultiEncoder` of the IEM Plugin Suite⁵.

(iii) a 13.28 s loop from the live-concert recording *Moment for Morricone* played by the same orchestra with equal spatial distribution of the spot microphones as (ii) but with added choir.

Ambisonic decoding was done using the `AllRAD` approach [16] with applied `max-rE` weights [17]. At zenith and nadir, an imaginary loudspeaker was added with zero gain to maintain the directional resolution at the horizon [18]. Playback used third-order Ambisonics to achieve optimally smooth panning on the given ring with eight loudspeaker arrays [19]. We applied amplitude compensation of the different loudspeaker distances to the center but omitted delay compensation as it can reduce the size of the sweet area [20].

In the second part, uncorrelated noise and recorded rain spatialized with the `GranularEncoder` of the IEM Plugin Suite are played back. The uncorrelated noise was routed directly to the corresponding loudspeaker arrays without Ambisonic processing, while the spatialized rain was decoded the same way as the scenes in the first part of the experiment. We added a low-pass filter with cut-off frequency at $f_c = 4\text{kHz}$ to reduce possible coloration caused by the phasing/beamforming and spatial aliasing due to the driver spacing.

3 Experimental procedure

Before the listening test started, we clarified the terms mixing balance and envelopment and performed demonstrations using different distance decay settings if necessary.

The experiment started at listening position P1, marked as cross in Figure 2, with the task of evaluating the mixing balance part followed by evaluation of the envelopment. Then, participants had to move to the second position P2, repeat both tasks, and continue at the third position P3 afterwards. To compare the different array configurations all at once, a Multi-Stimulus Test with Hidden Reference and Anchor (MUSHRA) [21] appeared to be a suitable test paradigm. The distance decay configurations were randomized within each trial, but participants were presented with the fixed order of

⁵<https://plugins.iem.at>

audio scenes at each position as the tracks increase in complexity in this order.

3.1 Mixing Balance including consistency of directional images

In the first part, the participants were asked to switch between the mono reproduction played back from the center array as a reference and the spatial reproduction using the surrounding arrays. They had to consider three questions gathered into a single answer, where 0 denoted the worst and 100 the best configuration. Listeners were asked to use the whole range. If the participant did not use the entire range, the results were normalized to the desired range between 0 and 100. The two other configurations had to be positioned relatively to the best and worst:

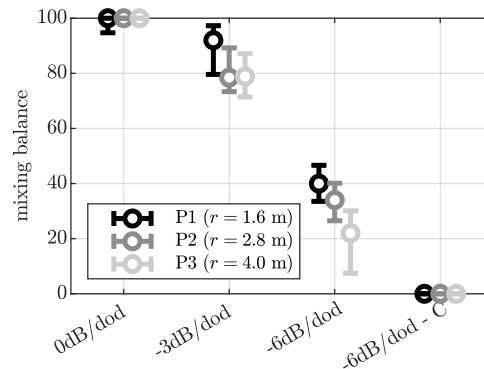
- (a) Is the mix balance preserved if you compare the spatial reproduction to the mono reproduction from the center?
- (b) Does the perceived distance change when comparing the sources positioned around the center of the spatial mix with the mono reproduction?
- (c) Are the directional voices well distributed across the frontal semicircle or is there a hole around the center?

3.2 Envelopment

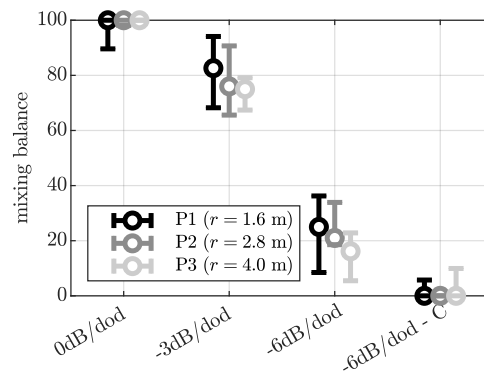
In the second part, they had to rate the envelopment, i.e. the feeling of being surrounded by sound. Here, 0 denoted not enveloping at all, which meant that the perceived sound collapses into a single direction. 100 denoted completely enveloping sound, i.e. there was no preferred perceived direction. The listeners were asked to rate a scene with highest score, when they had the feeling that the sound field had no preferred direction.

4 Results

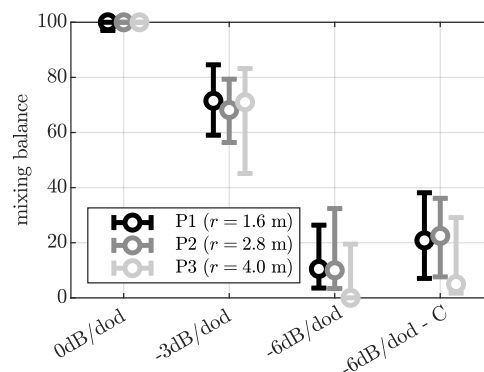
25 listeners (24 male, 1 female, 21 with experience in audio engineering) took part in the experiment with an average age of 33 years. The entire experiment took them on average 28 min 21 s.



(a) Results for *Waltz For My Victims*



(b) Results for *The Magical Music of Disney*



(c) Results for *Moment for Morricone*

Fig. 3: Medians and corresponding 95% confidence intervals of mixing balance for different array configurations.

	0dB −3dB	0dB −6dB	−3dB −6dB	−3dB −6dB-C	−6dB −6dB-C
P1	0.541	3.585	1.739	3.186	0.890
P2	1.041	4.197	1.635	3.106	0.846
P3	1.165	6.039	2.418	3.460	0.649

Table 1: Effect size for pairwise comparisons of pooled mixing balance for different array configurations, values greater 0.8 denote large effect.

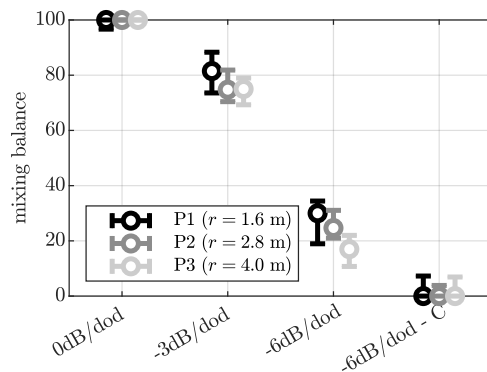


Fig. 4: Medians and corresponding 95% confidence intervals of mixing balance for different array configurations pooled over all audio scenes.

4.1 Mixing balance including consistency of directional images

Figure 3 shows the result for the first part of the listening experiment regarding the mixing balance including consistency of directional images. Comparing the results for each scene, it becomes clear that the participants rated the configuration with 0 dB/dod best. −3 dB/dod achieves slightly worse results. The ratings for the point-source configurations are clearly worse, especially for −6 dB/dod-C. The differences in the ratings across the audio scenes are significant, excepted for the most complex audio scene, *Moment for Morricone*, where a Wilcoxon signed-rank test with Bonferroni-Holm correction indicates $p > 0.5$. Also, ratings for 0 dB/dod and −3 dB/dod are only weakly significantly different ($p = 0.07$) for the first scene. We performed a correlation analysis between each scene at each position. The correlation coefficient is always above 0.85 and indicates strong correlation that allows the results of all scenes to be pooled, cf. Figure 4. It should be noted that the center loudspeaker increases clarity and stability (−6 dB/dod vs. −6 dB/dod - C)

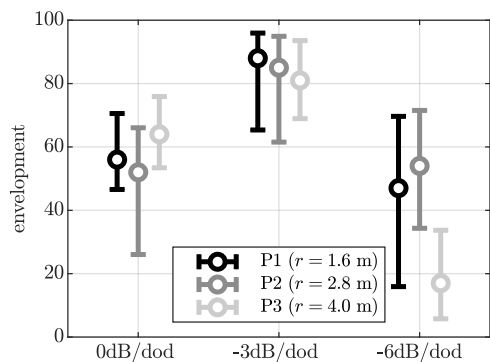
of a scene with a well defined voice in the center, cf. *Waltz For My Victims*. However, when considering a scene, in which instruments and a choir are distributed around the front semicircle without preference of a particular voice, cf. *Moment for Morricone*, the center loudspeaker becomes less important as the effects of stability and clarity are not as pronounced.

Comparing the pooled results of the two best configurations, 0 dB/dod with −3 dB/dod, the median differs about 20-30 points, cf. Figure 4. The signed-rank test reveals significant differences for all positions ($p < 0.001$). We also calculated the impact effect size [22] which indicates great effects for the two outermost positions, cf. Table 1. Although there are significant differences between these two configurations, it required a high level of attention to distinguish between the configurations which was reported by some participants after the experiment.

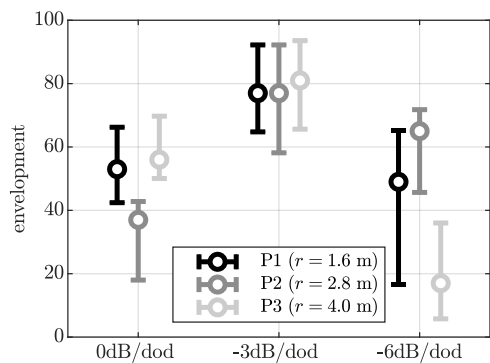
In terms of mixing balance, level decays 0 dB/dod and −3 dB/dod outperform the point-source configurations. Not only are the median values clearly different, the effect sizes also show a very large influence. Furthermore, −3 dB/dod and −6 dB/dod are worse for positions further out. The point-source configurations −6 dB/dod and −6 dB/dod-C were rated worst. The signed-rank test also indicates significant differences for all positions ($p < 0.01$) and the effect sizes from Table 1 show large effects. Furthermore, the participants noted that the voices are perceived more distantly, especially those placed around the center because the source directivity is higher for smaller distance decays cf. [11]. The effect sizes comparing 0 dB/dod with −6 dB/dod-C are not listed as the distribution of the results are clearly different which would result in extremely high values for the effect size effect size.

4.2 Envelopment

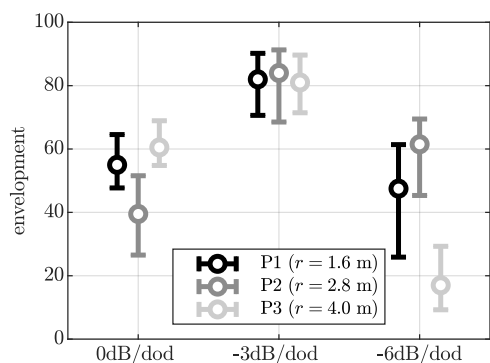
Array configurations with −3 dB/dod were rated best in terms of envelopment in the second part of the experiment, cf. Figure 5. The Wilcoxon signed-rank



(a) Results for decorrelated noise.



(b) Results for spatialized rain.



(c) Results pooled over all audio scenes.

Fig. 5: Medians and corresponding 95% confidence intervals of mixing envelopment for different array configurations.

	0dB/-3dB	0dB/-6dB	-3dB/-6dB
P1	0.554	0.348	0.617
P2	0.910	0.341	0.390
P3	0.444	1.170	2.143

Table 2: Effect size for pairwise comparisons of envelopment for different array configurations, values greater 0.8 denote large effect.

test with Bonferroni-Holm correction shows significant differences for all positions between the -3 dB/dod array and 0 dB/dod array and between -3 dB/dod array and -6 dB/dod array ($p < 0.01$). For position P2, there is only a weak difference between -3 dB/dod and -6 dB/dod ($p = 0.0558$). Between 0 dB/dod and -6 dB/dod significant results are denoted only on position P3. In contrast to the results of the previous part about mixing balance, the effect sizes indicate smaller effects, cf. Table 2 as the spread is larger.

Furthermore, some participants noted that the 0 dB/dod configuration leads to an unnatural behavior as the perceived direction pulls to the left, even though they were sitting to the right of the central position. Considering a circular setup in the free field with an infinite number of loudspeakers with 0 dB/dod placed on the horizon, the energy vector [23, 24, 25] is $r_E = 0$ in the center. Moving to the right, the direction of the energy vector is determined by more sound sources located on the left as the direct sound level of each loudspeaker is constant. This effect is also apparent when using a discrete set of loudspeaker directions.

5 Discussion

Our results clearly show that mixing balance is preserved best by the array configuration with 0 dB/dod, while envelopment is best for the configuration with -3 dB/dod. As a consequence, loudspeaker systems should optimally be able to realize these two targets at the same time. In practice, this would require two independent mix buses, to treat the direct sound objects and the enveloping parts individually. One drives line array in phase with curving designed for 0 dB/dod and the other one adds delays to each individual element of the line array to achieve -3 dB/dod. Optimal surround sound reinforcement using eight line arrays with eight elements each, has to consider a system of 64 amplifiers, a mixing console of two individual mix buses with eight channels each and a processor that distributes the

outputs of the mixer to the arrays and adds delays to the bus containing the enveloping parts. These delays have to be added with high precision as small deviations lead to a deviation of the distance decay. Furthermore, immersive audio productions must separate the direct part from the diffuse, enveloping part and provide both parts separately to enable separate processing at playback.

6 Conclusion

In this contribution, we compared mix balance including consistency of directional images and envelopment for surround sound reinforcement using a circle of eight miniature line arrays with different direct SPL supply profiles at three off-center listening positions in 10.3 m × 12 m room. The results of the listening experiment indicate that a dual-target design of the direct sound decay should be pursued for optimal surround sound reinforcement: 0 dB per distance doubling for preserving the mix balance at off-center listening positions and −3 dB per distance doubling for preserving the envelopment. Moreover, reducing the level of the center array while preserving its signal by distributing it to the neighboring arrays, decreases the mixing balance. Further work could investigate whether such a dual-target design is necessary with both direct and enveloping/diffuse parts separately rendered, or whether a single target of 0 dB, −1.5 dB or −3 dB per distance doubling achieves acceptable playback. Moreover, it would be interesting to find out whether further improvements can be achieved with planar arrays that are not only able to control the SPL profile along a line into the audience, but across the audience area.

7 Acknowledgments

Our research was funded by the Austrian Science Fund (FWF): P 35254-N (Envelopment in Immersive Sound Reinforcement, EnImSo). We thank all listeners for their participation in the experiment, Bergkapelle Leoben-Seegraben for providing the concert recordings for the listening experiment and the company Herzkraft for cooperation during the recording.

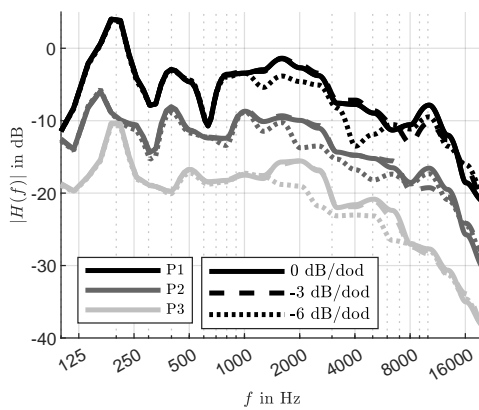
8 Data Availability

To support reproducible research, the results of the listening experiments are made available under [26].

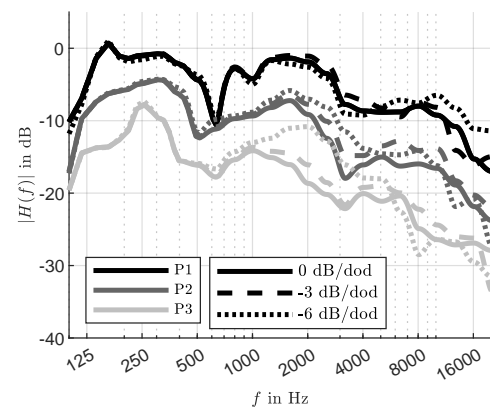
References

- [1] Patterson, J. and Lee, H., editors, *3D Audio, Perspective on Music Production*, Routledge, United States, 1st edition, 2021, ISBN 9781138590069, doi: 10.4324/9780429491214.
- [2] Mouterde, T., Epain, N., Moulin, S., and Corteel, E., “On the perception of musical groove in large-scale events with immersive sound,” in *Audio Engineering Society Conference: AES 2023 International Conference on Spatial and Immersive Audio*, 2023.
- [3] Mouterde, T., Epain, N., Moulin, S., and Corteel, E., “On the factors influencing groove fidelity in immersive live music events,” in *Audio Engineering Society Conference: AES 2024 International Acoustics & Sound Reinforcement Conference*, 2024.
- [4] Zotter, F., Riedel, S., Gölles, L., and Frank, M., “Acceptable Imbalance of Sound-Object Levels for Off-Center Listeners in Immersive Sound Reinforcement,” Hamburg (Deutschland), 2023.
- [5] Nettingsmeier, J. and Maier, P., “Scaling up: Making point-source multichannel material work for large listening areas,” 2015.
- [6] Heidegger, P., Brands, B., Langgartner, L., and Frank, M., “Sweet Area using Ambisonics with simulated Line Arrays,” Wien (Österreich), 2021.
- [7] Gölles, L. and Zotter, F., “Optimally Curved Arc Source for Sound Reinforcement,” Wien (Österreich), 2021.
- [8] Blochberger, M., Zotter, F., and Frank, M., “Sweet area size for the envelopment of a recursive and a non-recursive diffuseness rendering approach,” Ilmenau (Deutschland), 2019.
- [9] Riedel, S. and Zotter, F., “Surrounding line sources optimally reproduce diffuse envelopment at off-center listening positions,” *JASA Express Letters*, 2(9), p. 094404, 2022, doi: 10.1121/10.0014168.
- [10] Riedel, S., Gölles, L., Zotter, F., and Frank, M., “Modeling the Listening Area of Envelopment,” in *Fortschritte der Akustik, DAGA*, Hamburg, 2023.

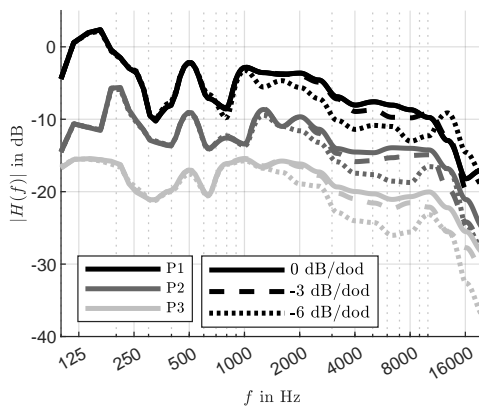
- [11] Gölles, L. and Zotter, F., “Theory of continuously curved and phased line sources for sound reinforcement,” *Acta Acust.*, 7, p. 52, 2023, doi: 10.1051/aacus/2023045.
- [12] Gölles, L., Zotter, F., and Merkel, L., “Miniature Line Array for Immersive Sound Reinforcement,” in *Audio Engineering Society Conference: AES 2023 International Conference on Spatial and Immersive Audio*, 2023.
- [13] Gölles, L. and Zotter, F., “Dual-Target Design for Large-Scale Sound Reinforcement: Simulation and Evaluation,” in *Audio Engineering Society Conference: AES 2024 International Conference on Acoustics & Sound Reinforcement*, 2024.
- [14] Gölles, Lukas, “Line Array Designer considering Two Targets,” <https://enimso.iem.sh/post/line-array-designer-two-target/>, 2023.
- [15] Rafii, Z., Liutkus, A., Stöter, F.-R., Mimitakis, S. I., and Bittner, R., “The MUSDB18 corpus for music separation,” 2017, doi: 10.5281/zenodo.1117372.
- [16] Zotter, F. and Frank, M., “All-Round Ambisonic Panning and Decoding,” *J. Audio Eng. Soc.*, 60(10), pp. 807–820, 2012.
- [17] Daniel, J., *Représentation de champs acoustiques, application à la transmission et à la reproduction de scènes sonores complexes dans un contexte multimédia*, Ph.D. thesis, Université de Paris 6, 2000.
- [18] Zotter, F., Riedel, S., and Frank, M., “All-Round Ambisonic Decoding: Spread and Correlation,” in *Fortschritte der Akustik, DAGA*, Stuttgart, 2022.
- [19] Frank, M., Gölles, L., Riedel, S., and Zotter, F., “Equalizing the coloration of different Ambisonic order weightings,” in *Fortschritte der Akustik, DAGA*, Hamburg, 2023.
- [20] Frank, M., “How to make Ambisonics sound good,” 2014.
- [21] “RECOMMENDATION ITU-R BS.1534-1 - Method for the subjective assessment of intermediate quality level of coding systems,” 2003.
- [22] Lötsch, J. and Ultsch, A., “A non-parametric effect-size measure capturing changes in central tendency and data distribution shape,” *PLoS ONE*, 15, 2020, doi: 10.1371/journal.pone.0239623.
- [23] Gerzon, M. A., “General metatheory of auditory localisation,” in *Audio Engineering Society Convention 92*, Audio Engineering Society, 1992.
- [24] Frank, M., “Localization using different amplitude-panning methods in the frontal horizontal plane,” in *Proc. of the EAA Joint Symposium on Auralization and Ambisonics*, Berlin, 2014.
- [25] Kurz, E. and Frank, M., “Prediction of the listening area based on the energy vector,” in *Proc. of International Conference on Spatial Audio*, Graz, 2017.
- [26] Lukas Gölles, “Supplementary Data for Improving Surround Sound Reinforcement at Off-center Listening Positions with Mini Line Arrays,” <https://phaidra.kug.ac.at/o:133352>, 2024.



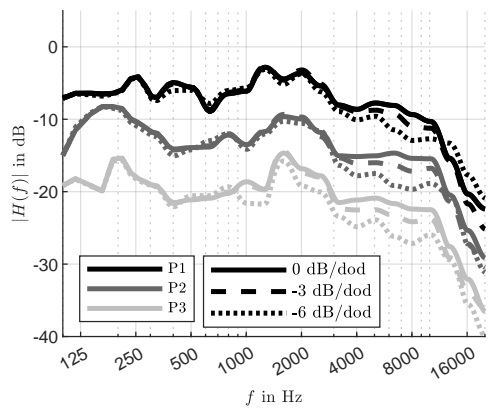
(a) Frequency responses of Loudspeaker 1



(b) Frequency responses of Loudspeaker 4



(c) Frequency responses of Loudspeaker 7



(d) Frequency responses of Loudspeaker 8

Fig. 6: Frequency responses of the first 2000 samples (41.67 ms at $f_s = 48$ kHz) of the impulse responses of the miniature line arrays at different observation points with different distance decay settings; for easier readability we applied offsets in steps of 6 dB.

Publication VII

This work was published as:

Lukas Gölles, Matthias Frank, and Franz Zotter, “Evaluating a dual-target line-array design for medium-scale surround sound reinforcement,” in Audio Engineering Society Convention 156, Madrid, June 2024. [Online]. Available: <https://aes2.org/publications/elibrary-page/?id=22560>



Audio Engineering Society

Convention Express Paper 214

Presented at the AES 156th Convention
2024 June 15–17, Madrid, Spain

This convention paper was selected based on a submitted abstract and 750-word precis that have been peer reviewed by at least two qualified anonymous reviewers. The complete manuscript was not peer reviewed. This convention paper has been reproduced from the author's advance manuscript without editing, corrections, or consideration by the Review Board. The AES takes no responsibility for the contents. This paper is available in the AES E-Library (<http://www.aes.org/e-lib>), all rights reserved. Reproduction of this paper, or any portion thereof, is not permitted without direct permission from the Journal of the Audio Engineering Society.

Evaluating a Dual-Target Line-Array Design for Medium-Scale Surround Sound Reinforcement

Lukas Göllles^{1,2}, Matthias Frank^{1,2}, and Franz Zotter^{1,2}

¹*Institute of Electronic Music and Acoustics, 8010 Graz, Austria*

²*University of Music and Performing Arts Graz, 8010 Graz, Austria*

Correspondence should be addressed to Lukas Göllles (goellles@iem.at)

ABSTRACT

Recent research shows that optimal surround sound reinforcement should consider a dual-target design of the direct sound: 0 dB per distance doubling (dod) to preserve the mixing balance at off-center listening positions and -3 dB/dod to preserve the envelopment. To enable this, direct sound objects and the diffuse, enveloping parts of an immersive mix need to be processed separately on two mix buses. This requires high software and hardware efforts to implement both targets with a single loudspeaker system which begs the question: Can a single target achieve sufficiently acceptable reproduction, when considering a typical scenario composed of frontally panned direct sound objects and complementing surrounding effects? This contributions presets the results of a listening experiment using eight surrounding miniature line arrays in a $10.3\text{ m} \times 12\text{ m}$ room to answer the question.

1 Introduction

Surround sound systems for live events have gained popularity recently, and guidelines for setting up immersive loudspeaker systems in large-scale sound reinforcement have been described by Corteel et al. [1, Ch. 2, p. 24ff]. According to recent studies, direct sound objects should only be positioned frontally in order to preserve the musical groove, while lateral and back loudspeakers should mainly be used for immersive sound components and effects [2, 3].

Considering medium-scale surround sound reinforcement for audiences up to 250 people, current research focuses on determining the optimal distance decay [4, 5, 6, 7, 8, 9, 10]. It has been shown that a dual-target

design for horizontally-placed line arrays would be optimal: 0 dB per distance doubling (dod) to preserve the mixing balance and -3 dB/dod to preserve the envelopment at off-center listening positions. To employ both within a single system, mixed line array designs were presented that combine curving and phasing/electronic beamforming [11], which was verified to be applicable to professional line source arrays [12]. Assuming an arrangement of eight surrounding line arrays with eight enclosures each, a dual-target design calls for a mixing desk with two eight-channel mix buses, 64 individually controllable amplifiers, and a processor that distributes the signals from the mix buses to the amplifiers. Additionally, the processor needs to be able to precisely apply sample-wise delays to each enclosure in the line



Fig. 1: IEM CUBE with mounted line arrays

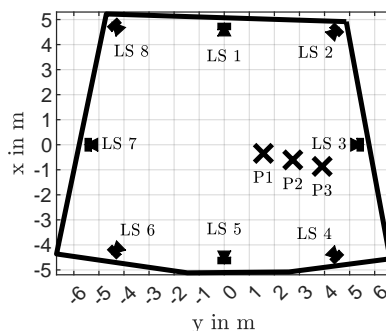


Fig. 2: Source and listening positions at the IEM CUBE

array loudspeaker chain as small deviations lead to deviations of the distance decay.

Compared with the dual-target design target as a reference, this contribution presents a listening experiment that examines if a uniform single-target design, such as 0 dB/dod, -1.5 dB/dod, -3 dB/dod, or -6 dB/dod can achieve acceptable playback in a scenario with frontal direct sound objects and surrounding reverberation.

2 Preparation of the Experiment

2.1 Room and Source Setup

A listening experiment was conducted at the IEM CUBE, a $10.3\text{ m} \times 12\text{ m}$ studio with a reverberation time of 0.5 s , cf. Figure 1. For playback, we used eight miniature line arrays with eight self-printed enclosures each [13] which were positioned in a circular layout as close to ear height (1.2 m for seated audiences) as

possible. The total length of one array was 65 cm . For curvature and phasing design, we used a web-based line array designer that solves the differential equation presented in [11] for a continuous curved source with phasing for a dual-target design. The tool discretizes the solution and outputs tilt angles and delays for a mixed array design. The curvature was calculated for the first target to achieve a direct sound level of 0 dB/dod , and delays were added for -1.5 dB/dod , -3 dB/dod and -6 dB/dod . Links to the tool with the parameters used to reproduce the design are provided, where the throw distance of the odd-numbered loudspeakers $1,2,3$ differed from the even-numbered loudspeakers $4,5,6$. This is because the even-numbered loudspeakers are placed near the corner and must therefore cover a larger distance. Note that the additional delays caused a position-dependent change of the frequency response; in default of a comprehensive compensation strategy, position dependency was accepted in the present study. The number of line arrays determines the optimal Ambisonic order, $N = 3$ [14], for which encoding and decoding was done using the *IEM Plugin Suite*⁷. We applied max r_E weights and amplitude compensation to the center but omitted delay compensation because it can reduce the size of the sweet area [15]. The decoder matrix was designed using the AllRAD approach [16]. At zenith and nadir, an imaginary loudspeaker was added to maintain the directional resolution on the horizon.

To comply with a prior listening experiment [10], the

¹<https://enimso.iem.sh/post/line-array-designer-two-target/?N=8&h=0.082&xr0=10&y0=1.1&q=0.31&beta=0&beta2=0.25&g2=0.482>

²<https://enimso.iem.sh/post/line-array-designer-two-target/?N=8&h=0.082&xr0=10&y0=1.1&q=0.31&beta=0&beta2=0.5&g2=0.693>

³<https://enimso.iem.sh/post/line-array-designer-two-target/?N=8&h=0.082&xr0=10&y0=1.1&q=0.31&beta=0&beta2=0.5&g2=0.693>

⁴<https://enimso.iem.sh/post/line-array-designer-two-target/?N=8&h=0.082&xr0=12&y0=1.1&q=0.283&beta=0&beta2=0.25&g2=0.455>

⁵<https://enimso.iem.sh/post/line-array-designer-two-target/?N=8&h=0.082&xr0=12&y0=1.1&q=0.283&beta=0&beta2=0.5&g2=0.668>

⁶<https://enimso.iem.sh/post/line-array-designer-two-target/?N=8&h=0.082&xr0=12&y0=1.1&q=0.283&beta=0&beta2=1&g2=1>

⁷<https://plugins.iem.at>

same setup and the same listening positions were used, cf. Figure 2.

2.2 Stimuli

Listeners were presented with a 15 s excerpt of the *The Marsh Marigold's Song* [17] by *Don Camillo Choir*. The first situation, which we refer to as the *wide mix*, had voices panned across the frontal half circle, i.e., $\varphi = \pm 90^\circ$ with an additional solo voice played back from the center, LS 1. The direct sound mix was complemented with the reverberation of two different rooms, York Minster cathedral ($T_{30} = 8.4$ s) [18] and Stefaniensaal of Congress Graz ($T_{30} = 1.7$ s) [19]. The reverberation was based on measured first-order Ambisonic impulse responses which were upmixed to third order using the 2DSE2 algorithm [20]. The direct sound was removed so that early reflections and diffuse components remained in the impulse response which were convolved with the direct sound objects using the *mcfx_convolver* of the *multichannel audio plug-in suite* by Matthias Kronlachner⁸.

The second scenario, denoted as the *narrow mix*, presented a more realistic live sound reinforcement scenario. The same piece was played back, but the choir was panned only to frontal angles between $\varphi = \pm 45^\circ$.

3 Experimental Procedure

To compare different configurations to a reference, a Multi-Stimulus Test with Hidden Reference and Anchor (MUSHRA) [21] appeared to be a suitable test paradigm. Participants were asked to rate the similarity between the five different conditions and the reference which rendered the direct sound objects with 0 dB/dod and the reverberation with -3 dB/dod. The single-target conditions were 0 dB/dod, -1.5 dB/dod, -3 dB/dod, and -6 dB/dod for which rendering did not separate direct sound objects and reverberation. The fifth condition was the hidden reference. In the experiment and the results, cf. Figure 3, 100 denoted perceptual identity to the reference, while 0 denoted maximum difference.

The listening experiment started at position P3, marked as cross in Figure 2. Participants were asked to rate the similarity between the reference and the other conditions for the wide mix, first with the long and afterwards with the short reverberation. Then, they repeated the

⁸<https://www.matthiaskronlachner.com/mcfx-v0-1-multichannel-cross-plattform-audio-plug-in-suite/>

task for the narrow mix with both reverb and changed the listening position afterward. In each trial, we randomized the different conditions to be evaluated.

4 Results

20 expert listeners (1 diverse, 2 female, and 17 male) with an average age of 35.7 years (minimum: 27, maximum: 61 years) took part in the listening experiment. On average, the participants needed 24 minutes and 47 seconds (minimum: 10 min 56 sec, maximum: 40 min 03 sec) to complete the listening experiment.

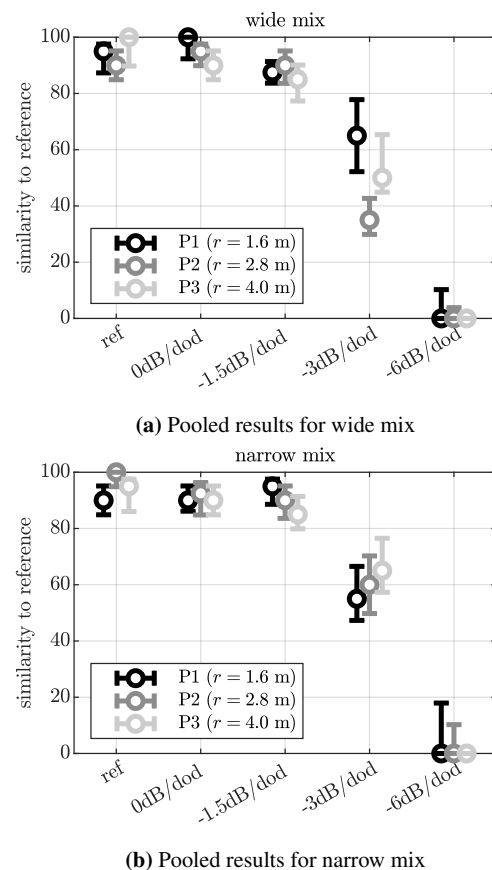


Fig. 3. Medians and corresponding 95% confidence intervals for different array configurations.

Regardless of the listening position and for both the narrow and the wide mix scenarios, the correlation

	refl0dB	refl-1.5dB	refl-3dB	0dBI-3dB	-1.5dBI-3dB	-3dBI-6dB
P1	0.737	0.089	≪ 0.001	≪ 0.001	≪ 0.001	≪ 0.001
P2	1.086	1.162	≪ 0.001	≪ 0.001	≪ 0.001	≪ 0.001
P3	0.282	0.021	≪ 0.001	≪ 0.001	≪ 0.001	≪ 0.001

Table 1: Bonferroni-corrected p -values for pairwise comparisons of the wide mix for different array configurations; values smaller 0.05 denote significant differences.

	refl0dB	refl-1.5dB	refl-3dB	0dBI-3dB	-1.5dBI-3dB	-3dBI-6dB
P1	-0.026	0.172	1.157	0.679	0.858	2.794
P2	-0.114	0.113	2.994	3.220	2.587	2.366
P3	0.309	0.425	2.416	1.900	1.173	6.293

Table 2: Effect size for pairwise comparisons of the wide mix for different array configurations; values greater 0.6 denote medium effects; values greater 0.8 denote large effects.

coefficients for pairwise comparisons between both reverberation conditions stayed nearly always above 0.9. Therefore, the following analyses were performed on the pooled data from both reverberation conditions.

4.1 Wide mix

For the wide mix, ratings show a pronounced similarity of the dual-target reference with some of the uniform, single-target array configurations: 0 dB/dod and -1.5 dB/dod are similarly good when comparing the median and confidence intervals, cf. Figure 3a. A Wilcoxon signed-rank test with Bonferroni correction indicated that there was no statistically significant difference between the reference and 0 dB/dod for all positions ($p > 0.28$), cf. Table 1. Comparing the answers for the hidden reference with -1.5 dB/dod yielded a weakly significant difference at position 1 ($p = 0.09$), no significance at position 2 ($p = 1.16$), and significant difference at position 3 ($p = 0.02$), for which apparently the direct sound objects being played back by the right loudspeakers were becoming too loud as the listener went outwards.

Greater differences were observed for -3 dB/dod and -6 dB/dod which were clearly rated worse, and the differences of their results were significant to the hidden reference and also to 0 dB/dod and -1.5 dB/dod for all positions ($p < 0.01$). Significant differences were also observed between -3 dB/dod and -6 dB/dod at all positions ($p < 0.01$).

To examine the effect sizes of these array configurations, we employed the impact effect size which incorporates the probability distributions of two data sets

compared to other effect size measures [22]. Table 2 showed that there was only a weak effect when comparing 0 dB/dod and -1.5 dB/dod to the reference. On the first and second position, the negative sign indicated that 0 dB/dod yields even slightly better results than the reference itself. In contrast, there were medium to large effects comparing -3 dB/dod and -6 dB/dod to all other configurations.

The number of responses in which the hidden reference ranks highest is an interesting overall indicator for the difference to similar array configurations, too. Only three participants rated the hidden reference as the exclusively best configuration for all reverberation conditions and listening positions. In contrast, the hidden reference was rated on top of the scale in 57.5% of the answers on average, so there may have been another arrangement that received the same rating. When the hidden reference was not rated as the best configuration, participants favored 0 dB/dod in most cases, which received top ratings in 47.5 % of the responses. In 35% of the responses, -1.5 dB/dod received top ratings.

4.2 Narrow mix

Similar results were found for the narrow mix scenario. The worst rating was observed for the -6 dB/dod configuration, followed by -3 dB/dod. For the more similar cases 0 dB/dod, and -1.5 dB/dod, median and confidence intervals only indicate slight differences to the hidden reference, cf. Figure 3b. A Wilcoxon signed-rank test with Bonferroni correction indicates no significant difference between 0 dB/dod and the hidden reference ($p > 0.12$) at all positions, cf. Table 3. Neither was the -1.5 dB/dod case significantly different

	refl0dB	refl-1.5dB	refl-3dB	0dBI-3dB	-1.5dBI-3dB	-3dBI-6dB
P1	1.108	1.108	≪ 0.001	≪ 0.001	≪ 0.001	≪ 0.001
P2	0.122	0.094	≪ 0.001	≪ 0.001	≪ 0.001	≪ 0.001
P3	0.790	0.695	≪ 0.001	≪ 0.001	≪ 0.001	≪ 0.001

Table 3: Bonferroni-corrected p -values for pairwise comparisons of the narrow mix for different array configurations; values smaller 0.05 denote significant differences.

	refl0dB	refl-1.5dB	refl-3dB	0dBI-3dB	-1.5dBI-3dB	-3dBI-6dB
P1	-0.107	-0.154	1.212	1.298	1.589	2.072
P2	0.211	0.277	1.945	1.122	1.109	2.700
P3	0.103	0.244	1.045	0.777	0.618	3.560

Table 4: Effect size for pairwise comparisons of the wide mix for different array configurations; values greater 0.6 denote medium effects; values greater 0.8 denote large effects.

to the hidden reference ($p > 0.6$), except weakly at position 2 ($p = 0.094$). -3 dB/dod and -6 dB/dod differed significantly from either the hidden reference or 0 dB/dod, or -1.5 dB/dod, at all positions ($p < 0.005$). Moreover, significant differences were found between -3 dB/dod and -6 dB/dod at all positions ($p < 0.001$). Three participants (not the same as for the wide mix) identified the hidden reference as the exclusively best configuration for all reverberation conditions and listening positions. On average, the hidden reference was rated on top of the scale in 56.66 % of the responses. Similar to the results for the wide mix, the 0 dB/dod configuration received top ratings in 41.67 % of the responses, and -1.5 dB/dod in 36.67 %.

5 Discussion

Previous experiments showed that preserving the mixing balance of direct sound objects required a line-array design with 0 dB/dod, while preserving envelopment required -3 dB/dod [10]. Thus, an optimal system would need to combine both in a dual-target design, with separate rendering of both components of an immersive mix. However, for typical content, our experiment showed there are no appreciable benefits from the complication of a dual-target line-array design as a reference, when compared to some single-target design that renders both components the same way, yet with more control than what point sources offer. In nearly all cases, listeners were not able to clearly distinguish between the single-target designs 0 dB/dod or -1.5 dB/dod versus the hidden dual-target reference (maximum effect size of 0.425).

It seems that a preserved mixing balance was more important than envelopment considering a live concert scenario with frontally placed direct sound objects that are complemented with surround effects, e.g. reverberation. In terms of the mixing balance, the -3 dB/dod design yielded better results for the narrow mix than for the wide one, because loudspeaker array LS 3 (right side and close to the listening position) mainly contains reverberation in the narrow mix. In contrast, the -1.5 dB/dod configuration was a little worse in the wide mix, where more lateral loudspeakers contribute to the mixing balance. Interestingly, the -3 dB/dod configuration performed better at position 3 than at position 2 in the wide mix, although the listener is closer to loudspeaker LS 3 at position 3. This behavior can be argued with the directivity of the loudspeakers. According to the direct sound level maps shown in [11] and to the directivity measurements in [13], a listener at position 3 is outside the main lobe of the line array for higher frequencies and therefore loudspeaker LS 3 becomes less important.

In summary, acceptable playback is achieved when using loudspeaker arrays whose direct-sound level decay stays limited by -1.5 dB/dod. For practical applications, this allows more relaxed line array designs, which also improve frequency homogeneity over distance. In a scenario where the direct sound objects are only placed frontally, the frontal loudspeaker arrays must fulfill this criterion. However, the other loudspeakers may be even designed to produce a direct sound that rolls off by -3 dB/dod, because this is an optimal target for envelopment.

6 Conclusion

In this contribution, we compared a dual-target line array design, i.e. 0 dB/dod for constant mixing balance of the direct sound objects and -3 dB/dod for envelopment, to different single-target designs in a listening experiment. The experiment employed typical live sound reinforcement content with frontally placed direct sound and reverberation from lateral and back directions at three off-center listening positions. While the single-target designs with -3 dB/dod and -6 dB/dod were clearly rated worse than the reference dual-target design in all cases, the single-target design with 0 dB/dod was indistinguishable from the reference. Similarly, -1.5 dB/dod could only be distinguished from the reference at the outmost listening position for a wide mix, where direct sounds were distributed within the entire frontal semicircle, i.e. $\pm 90^\circ$ around the front.

According to our results, listeners are more sensitive regarding the preservation of the mixing balance for typical content, while preservation of envelopment seems to be less important. Thus, a single-target design with 0 dB/dod or even a slightly relaxed design with -1.5 dB/dod that exhibits a less position-dependent frequency response are sufficient. In practice, the effort could even be reduced by using shorter arrays with -3 dB/dod at lateral and back directions, where typically no direct sound is coming from.

Further work should deal with the question whether planar arrays could further improve rendering for off-center listening positions which would not be covered by the horizontal directivity of the miniature line array. Furthermore, the size of the sweet area for large venues should be investigated in situ or via simulated scenarios.

7 Acknowledgments

Our research was funded by the Austrian Science Fund (FWF): P 35254-N (Envelopment in Immersive Sound Reinforcement, EnImSo). We want to thank all listeners for their participation in the experiment.

8 Data Availability

To support reproducible research, the results of the listening experiments are made available under [23].

References

- [1] Patterson, J. and Lee, H., editors, *3D Audio*, Perspective on Music Production, Routledge, United States, 1st edition, 2021, ISBN 9781138590069, doi:10.4324/9780429491214.
- [2] Mouterde, T., Epain, N., Moulin, S., and Corteel, E., "On the perception of musical groove in large-scale events with immersive sound," in *Audio Engineering Society Conference: AES 2023 International Conference on Spatial and Immersive Audio*, 2023.
- [3] Mouterde, T., Epain, N., Moulin, S., and Corteel, E., "On the factors influencing groove fidelity in immersive live music events," in *Audio Engineering Society Conference: AES 2024 International Acoustics & Sound Reinforcement Conference*, 2024.
- [4] Blochberger, M., Zotter, F., and Frank, M., "Sweet area size for the envelopment of arecursive and a non-recursive diffusenessrendering approach," in *Proceedings of 5th International Conference on Spatial Audio ICSA*, Ilmenau (Deutschland), 2019.
- [5] Heidegger, P., Brands, B., Langgartner, L., and Frank, M., "Sweet Area using Ambisonics with simulated Line Arrays," in *Fortschritte der Akustik, DAGA*, Wien (Österreich), 2021.
- [6] Gölles, L. and Zotter, F., "Optimally Curved Arc Source for Sound Reinforcement," in *Fortschritte der Akustik, DAGA*, Wien (Österreich), 2021.
- [7] Riedel, S. and Zotter, F., "Surrounding line sources optimally reproduce diffuse envelopment at off-center listening positions," *JASA Express Letters*, 2(9), p. 094404, 2022, doi:10.1121/10.0014168.
- [8] Riedel, S., Gölles, L., Zotter, F., and Frank, M., "Modeling the Listening Area of Envelopment," in *Fortschritte der Akustik, DAGA*, Hamburg, 2023.
- [9] Gölles, L., Frank, M., and Zotter, F., "Improving Surround Sound Reinforcement at Off-center Listening Positions with Miniature Line Arrays," in *Fortschritte der Akustik, DAGA*, Hannover, 2024.

- [10] Gölles, L., Frank, M., and Zotter, F., “Improving Surround Sound Reinforcement at Off-center Listening Positions with Miniature Line Arrays,” in *AES 156th Convention*, Madrid, 2024.
- [11] Gölles, L. and Zotter, F., “Theory of continuously curved and phased line sources for sound reinforcement,” *Acta Acust.*, 7, p. 52, 2023, doi:10.1051/aacus/2023045.
- [12] Gölles, L. and Zotter, F., “Dual-Target Design for Large-Scale Sound Reinforcement: Simulation and Evaluation,” in *Audio Engineering Society Conference: AES 2024 International Conference on Acoustics & Sound Reinforcement*, 2024.
- [13] Gölles, L., Zotter, F., and Merkel, L., “Miniature Line Array for Immersive Sound Reinforcement,” in *Audio Engineering Society Conference: AES 2023 International Conference on Spatial and Immersive Audio*, 2023.
- [14] Frank, M., Gölles, L., Riedel, S., and Zotter, F., “Equalizing the coloration of different Ambisonic order weightings,” in *Fortschritte der Akustik, DAGA*, Hamburg, 2023.
- [15] Frank, M., “How to make Ambisonics sound good,” in *Proceedings of Forum Acusticum*, Krakau, 2014.
- [16] Zotter, F. and Frank, M., “All-Round Ambisonic Panning and Decoding,” *J. Audio Eng. Soc.*, 60(10), pp. 807–820, 2012.
- [17] don camillo chor e.V., “The Marsh Marigold’s Song from Kasimir’s Adventure,” <https://cambridge-mt.com/ms/mtk/#KasimirsAdventure>, 2016.
- [18] Murphy, D. T., “Impulse Responses of York Minster cathedral,” https://www.openair.hosted.york.ac.uk/?page_id=797, 2006.
- [19] Gölles, L., “Impulse Responses of Stefaniensaal Graz,” https://git.iem.at/lukasgoelles/impulse_responses_stefaniensaal_congress_graz, 2023.
- [20] Gölles, L. and Zotter, F., “Directional Enhancement of First-Order Ambisonic Room Impulse Responses By The 2+2 Directional Signal Estimator,” in *Proceedings of the Audio Mostly*, Graz (Österreich), 2020.
- [21] Union, I. T., “RECOMMENDATION ITU-R BS.1534-1 - Method for the subjective assessment of intermediate quality level of coding systems,” *International Telecommunications Union*, Geneva, 2001.
- [22] Lötsch, J. and Ultsch, A., “A non-parametric effect-size measure capturing changes in central tendency and data distribution shape,” *PLoS ONE*, 15, 2020, doi:10.1371/journal.pone.0239623.
- [23] Gölles, L., “Supplementary Data for Evaluating a Dual-Target Line-Array Design for Medium-Scale Surround Sound Reinforcement,” <https://phaidra.kug.ac.at/o:133364>, 2024.

Publication VIII

This work was published as:

Lukas Gölles, and Maximilian Herczegh, “MCPyPan3D: mixing console’s python-based panning tool for 3D audio at live events,” in Proceedings of LEaTcon Science Talks, Hamburg: October 2024. [not yet published]

MCPyPan3D: Mixing Console’s Python-Based Panning Tool for 3D Audio at Live Events

Lukas Göllés¹, Maximilian Herczegh², Matthias Frank¹

¹*Institute of Electronic Music and Acoustics, University of Music and Performing Arts, 8010 Graz, Austria*

²*Graz, University of Technology, 8010 Graz, Austria*

Email: goelles@iem.at, m.herczegh@student.tugraz.at, frank@iem.at

Introduction

Recently, spatial audio increased in popularity at live events. In spatial audio systems at live events, a processor is commonly employed that distributes the signals from a digital mixing console to the loudspeaker arrangement with corresponding gains and, in some instances, delays. A number of loudspeaker manufacturers^{1,2} have already developed such processors successfully, using MADI or network-based protocols like AVB/MILAN or DANTE to establish convenient connections with all sound devices. However, the question arises: It is possible to achieve surround sound reinforcement with a conventional stereo mixing console alone?

This contribution presents a network-based solution using a conventional Allen & Heath SQ5 mixing console. MCPyPan3D is a python-based tool with a graphical interface that allows the sound engineer to place direct sound objects on the upper hemisphere. The objective of this tool is to calculate loudspeaker gains using Ambisonics [1] and then apply them as gains of the aux channels in the mixing console. Furthermore, these direct sound objects can be complemented with surrounding effects, such as reverberation and delay. These are typically implemented as stereo effects in the mixing console and can be spatialized using first-order Ambisonic encoding and decoding. Simulations of the sweet area and a listening experiment investigate the applicability of MCPyPan3D in practice.

Loudspeaker Gains

MCPyPan3D uses the surround sound format Ambisonics [1] to obtain proper loudspeaker gains. Encoding and decoding requires the encoder vector $\mathbf{y}_N(\boldsymbol{\theta}_S)$ and a decoder matrix \mathbf{D} . The column vector $\mathbf{y}_N(\boldsymbol{\theta}_S) = [Y_0^0(\boldsymbol{\theta}_S) \ Y_{-1}^1(\boldsymbol{\theta}_S) \ \dots \ Y_N^N(\boldsymbol{\theta}_S)]^T$ contains the spherical harmonics up to the desired order N evaluated at the desired source position $\boldsymbol{\theta}_S = [\cos \varphi_S \cos \vartheta_S \ \sin \varphi_S \cos \vartheta_S \ \sin \vartheta_S]^T$. φ_S denotes the azimuth angle, and ϑ_S the elevation angle.

We assume a hemispherical setup of full-range loudspeakers with additional subwoofers positioned on the floor around the audience. In order to decode the subwoofers separately, MCPyPan3D expects two decoder matrices \mathbf{D} . The dimensions of \mathbf{D} , $L \times (N+1)^2$, defines the number of used loudspeakers L and the desired Ambisonic order N . State-of-the-art Ambisonic decoding to loudspeakers

typically employs the AllRAD approach as it ensures smooth playback on arbitrary loudspeaker arrangements [2]. Configuration files containing the decoder matrix \mathbf{D} may be generated by the VST plugin AllRADecoder of the IEM plugin suite³.

Max- r_E weights [3], $a_N = P_N \left[\cos \left(\frac{137.9^\circ}{N+1.51} \right) \right]$, are applied to increase the sweet area [1, 4]. P_N denote the Legendre polynomials. These weights cause a side-lobe suppression and the application requires a diagonal matrix $\text{diag}\{\mathbf{a}_N\}$ of size $(N+1)^2 \times (N+1)^2$ whose entries in the main diagonal correspond to the entries of the vector \mathbf{a}_N . The matrix-vector operation yields loudspeaker gains

$$\mathbf{g}_L = \mathbf{D} \text{diag}\{\mathbf{a}_N\} \mathbf{y}_N(\boldsymbol{\theta}_S). \quad (1)$$

However, these calculations may provide loudspeaker gains with different signs, which would require an additional channel strip with inverted phase. In order to maximize the number of usable channels, MCPyPan3D omits the sign of the gains because negative values are only to be expected for the side lobes, which are reduced by the max- r_E weights anyway and therefore only reproduced very quietly. Furthermore, omitting the sign of the gains does not change the predicted localization.

Stereo Auxiliary Channels

To keep the maximum number of usable loudspeakers as high as possible, stereo auxiliary channels have to be used which require to adjust the level and panorama appropriately. With the Allen & Heath SQ-5, a setup with a maximum of 24 loudspeakers is feasible. Through measurements, we obtained the panning law and the resulting level differences ΔL in dB depending on the panorama setting, for which we use the approximation

$$\Delta L(\text{pan}) = 6 \tan \left(\frac{\text{pan}}{41} \frac{\pi}{2} \right), \quad (2)$$

where pan is the panorama setting of the mixer that ranges from -37 to 37 and uses integer values. The error between the measured and the approximated level remains within a value of ± 0.7 dB for the range of high interest $|\Delta L| < 16$ dB, cf. Figure 1.

The loudspeaker gains of Equation 1 are grouped into pairs for which the level differences are calculated. The value of the panorama is set through the approximation of Equation 2. The level of the auxiliary channel is set, so that the higher gain with applied panning corresponds to the optimal gain from Equation 1.

¹L-Acoustics L-ISA: <https://l-isa.l-acoustics.com/>

²d&b Soundscape: <https://www.dbsoundscape.com/global/en/>

³<https://plugins.iem.at>

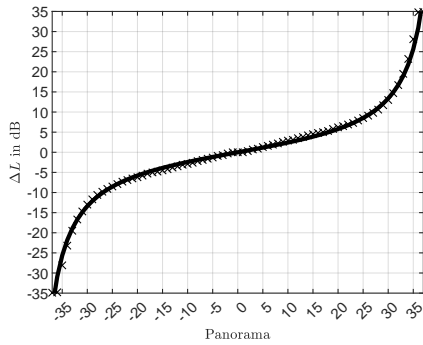


Figure 1: Measured level differences ΔL of the auxiliary channels using the console’s panorama between -37 and 37 (black crosses) and approximated function (solid black line).

Python: Graphical Interface & Network Commands

We selected Python as our preferred language for implementing all calculations and the graphical interface due to its flexibility and independence from a platform. For the design of the graphical interface, cf. Figure 2, Pygame⁴ offers the possibility to draw, add and move colored balls which represent the direct sound objects. The number inside the balls corresponds to the channel number on the mixing console. The stacking order of overlapping objects can be altered by clicking the middle mouse button. The interface shows a circle that represents the top view of an upper hemisphere. For smooth panning in height, we decided to map the radius linearly to the elevation angle. When objects are moved, a gain calculation is performed and the corresponding send gains of the console’s auxiliary channels are updated.

Numpy⁵ is required for the gain calculations. Currently, MCPyPan3D is intended to be used with the Allen & Heath SQ-5 mixer. The gains are transmitted to the mixing console via Transmission Control Protocol (TCP) for which the library socket⁶ is used. The modular structure of MCPyPan3D supports adaption to any other mixing console that can be controlled via network commands. In the configuration file, azimuth and elevation of the effects channel, as well as the IP address of the mixing console are set. The paths to .json files containing the decoding matrices are also provided in the configuration file. Furthermore, users can save and load presets which are stored in .json format. These presets contain azimuth angle, elevation angle, and color of each audio object.

Error evaluation

To evaluate the error produced by the gain modification when using auxiliary channels, we use the extended energy vector model [5, 6] that has already been used to predict the sweet area of Ambisonic playback systems successfully [7, 8, 9]:

⁴<https://github.com/pygame/pygame>

⁵<https://numpy.org/>

⁶<https://docs.python.org/3/library/socket.html>

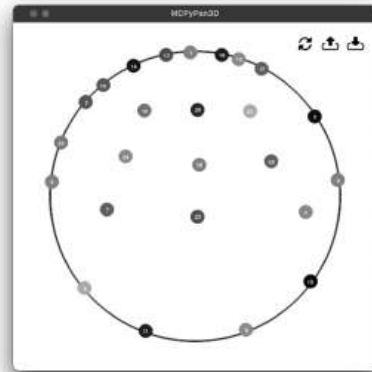


Figure 2: MCPyPan3D: graphical interface

$$r_E = \frac{\sum_L (w_{\tau,l} \cdot w_{d,l} \cdot g_l)^2 \theta_l}{\sum_L (w_{\tau,l} \cdot w_{d,l} \cdot g_l)^2}. \quad (3)$$

θ_l is a unit vector pointing from the listening position to the l th loudspeaker and g_l is the corresponding loudspeaker gain. $w_{d,l}$ is an additional weighting to account for the relative damping of direct sound at off-center listening positions. $w_{\tau,l} = 10^{\frac{w_{\tau} \cdot \tau_l}{1000}}$ is a weight to incorporate the time of arrival, where τ_l denotes the acoustic delay of the l -th loudspeaker to the listening position. $w_{\tau} = -1 \frac{\text{dB}}{\text{ms}}$ is a multiplication factor that is known from the echo threshold and chosen as trade-off between transient and stationary signals [8, 9].

For the evaluation, we assume a circular setup of eight loudspeakers on the horizon of the IEM CUBE, a 10.3 m \times 12 m studio with a reverberation time of $T_{30} \approx 0.5$ s, cf. Figure 3. It has been proposed to use line arrays whose direct sound decays by -1.5 dB per distance doubling (dod) for a surround sound scenario with frontally placed direct sound objects that are complemented with surrounding reverberation [10]. This is achieved by eight mini line arrays consisting of eight enclosures each with 65 cm total length [11]. To show broadband results, the damping weights w_d use the A-weighted results of the simulated direct sound pressure levels of arrays. We use third-order Ambisonics with max- r_E weighting to ensure optimally smooth playback on this arrangement [12].

Figure 4 shows the localization error (root mean square) for panning on the horizon in steps of 1° using the gains resulting from optimal Ambisonic encoding and decoding (right half of the room) compared to gains realized with MCPyPan3D (left). For the majority of the audience area, the localization error stays below 10° (white contour) in both cases. The difference in the localization error between optimal gains and gains realized by MCPyPan3D stays between $\pm 1^\circ$ for the relevant region. Therefore, the approximations of the gains realized by MCPyPan3D can be expected not to have any significant disadvantage in practice.

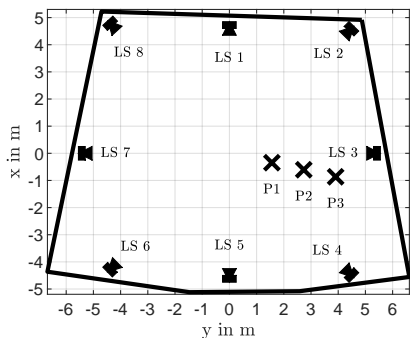


Figure 3: Loudspeaker setup at the IEM CUBE with positions for the listening experiments marked as crosses as used in [8, 10, 13].

Surrounding Effects

In typical live concert scenarios, reverberation is mostly used as surrounding effect. However, a conventional stereo mixing console is not able to render surrounding or 3D reverberation by default, which requires a solution using stereo effects. For example, the stereo signals of the effect bus can be panned to left and right on the horizon, i.e. $\varphi_S = \pm 90^\circ$, and decoded to the loudspeaker arrangement using first-order Ambisonics. We performed a listening experiment to find out whether such a configuration achieves acceptable playback.

Methods and Conditions

The listening experiment took place at the IEM CUBE. We used the same setup as described for the simulation, cf. Figure 3. As proposed in [10], we used our miniature line arrays [11] in -1.5 dB/dod setting. We applied amplitude compensation to the center, but omitted delay compensation as it makes no sense for a large listening area [4].

As audio scenes, we used a short excerpt of the *Cello Concerto in A Minor* by *Ethan Winer* [14] with a reverberation time of 4 s and two short excerpts of *All The Gin Is Gone* played by the *Maurizio Pagnutti Sextet* [15] with a reverberation time of 2 s. For all 3 audio scenes, the direct-sound objects were positioned between $\varphi_S = \pm 45^\circ$ using third-order Ambisonics, assuming a wide stage in front of the audience, and were presented together with the reverberation.

The listeners had to rate the envelopment of the reverberation comparing four conditions. We used a 16×16 feedback delay network (*FDN*), which was encoded to third-order Ambisonics using 16 points on a sphere (sphconv16 preset of the SPARTA plugin suite⁷) and decoded to 8 loudspeakers using the *AllRADecoder* with additional imaginary loudspeakers at nadir and zenith with 0 gain. Condition *o1* simulated a spatialized 2-channel stereo reverberation. The 2 channels were generated from the Ambisonics signals by first decoding only to 4 loudspeakers at $\varphi = 0^\circ, 90^\circ, 180^\circ, -90^\circ$ together with the

⁷<https://leomccormack.github.io/sparta-site/>

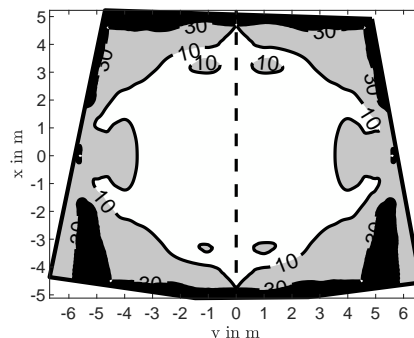


Figure 4: Mean localization error vector contours in degrees simulated by the extended energy vector model for third-order Ambisonics using ideal gains (right) compared to the realization with MCPyPan3D (left).

two imaginary loudspeakers. Then, the signals for the loudspeakers in the front (0°) and in the back (180°) were omitted and the remaining two lateral loudspeaker signals were re-encoded at $\varphi_S = \pm 90^\circ$ and decoded to the loudspeaker setup using first-order Ambisonics. We also added a *mono* version of the same reverberation distributed equally to all eight loudspeakers. As alower anchor, we used playback without reverberation, abbreviated as *w/o*.

The listeners started at position 1 and continued at position 2 and then 3. The conditions were randomized in each trial, however the audio scenes were always presented in the same order with decreasing reverberation time.

Results

In total, 17 listeners with experience in spatial audio (average age: 33 years) took part in the experiment. The entire experiment took them on average 11 min 31 s. Figure 5 shows the median and 95 % confidence intervals of the pooled results of all audio scenes. It is noticeable that the *FDN* tends to be the best condition. However, the *FDN* was sometimes confused with the *o1* condition. At position 1, the *FDN* was rated best in 66% of the ratings, in 33% *o1* was best. At position 2, the *FDN* was rated best in 71% of the ratings and *o1* in 25%. At position 3, the *FDN* was only rated best in 52% of the ratings. A sign rank test with Bonferroni correction indicates no significant differences between *FDN* and *o1* at positions 1 and 3 ($p \geq 0.09$), however at position 2 ($p = 0.013$). Comparing to the *mono* reverberation, the *FDN* was rated significantly better at all positions ($p \leq 4 \cdot 10^{-4}$).

The impact effect size [16] for pairwise comparison between *FDN* and *o1* reveals a weak effect at all positions ($d \leq 0.6$). Comparing *FDN* and the *mono* reverberation, large effects can be observed at all positions ($d \geq 2.29$). As experts participated in this listening experiment and paid attention to the reverberation explicitly, we can conclude that the *o1* condition would achieve acceptable results in live concert scenarios, where background noise

is usually to be expected in addition to the musical performance. Furthermore, listeners there would not focus on the comparison between different reproductions of the reverberation.

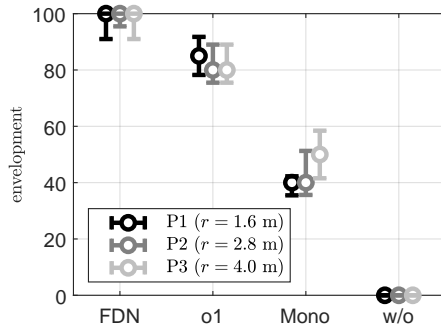


Figure 5: Medians and corresponding 95% confidence intervals of envelopment ratings in dependence of the listening position, pooled across all audio scenes.

Conclusion and Outlook

In this contribution, we presented MCPyPan3D, a python-based panning tool based on Ambisonics, which allows to spatialize sound objects at live events using a conventional stereo mixing console. Spatialization is done by controlling gain and panorama settings of the auxiliary channels of the mixing console via network commands. In order to save channels, only the absolute values of the gains are applied and signs are omitted. Simulations indicate that the expected localization error is not significantly affected by the proposed modification. The results of a listening experiment show that stereo reverberation panned laterally using first-order Ambisonics achieves similar envelopment than a surrounding multi-channel reverberation, even at off-center listening positions. Further work should consider the implementation of automatization strategies to provide non-static mixes based on a timecode.

Data Availability

The results of the listening experiments and the simulated A-weighted sound pressure levels are available online⁸. The source code⁹ of this tool can be downloaded freely and modified for other mixing consoles.

Acknowledgment

Our research was partly funded by the Austrian Science Fund (FWF): P 35254-N (Envelopment in Immersive Sound Reinforcement, EnImSo). The authors want to thank all participants of the listening experiment.

References

- [1] F. Zotter and M. Frank, *Ambisonics: A Practical 3D Audio Theory for Recording, Studio Production, Sound Reinforcement, and Virtual Reality*, ser.

Springer Topics in Signal Processing. Springer International Publishing, 2019.

- [2] —, “All-round ambisonic panning and decoding,” *Journal of the Audio Engineering Society. audio, acoustics, applications*, vol. 60, no. 10, pp. 807–820, 11 2012.
- [3] J. Daniel, “Représentation de champs acoustiques, application à la transmission et à la restitution de scènes sonores complexes dans un contexte multimédia,” Ph.D. dissertation, Université de Paris 6, 2000.
- [4] M. Frank, “How to make ambisonics sound good,” in *Proceedings of Forum Acusticum*, Krakau, 09 2014.
- [5] M. A. Gerzon, “General metatheory of auditory localisation,” in *Audio Engineering Society Convention 92*. Audio Engineering Society, 03 1992.
- [6] P. Stitt, S. Bertet, and M. van Walstijn, “Extended energy vector prediction of ambisonically reproduced image direction at off-center listening positions,” *J. Audio Eng. Soc.*, vol. 64, no. 5, pp. 299–310, 2016.
- [7] E. Kurz and M. Frank, “Prediction of the listening area based on the energy vector,” in *International Conference on Spatial Audio*, 09 2017.
- [8] L. Göllés, M. Frank, and F. Zotter, “Simulating the sweet area of immersive sound reinforcement with surrounding mini line arrays,” in *Fortschritte der Akustik*, Hannover, 03 2024.
- [9] M. Frank and J. Kristl, “Perceptual sweet area of 2-channel stereo playback,” in *VDT International Convention*, 03 2024.
- [10] L. Göllés, M. Frank, and F. Zotter, “Evaluating a dual-target line-array design for medium-scale surround sound reinforcement,” in *AES 156th Convention*, Madrid, 06 2024.
- [11] L. Göllés, F. Zotter, and L. Merkel, “Miniature line array for immersive sound reinforcement,” in *Audio Engineering Society Conference: AES 2023 International Conference on Spatial and Immersive Audio*, Aug 2023.
- [12] M. Frank, L. Göllés, S. Riedel, and F. Zotter, “Equalizing the coloration of different ambisonic order weightings,” in *Fortschritte der Akustik, DAGA*, Hamburg, 03 2023.
- [13] L. Göllés, M. Frank, and F. Zotter, “Improving surround sound reinforcement at off-center listening positions with miniature line arrays,” in *AES 156th Convention*, Madrid, 06 2024.
- [14] E. Winer, “Concerto for cello and orchestra in a minor,” <https://ethanwiner.com/concerto.html>, 1999.
- [15] M. P. Sextet, “All the gin is gone,” <https://cambridge-mt.com/ms/mtk/#MaurizioPagnuttiSextet>.
- [16] J. Lötsch and A. Ultsch, “A non-parametric effect-size measure capturing changes in central tendency and data distribution shape,” *PLoS ONE*, vol. 15, 09 2020.

⁸<https://phaidra.kug.ac.at/o:134336>

⁹https://git.iem.at/lukasgoelles/2024_ambisonics_sq5

